

**CONCEPTUAL DESIGN OF A MODEL SUPPORT SYSTEM AND ITS
CONTROLLER FOR ANKARA WIND TUNNEL**

**A THESIS SUBMITTED TO
THE GRADUATE SCHOOL OF NATURAL AND APPLIED SCIENCES
OF
MIDDLE EAST TECHNICAL UNIVERSITY**

BY

NEJAT ULUSAL

**IN PARTIAL FULFILLMENT OF THE REQUIREMENTS
FOR
THE DEGREE OF MASTER OF SCIENCE
IN
MECHANICAL ENGINEERING**

DECEMBER 2005

Approval of the Graduate School of Natural and Applied Sciences

Prof. Dr. Canan Özgen
Director

I certify that this thesis satisfies all the requirements as a thesis for the degree of Master of Science.

Prof. Dr. Kemal İder
Head of Department

This is to certify that we have read this thesis and that in our opinion it is fully adequate, in scope and quality, as a thesis for the degree of Master of Science.

Prof. Dr. Bülent E. Platin
Co-Supervisor

Prof. Dr. Tuna Balkan
Supervisor

Examining Committee Members

Prof. Dr. Kahraman Albayrak (Chairman)	(METU,ME)	_____
Prof. Dr. Tuna Balkan	(METU,ME)	_____
Prof. Dr. Bülent E. Platin	(METU,ME)	_____
Asst. Prof. Dr. İlhan Konukseven	(METU,ME)	_____
Dr. Gökmen Mahmutyazıcıoğlu	(TÜBİTAK-SAGE)	_____

I hereby declare that all information in this document has been obtained and presented in accordance with academic rules and ethical conduct. I also declare that, as required by these rules and conduct, I have fully cited and referenced all material and results that are not original to this work.

Nejat ULUSAL

ABSTRACT

CONCEPTUAL DESIGN OF A MODEL SUPPORT SYSTEM AND ITS CONTROLLER FOR ANKARA WIND TUNNEL

Ulusal, Nejat

M.Sc., Department of Mechanical Engineering

Supervisor: Prof. Dr. Tuna Balkan

Co-Supervisor: Prof. Dr. Bülent E. Platin

December 2005, 119 pages

Ankara Wind Tunnel (AWT) operated by TÜBİTAK-SAGE is the only big sized wind tunnel in Turkey. The AWT was constructed in late 1940's but was not operated until 1993 when the tunnel was turned over TÜBİTAK-SAGE. Since 1993, a series of modernization work has been undergoing in order to match the demands of the 21st century.

In wind tunnels, models are positioned by special mechanisms that are instrumented to get the test data specific to the test performed. Models are assembled from their rear sides on these mechanisms called model support systems in order not to influence the flow around them.

In this thesis, a conceptual design of a 6 degrees-of-freedom model support system for AWT is accomplished. A detailed system model is developed for the controller design. A force controller to perform store separation tests in real time is designed, tuned, and validated with computer simulations.

Keywords: Wind Tunnel, Model Support System, Force Controller

ÖZ

ANKARA RÜZGAR TÜNELİ İÇİN MODEL DESTEK SİSTEMİ VE DENETİMCİSİNİN KAVRAMSAL TASARIMI

Ulusal, Nejat

Yüksek Lisans, Makine Mühendisliği Bölümü

Tez Yöneticisi : Prof. Dr. Tuna Balkan

Ortak Tez Yöneticisi : Prof. Dr. Bülent E. Platin

Aralık 2005, 119 sayfa

TÜBİTAK-SAGE tarafından çalıştırılan Ankara Rüzgar Tüneli Türkiye'nin tek büyük çaplı rüzgar tünelidir. Tünel 1940'ların sonlarında inşa edildikten sonra TÜBİTAK-SAGE'ye devredildiği 1993 yılına kadar kullanılmamıştır. 1993 yılından bu yana tüneli 21. yüzyılın ihtiyaçlarını karşılar hale getirebilmek için modernizasyon çalışmaları yürütülmektedir.

Rüzgar tünellerinde modeller, yapılan teste uygun algılayıcılarla donatılmış özel mekanizmalar tarafından konumlandırılırlar. Model destek sistemi adı verilen bu mekanizmalara modeller, etraflarındaki hava akımını etkilememek için akışın terk ettiği taraflarından bağlanırlar.

Bu tez kapsamında 6 serbestlik dereceli bir model destek sisteminin kavramsal tasarımı yapılmıştır. Denetimci tasarımı için ayrıntılı bir sistem modeli geliştirilmiştir. Gerçek zamanlı olarak ayrılma testleri yapabilecek bir kuvvet denetimcisi tasarlanmış, parametreleri ayarlanmış ve bilgisayar benzetimleri ile doğrulanmıştır.

Anahtar Kelimeler: Rüzgar Tüneli, Model Destek Sistemi, Kuvvet Denetimcisi

ACKNOWLEDGMENTS

I want to express my deepest thanks to my supervisor, Prof. Dr. Tuna Balkan for his supervision, guidance, advice, encouragements, support and endless tolerance during all stages of the thesis.

I would also like to express my special appreciation to my co-supervisor Prof. Dr. Bülent Platin for his suggestions and comments, and continuous support.

I am grateful to my colleague Mesut Özel for his great efforts to share my responsibilities in the office to create me more time to complete this thesis.

I want to thank to my chiefs Mahmut Beşir, Turgay Şahin and Gülay Sandıkçioğlu for their continuous motivation and desire to help me during this study.

TÜBİTAK-SAGE, which supported this work, is acknowledged.

I want to thank to my family and especially my sister Elif for their consistent support during this work.

Finally I want to express my deepest thanks to N. Deniz Yücel and Onur Albayrak for making my dreams come true.

TABLE OF CONTENTS

PLAGIARISM	iii
ABSTRACT	iv
ÖZ	vi
ACKNOWLEDGMENTS	viii
TABLE OF CONTENTS	ix
LIST OF TABLES	xii
LIST OF FIGURES	xiii
LIST OF SYMBOLS	xvi
CHAPTERS	
1. INTRODUCTION	1
1.1. WIND TUNNEL TESTING	1
1.2. ANKARA WIND TUNNEL	2
1.3. MODEL SUPPORT SYSTEMS	4
1.4. AIM OF THE STUDY	8
1.5. SCOPE OF THE STUDY	8
2. LITERATURE SURVEY	10
2.1. SIMILAR SYSTEMS	10

2.2. STORE SEPARATION TEST METHODS USING MSS	17
2.3. POSITION / FORCE CONTROL ALGORITHMS	17
3. CONCEPTUAL DESIGN AND ANALYSIS OF THE MSS	21
3.1. DESIGN SPECIFICATIONS	21
3.2. COORDINATE FRAMES	23
3.3. THE R-R-P-R-R-R CONFIGURATION	25
3.4. CONCEPTUAL DESIGN	30
3.5. FORWARD KINEMATICS OF THE MSS	39
3.6. INVERSE DYNAMICS OF THE MSS	47
4. CONTROLLER DESIGN	52
4.1. CONTROLLER TOPOLOGY	52
4.2. PRELIMINARY WORK	55
4.3. CONTROL SYSTEM FOR THE MSS	71
4.3.1. MODEL SUPPORT SYSTEM BLOCK	72
4.3.2. COMPUTED TORQUE BLOCK	75
4.3.3. AERODYNAMIC MODULE BLOCK	75
4.3.4. CARTESIAN TO JOINT SPACE CONVERTER BLOCK	79
4.3.5. CONTROLLER BLOCK	80
5. SIMULATIONS OF THE MSS	82
5.1. THE MODEL MISSILE	82
5.2. CASE STUDIES	83
5.3. DISCUSSION	93

6. SUMMARY AND CONCLUSIONS	95
6.1. SUMMARY	95
6.2. CONCLUSIONS	97
6.3. RECOMMENDATIONS FOR FUTURE WORK.....	98
REFERENCES	100
APPENDICES	
APPENDIX A. SINGULARITY ANALYSIS FOR DOUBLE PENDULUM	103
APPENDIX B. SUPPLEMENTARY MATLAB® FILES	105
APPENDIX C. INFORMATION RELATED TO THE SIMULATIONS	109
SECTION 1. Technical Drawing of Basic Finner Geometry	109
SECTION 2. Missile DATCOM Code to Obtain the Aerodynamic	
Coefficients	111
SECTION 3. Tables Aerodynamic Coefficients of	
Basic Finner Geometry	114

LIST OF TABLES

Table.3.1 The Working Volume Defined in TSP.....	22
Table.3.2 External Loading Defined by the TSP.....	23
Table.3.3 Information about the Points Given In Figure.3.9.....	32
Table.3.4 Denavit and Hartenberg Parameters.....	41
Table.4.1 Parameters of the Double Pendulum Model	58
Table.4.2 Resulting Optimal PID Parameters for Double Pendulum.....	60
Table.4.3 Constants Used in Equations (4.3) to (4.8)	78
Table.4.4 Constants Used to Calculate Aerodynamic Forcing On the Links..	79
Table.4.5 Initial Conditions Used in Optimization.....	80
Table.4.6 Initial Guesses of the PID Parameters	81
Table.4.7 Resulting Optimal PID Parameters	81
Table.5.1 The Initial Conditions of the Test Cases.....	83
Table.5.2 The Actuator Requirements for the Results Obtained.....	93

LIST OF FIGURES

Figure.1.1 Side View Diagram of AWT Test Section.....	3
Figure.1.2 Current Model Handling System in AWT	4
Figure.1.3 A Poor Release Damaging the Aircraft Components.....	5
Figure.1.4 Multiple-flash Drop Test Photograph (With Catch-net).....	6
Figure.1.5 Multiple-flash Drop Test Photograph (Without Catch-net).....	7
Figure.2.1 Two Sting Rig	11
Figure.2.2 Motion Details of TSR.....	12
Figure.2.3. MSS in DNW-HST	13
Figure.2.4. Interior Schema of MSS in DNW-HST	13
Figure.2.5 DNW-HST Missile Support Extension.....	14
Figure.2.6 Test Rig in DNW-NWB Using a Stewart Platform	15
Figure.2.7 MSS in DNW-LLF during A340-500 Tests	16
Figure.2.8 MSS in DNW-LLF with A318 Model.....	16
Figure.2.9 The Conceptual Organization of Hybrid Controller	19
Figure.3.1 Earth-Fixed and Body-Fixed Coordinate Frames.....	24
Figure.3.2 Three Prismatic Joint Configuration in x-y-z Order	25
Figure.3.3 Three Prismatic Joint Configuration in y-z-x Order	26
Figure.3.4 One Revolute and Two Prismatic Joint Configuration.....	26
Figure.3.5 Two Revolute and One Prismatic Joint Configuration.....	27
Figure.3.6 The Two Revolute One Prismatic Joint Configuration in the Tunnel.	28
Figure.3.7 Actuating the Degrees of Freedom in the Test Section.....	29

Figure.3.8 R-R-P-R-R-R Configuration.....	30
Figure.3.9 Workspace In x-y Plane	31
Figure.3.10 Bottom View of the Test Section with the First Two Links.....	33
Figure.3.11 Top View of the Test Section with the First Two Links.....	34
Figure.3.12 Side View of the Prismatic and Fourth Revolute Joint	35
Figure.3.13 Limits of the Motion in z-Axis	36
Figure.3.14 Last Two Links of the MSS	38
Figure.3.15 Coordinate Frames Attached to the MSS According to Denavit and Hartenberg Notation.....	40
Figure.4.1 Force Controller Block Diagram	54
Figure.4.2 Modeled Double Pendulum.....	55
Figure.4.3 View of the MATLAB Simulink® Model for the Double Pendulum..	56
Figure.4.4 Simmechanics® Model of Double Pendulum.....	57
Figure.4.5 Details of the Revolute Joint Blocks.....	57
Figure.4.6 Free Fall Trajectory.....	61
Figure.4.7 Position Error Occurred During Free Fall.....	62
Figure.4.8 Force Sensor Measurement on x-Axis.....	62
Figure.4.9 Force Sensor Measurement on y-Axis.....	63
Figure.4.10 Force Error on y-Axis	63
Figure.4.11 Forced Motion Trajectory	64
Figure.4.12 Position Error Occurred During Forced Motion without Computed Torque Compensation.....	65
Figure.4.13 Force Sensor Measurement on x-Axis without Computed Torque Compensation	65
Figure.4.14 Force Error on x-Axis without Computed Torque Compensation	66
Figure.4.15 Force Sensor Measurement on y-Axis without Computed Torque Compensation	66
Figure.4.16 Force Error on y-Axis without Computed Torque Compensation	67
Figure.4.17 Force Error on y-Axis without Computed Torque Compensation	67

Figure.4.18 Force Sensor Measurement on x-Axis with Computed Torque Compensation	68
Figure.4.19 Force Error on x-Axis with Computed Torque Compensation	68
Figure.4.20 Force Sensor Measurement on y-Axis with Computed Torque Compensation	69
Figure.4.21 Force Error on y-Axis with Computed Torque Compensation	69
Figure.4.22 Block Diagram of the MATLAB Simulink® Model for the MSS	71
Figure.4.23 MATLAB® Simmechanics Model of the MSS	73
Figure.4.24 Linear Actuator Model	74
Figure.4.25 Coordinate System of Missile DATCOM	76
Figure.5.1 The Model Missile with Basic Finner Geometry	82
Figure.5.2 Wire Frame View of MSS at Specific Time Intervals of Case 1	84
Figure.5.3 Force Error Occurred During Free Fall	85
Figure.5.4. Torque Error Occurred During Free Fall	85
Figure.5.5 Position Error with Unconstrained Motion	86
Figure.5.6 Orientation Error with Unconstrained Motion	86
Figure.5.7 Wire Frame View of MSS at Specific Time Intervals of Case 2	87
Figure.5.8 Force Error Occurred During Case 2	88
Figure.5.9 Torque Error Occurred During Case 3	88
Figure.5.10 Position Error with Unconstrained Motion	89
Figure.5.11 Orientation Error with Unconstrained Motion	89
Figure.5.12 Wire Frame View of MSS at Specific Time Intervals of Case 3	90
Figure.5.13 Force Error Occurred During Case 3	91
Figure.5.14 Torque Error Occurred During Case 3	91
Figure.5.15 Position Error with Unconstrained Motion	92
Figure.5.16 Orientation Error with Unconstrained Motion	92
Figure.A.1 A Simple R-R Configuration	103

LIST OF SYMBOLS

a_k	Distance between $A_k O_k$
A	Cross sectional area of the object
A_k	Intersection point of $\bar{u}_3^{(k-1)}$ and $\bar{u}_1^{(k)}$
ARA	Aircraft Research Association
AWT	Ankara Wind Tunnel
c	Cosine trigonometric function
C_D	Drag coefficient
C_A	Axial force coefficient
C_Y	Side force coefficient
C_N	Normal force coefficient
C_{LL}	Rolling moment coefficient
C_M	Pitching moment coefficient
C_{LN}	Yawing moment coefficient
$\hat{C}^{(a,b)}$	Direction cosine matrix from the reference frame $\mathfrak{S}^{(b)}$ to reference frame $\mathfrak{S}^{(a)}$
d	Diameter of the object
DNW	German Dutch Wind Tunnels
DOF	Degree of Freedom
${}^i \underline{f}_i$	Force exerted on link i by link $i-1$
${}^i \underline{E}_i$	Inertial force on the center of mass of link i in frame i

F_D	Desired force/torque vector
$F_{DESIRED}$	Force and torque vector of 6 components whose third component is the compensation for the weight of the model.
$F_{EXTERNAL}$	External force applied to object carried by the manipulator
F_{SENSOR}	Forcing on the end-effector by the object
g	Gravity
G_C	Controller gain
HST	High Speed Tunnel of DNW
i	Link index
I	Identity matrix
I_s	Diagonal selection matrix
J_i	Moment of inertia of link i
J	Jacobian Matrix
J^T	Transpose of the Jacobian matrix
J^{-1}	Inverse of the Jacobian matrix
${}^0J(\Theta)$	Manipulator Jacobian for earth-fixed frame (frame 0)
K_p	Proportional Controller Gain
K_i	Integral Controller Gain
K_d	Derivative Controller Gain
L	Rolling moment
LLF	Large-Low-Speed Facility of DNW
m_i	Mass of the link i
M	Pitching moment
M	Mach number
MSS	Model support system
N	Yawing moment
iN_i	Inertial moment on center of mass of the link i in frame i

${}^i \underline{n}_i$	Moment exerted on link i by link $i-1$
NWB	Low-Speed Wind Tunnel Braunschweig of DNW
O_k	Intersection point of $\bar{u}_3^{(k)}$ and $\bar{u}_1^{(k)}$
PI	Proportional Integral Controller
PD	Proportional Derivative Controller
PID	Proportional Integral Derivative Controller
\underline{Q}_i	Force or torque exerted by the actuator at joint i
\dot{q}_{i+1}	Rate of change of joint variable
$\bar{r}_{ab}^{(0)}$	Vector from <i>the tip point of link a</i> to <i>the tip point of link b</i> expressed in frame 0
s	sine trigonometric function
s_k	Distance between $\bar{u}_1^{(k-1)}$ and $\bar{u}_1^{(k)}$ on $\bar{u}_3^{(k-1)}$
\underline{s}_i	Position vector of the center of mass of link i with respect to frame i
TSP	Technical Specification of Purchase
TSR	Two sting rig
$\bar{u}_3^{(k)}$	Unit vector long the axis of joint $(k+1)$
$\bar{u}_1^{(k)}$	Unit vector along the common normal from $\bar{u}_3^{(k-1)}$ to $\bar{u}_3^{(k)}$
${}^{i+1} \underline{w}_i$	Angular velocity of frame i in frame $i+1$
${}^{i+1} \dot{\underline{w}}_i$	Angular acceleration of frame i in frame $i+1$
${}^{i+1} \underline{v}_i$	Linear velocity of frame i in frame $i+1$
${}^{i+1} \dot{\underline{v}}_i$	Linear acceleration of frame i in frame $i+1$
${}^i \dot{\underline{v}}_i$	Linear acceleration of the center of mass of link i in frame i
V	Air velocity
x, \dot{x}, \ddot{x}	Vectors of joint variables and their derivatives
X_D	Desired position vector in the task space

\underline{z}_0	Unit vector in z-direction
θ	Pitch Angle of MSS end-effector
Q_d	Dynamic pressure
θ_k	Angle from $\bar{u}_1^{(k-1)}$ to $\bar{u}_1^{(k)}$ about $\bar{u}_3^{(k-1)}$ (Rotation angle)
θ_1	First Joint Angle of MSS
θ_2	Second Joint Angle of MSS
θ_4	Fourth Joint Angle of MSS
α_k	Angle from $\bar{u}_3^{(k-1)}$ to $\bar{u}_3^{(k)}$ about $\bar{u}_1^{(k)}$ (Twist angle)
Θ	Vector of joint angles of the manipulator
0v	Vector of Cartesian velocities in the earth-fixed frame (frame 0)
ΔF	Force error in Cartesian Space
Δf	Force error in Joint Space
τ_{CONT}	Vector of torque input to the joints associated with the force controller
$\tau_{\text{INV DYN}}$	Vector of torque input to the joints associated with the inverse dynamics
τ_{ACTUATOR}	Vector of total torque demand
ρ	Air density
Ψ	Rotation angle about the z-axis
Θ	Rotation angle about the y-axis
ϕ	Rotation angle about the x-axis

CHAPTER I

INTRODUCTION

1.1 WIND TUNNEL TESTING

Our planet, Earth, is covered by the atmosphere where air flow from gentle breezes to storms occurs. Mankind has benefited from the naturally produced motions due to the winds since before the earliest existence recorded in history and always was jealous of the flying birds. As an obvious result of the air's effect on the life of mankind, s/he began to investigate the secrets of the air flow resulting in the concept of aerodynamics.

Today the final exterior design of products which are subject to air flow is determined by aerodynamic considerations. The aerodynamic coefficients which relate the flow parameters to the aerodynamic forcing on a solid body are the tools to evaluate an aerodynamic design. The most common four methods for the aerodynamic coefficient estimation are computational fluid dynamics, theoretical and empirical fluid dynamics, experimental flight mechanics, and experimental aerodynamics [1].

Computational fluid dynamics is a widely used as a predictive tool with the disadvantages such as accuracy, computational cost, and speed. In theoretical and empirical fluid dynamics, the quick estimations of the coefficients are made

based on databases of experimental and theoretical data by software packages like Missile DATCOM[®]. In experimental flight mechanics, aeroballistic range experiments are held by scaled down models in free-flight. In experimental flight mechanics, the workload to extract aerodynamic coefficients is the main disadvantage [1].

In experimental aerodynamics, wind tunnels are used to test models of aircrafts, missiles, fuel tanks of aircrafts, ground vehicles, and even sportsmen. In the safe environment of wind tunnels, the engineers can obtain important aerodynamic data about the interaction of the object with the blowing wind.

During the wind tunnel tests, models are placed in the test sections of tunnels and instrumented to obtain the test data under the effect of blowing wind in the tunnel. In order this data to be meaningful, they have to be revised with similarity parameters like Mach number, Reynolds number, and Froude number. By this method, the test data match real conditions.

The two basic types of wind tunnels are open circuit and closed circuit. The air flowing through an open circuit tunnel follows a straight path from the entrance to an exhaust. On the other hand, the air flowing through a closed circuit wind tunnel re-circulates continuously with little or no exchange of air with the exterior.

1.2 ANKARA WIND TUNNEL

Ankara Wind Tunnel (AWT) is a low speed ($M < 0.3$) and closed circuit wind tunnel constructed in late 1940's. The dimensions of the wooden test section are 2.44 m x 3.05 m x 6.10 m (8 ft x 10 ft x 20 ft) in height, width, and length,

respectively. The side view of the test section can be seen in Figure.1.1. The maximum speed of the wind in the tunnel is 100 m/s and the air flow is supplied by a DC electric motor driven fan.

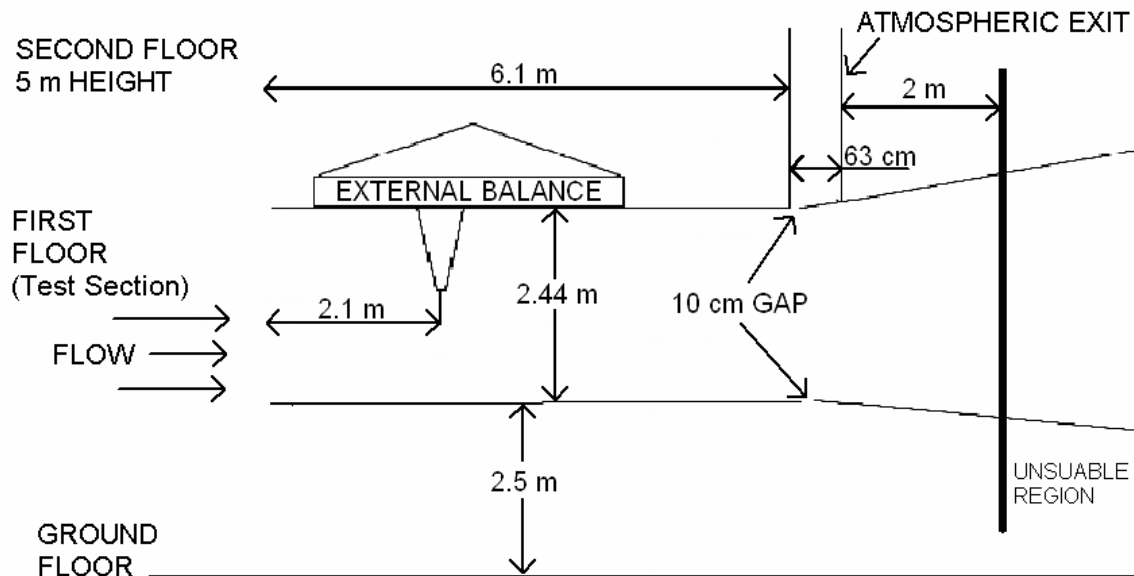


Figure.1.1 Side View Diagram of AWT Test Section [2]

AWT has a pyramidal external balance system at the upper part of the test section to carry the forces and moments on the model, outside the test section to be measured there.

There are turntables on the floor and ceiling of the test section exactly under the external balance to give side-slip (yaw) angle to the model. In addition, the model has a degree of freedom in pitch that is actuated with a ball screw attached to the back part of the model. Therefore, the total degree of freedom of the model is two. The current model handling system of AWT is seen in Figure.1.2 Currently; AWT can manage aerodynamic performance tests and

external load effect tests for aviation industry, performance analysis for automotive industry, and some other tests related to wind energy, civil, and environmental engineering fields.

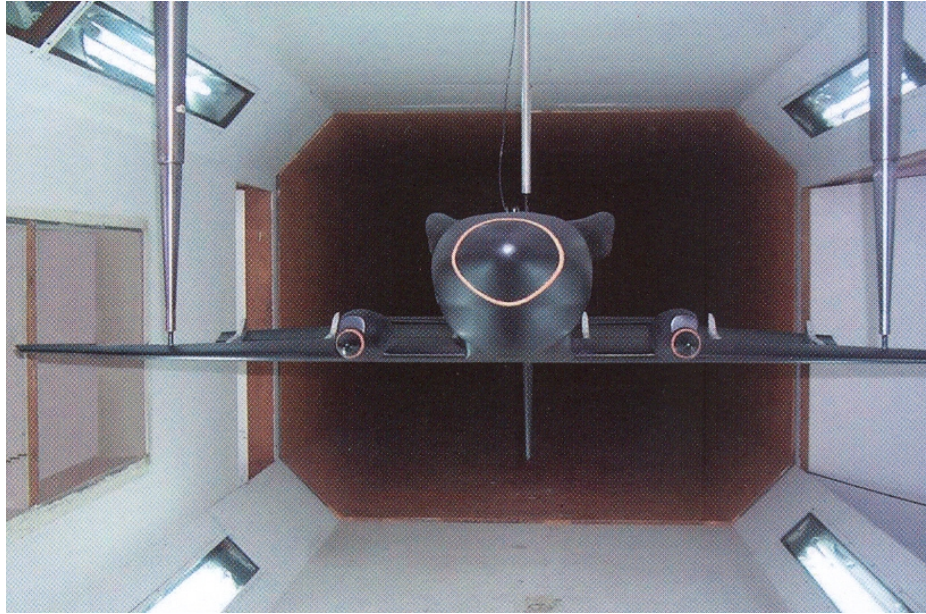


Figure.1.2 Current Model Handling System in AWT [2]

1.3 MODEL SUPPORT SYSTEMS

Model support systems (MSS) are mechanisms that are used to position a model in wind tunnels precisely. MSS are instrumented with internal balances which are special equipment to obtain the aerodynamic and gravitational loading on the model and send the obtained force data by electrical means. The models are assembled to the MSS via the mechanical interface formed by these balances.

In wind tunnels, apart from the testing of a single object's interaction with the flow, the interaction of two objects in the flow can be tested, like the tests in which the release characteristics of external objects like fuel tanks, stores, bombs under an aircraft are observed. This problem is named as the store separation. By the help of these store separation tests, poor releases (wild pitching or hitting the airplane with the store) resulting in loss of human life and air vehicles can be prevented. Figure.1.3 shows a poor release of an ammunition breaking the fuel tank of the aircraft.



Figure.1.3 A Poor Release Damaging the Aircraft Components

Two different techniques are used in store separation tests: (i) free dropping of the store, and (ii) utilization of the store MMS.

In free drop tests, drop data can be obtained in the form of high speed video or multiple-flash pictures. Two examples of multiple-flash stop motion recordings are shown in Figure.1.4 [3] and Figure.1.5 [4].

The free drop technique is advantageous from the point of view that there is no interference of the MSS to the store model. However, there are some inferior points of the free drop technique when compared to the MSS technique. One of the disadvantages is that the manufacturing of the store model is an expensive and a complex process. In addition to that, the breaking of the model might cause a serious damage to the wind tunnel test section and the propellers. On the other hand, an attentive removal of the remains is required after each test. A catch net solution to minimize the damage to the model and the tunnel results in another problem as it causes drag and disturbance to the air flow. Another disadvantage of the drop tests is the difficulty in scaling the model. When the model is scaled down, the gravitational, inertial and aerodynamic forces on the model are affected by different ratios, which arises a model matching problem [3].

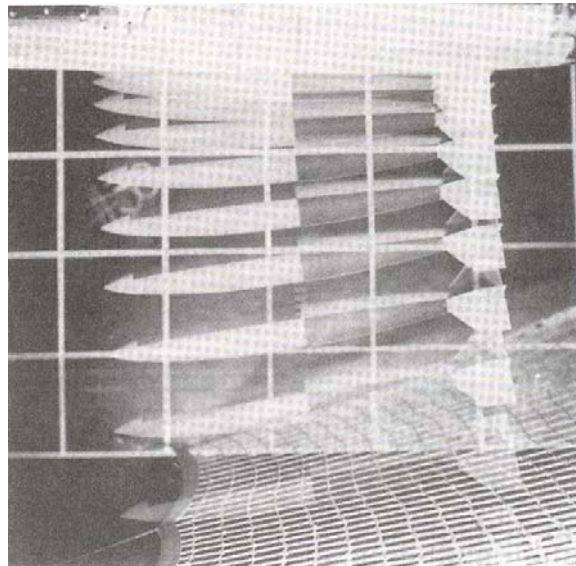


Figure.1.4 Multiple-Flash Drop Test Photograph (with Catch-Net) [3]

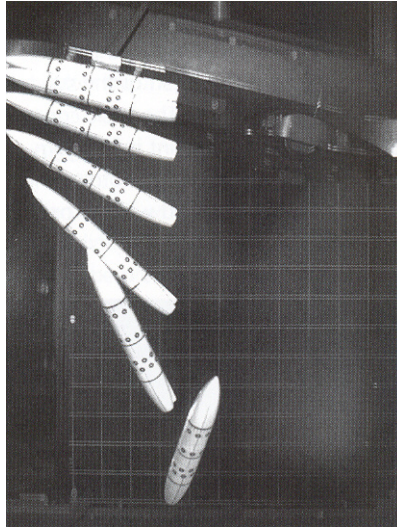


Figure.1.5 Multiple-Flash Drop Test Photograph (without Catch-Net) [4]

The utilization of an MSS in store separation tests is a complicated approach. By using the MSS, the relative motion between the aircraft model and store model can be simulated according to the force measurements on the internal balance assembled between the model and the MSS. The behavior of a store under an aircraft wing observed with these tests can be used to achieve a safe separation.

Although the use of MSS is an expensive investment for a wind tunnel, it allows the engineers to perform their tests faster since there is no need to stop the test in order to re-position the model manually. The use of MSS eliminates the model-matching problem since the force data obtained from the internal balance can be modified for similarity aspects. Another advantage of the MSS is its relatively small disturbing effect on the flow, since there is no need for a catch-net decreasing the quality of the flow in the test section.

1.4 AIM OF THE STUDY

The AWT, as the only big sized wind tunnel of Turkey, requires some additional modernization in order to be a test facility satisfactorily meeting the demands of the 21st century. The model support concept currently used in the AWT is a rather old 2-DOF system and it requires an enhancement to increase the test capabilities. With a new MSS, the AWT should be capable of performing wind tunnel separation tests, to certify the safety of genuine ammunitions, which military standards insist on before flight tests.

The aim of this study is to propose a mechanical design and control algorithm for a model support system for the AWT. For this purpose, a conceptual design of the MSS and its detailed model are needed for the controller design whose performance is to be tested by computer simulations. The results of this study are also expected to establish a base work for a model support system for a high-speed wind tunnel.

1.5 SCOPE OF THE STUDY

To form a basic understanding of the concept in this introduction chapter, it is necessary to go through the concept of aerodynamic testing using wind tunnels. AWT is also introduced and the benefits of using Model Support Systems for the wind tunnel tests are discussed.

In Chapter 2, some similar systems assembled in wind tunnels are covered with their positioning capabilities. In this chapter, the store separation test methods used with these model support systems are also introduced. Finally, a literature survey on position/force control algorithms is summarized.

In Chapter 3, the conceptual design of the MSS for AWT is introduced after the design specifications are clarified. Forward kinematics and inverse dynamics of the proposed system are formulated.

In Chapter 4, a control approach is proposed and the preliminary work held with a double pendulum in MATLAB[®] Simulink environment is discussed in order to validate the effectiveness of the proposed approach. The implementation of the proposed and validated approach to MSS is explained.

Chapter 5 is devoted to the simulations held in MATLAB[®] Simulink environment. The geometry of the model missile is introduced; some test cases and results of their simulations are discussed.

In Chapter 6, a review of chapter discussions, concluding remarks and recommendations for future work are presented.

CHAPTER II

LITERATURE SURVEY

As stated in the previous chapter, model support systems are rational solutions for the store separation tests. In addition, these systems can easily be used in tests other than store separation tests for model positioning purposes. In this chapter, some of these model support systems of the wind tunnels constructed in Europe and USA will be introduced. Test methods used in separation tests will be explained and finally some well-known methods of manipulator position and force control will be summarized.

2.1 SIMILAR SYSTEMS

Two Sting Rig of Aircraft Research Association

Two Sting Rig (TSR) has been used since 1979 in the Aircraft Research Association (ARA) 2.74 m x 2.44 m Transonic Wind Tunnel to provide aerodynamic data to be collected in order to examine the release characteristics of stores from various aircraft models.

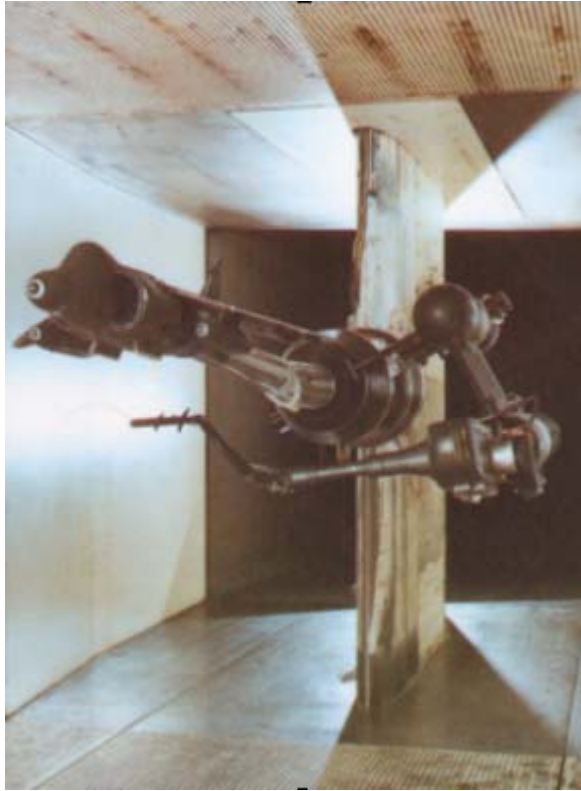


Figure.2.1 Two Sting Rig [5]

TSR, seen in Figure.2.1, is capable of positioning a store with 6-degrees of freedom. The translational motion of TSR is in a cubic space of approximately 750 mm side. All the rotations use hydraulic actuators except roll which uses an electrical stepper motor. The angular ranges are $\pm 29^\circ$ in pitch and $\pm 160^\circ$ in roll and -8° to 15° in yaw. The details of motion capabilities are indicated in Figure.2.2.

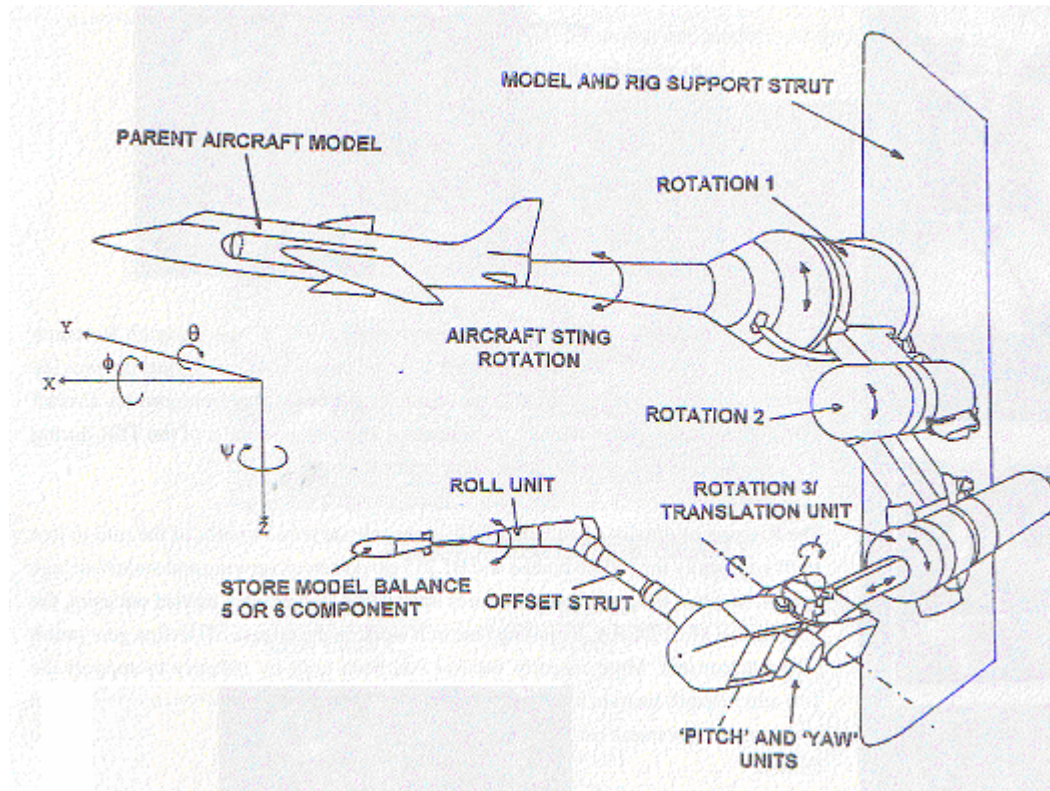


Figure.2.2 Motion Details of TSR [5]

MSS In High Speed Tunnel of German-Dutch Wind Tunnels

The High Speed Tunnel (HST) of German-Dutch Wind Tunnels (DNW) is a closed circuit pressurized wind tunnel with test section dimensions of 2 m to 1.8 m operating in a Mach range of 0.1 to 1.35. A photograph of the model support system in this tunnel can be seen in Figure.2.3 and a schema about the actuation mechanisms of this 4-DOF system is given in Figure.2.4. It should be noticed that this system can not perform store separation tests.



Figure.2.3. MSS in DNW-HST [6]

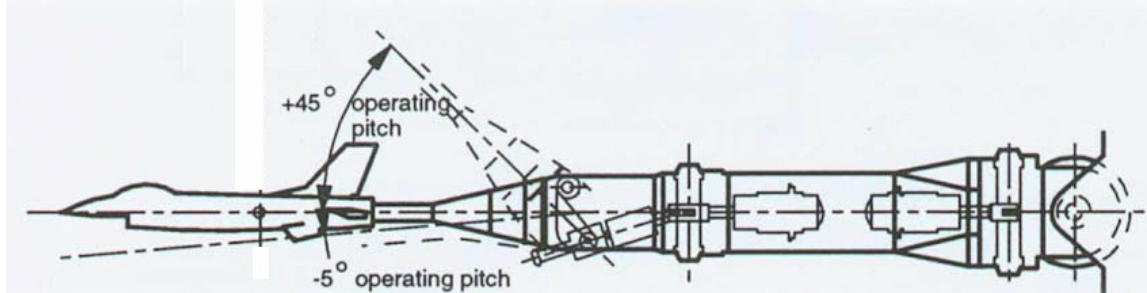


Figure.2.4 Interior Schema of MSS in DNW-HST

A missile support extension seen in Figure.2.5 can be attached to this MSS in order to increase the motion limits and positioning accuracy. The motion limits of this missile model support is $\pm 30^\circ$ in yaw, $\pm 45^\circ$ in pitch and 0° to 370° in roll with a precision less than 0.20° .



Figure.2.5 DNW-HST Missile Support Extension [7]

MSS In Low-Speed Wind Tunnel Braunschweig of DNW

The Low-Speed Wind Tunnel Braunschweig (NWB) of DNW is a closed circuit atmospheric low-speed wind tunnel. It can be operated optionally with a closed, a slotted or an open test section of dimensions 3.25 m x 2.8 m operating in a Mach range of 0 to 0.26.

Although there are more than 6 model handling systems in DNW-NWB, the most interesting one is the one used to determine dynamic derivatives of models in open test section configuration (Figure.2.6). The major difference of this test rig is its actuation mechanism being a Stewart platform. The advantage of using a Stewart platform is the resulting high dynamic capability combined with high constant stiffness over the whole workspace of 1100 mm in flow direction (by additional movement of the system on rails), 300 mm in lateral and 500 mm in vertical.



Figure.2.6 Test Rig in DNW-NWB Using a Stewart Platform [8].

MSS In Large-Low Speed Facility of German-Dutch Wind Tunnels

The Large-Low-Speed Facility (LLF) of DNW is a closed circuit atmospheric low-speed wind tunnel. It can be operated optionally with different test section dimensions of 6 m x 6 m (closed or slotted walls), 8 m x 6 m (closed, slotted or open jet), or 9.5 m x 9.5 m (closed walls). The operating Mach number range in LLF is 0 to 0.44.

The system is designed to withstand large forces and for this reason the system has only two degrees of freedom, having $\pm 60^\circ$ motion range both in yaw and pitch angles. The photographs of this system are given in Figure.2.7 and Figure.2.8.



Figure.2.7 MSS in DNW-LLF during A340-500 Tests [6]



Figure.2.8 MSS in DNW-LLF with A318 Model [4]

2.2 STORE SEPARATION TEST METHODS USING MSS

In literature, there are two common types of store separation test methods using MSS; namely, continuous method and grid method.

In the continuous method, the store is positioned under the aircraft model. At the beginning of the test, MSS gives an initial velocity to the store model. This simulates the separation velocity relative to the aircraft due to the ejector forces. The loads occurring on the store model is measured by the internal balance. These internal balance measurements are then used in computations in order to calculate the next position of the store model for a defined time step. Then MSS takes the store model to the calculated position and then new force data is gathered in the new position while the actuators are locked. By this method, the motion of the store model for specific ejector forces and specific Mach numbers can be examined in the wind tunnel environment.

In the grid method, MSS positions the model in the measurement locations at the desired orientations that are defined in the grid table before the tests. At these grid points, the force and moment data are collected by the internal balance to form a database of forcing versus position and orientation. After the test, this database is used during the calculations of the grid interpolation program to calculate the trajectory of the store in the computer environment.

2.3 POSITION / FORCE CONTROL ALGORITHMS

Considerable effort has been focused on the problem of control of manipulators during the execution of tasks in which the manipulator interacts with the environment. Several methods are proposed for this purpose.

Stiffness Control

By adjusting the stiffness of servos of robot joints, a desired stiffness of the end-effector can be achieved in order to apply the desired force to the environment without losing the control on position [9].

The sensor measurements are used to correct the desired position trajectory in proportion to the inverse stiffness and then the modified position demand is fed to the inner control loops.

Impedance Control

The aim of the impedance control proposed by Hogan [10] is to establish relationship between the end-effector motion and the applied force. For this purpose a position trajectory and a relationship between interaction forces and displacements from the assigned trajectory are given.

The impedance control approach allows closed loop position control in an inertial environment like carrying a payload. This approach is suitable in all tasks in which the end-effector imposes its motion on the environment. In case of a contact with a rigid environment, this approach can react with only open-loop force control capabilities [11].

Admittance Control

Admittance control also uses the relationship between the velocity and the applied force. This approach is mainly the dual of the impedance approach focusing more on the force control.

The admittance control approach exhibits closed-loop force control capabilities when in contact with the environment. This results in the control of interaction forces and makes the approach beneficial in all tasks in which the motion of the end-effector must be guided by the environment [11].

Hybrid Force/Position Control

In this approach the position and force information is combined into one control scheme. The basic idea of this controller is to use a diagonal matrix (seen as I_s in the figure) to select force or position controlled axis as shown in Figure.2.9.

For example, in a surface-tracking example, the normal direction is force controlled and the tangential directions are position controlled. Although it is required to know the normal direction in order to make the decision, this information can be easily obtained from the force measurements.

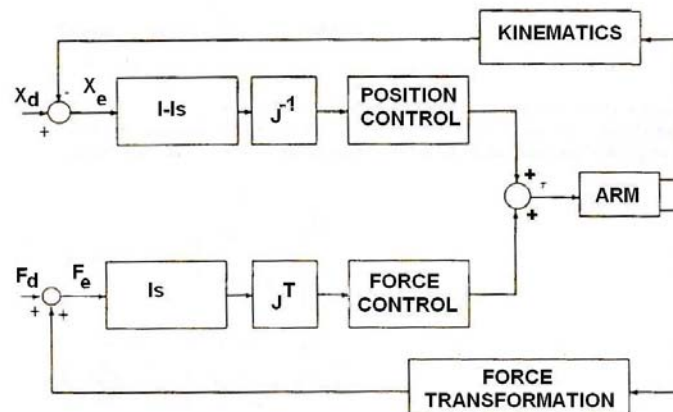


Figure.2.9 The Conceptual Organization of Hybrid Controller [11]

As a disadvantage, the hybrid controller results in a control approach whose structure has to be changed during performing the given task, which requires entering a new environment with different mechanical behavior. The need of a changing control structure to guarantee the effectiveness of the approach requires a detailed knowledge of the manipulator environment. Therefore, it is not possible to perform operations such as self-adjusting or recovery from unexpected impacts where large contact forces may arise [11].

Parallel Control

This method combines the simplicity and robustness of the impedance and admittance control approaches with the ability of controlling both position and force variables as in hybrid control. Since the primary goal is to accommodate the motion to environment constraints, the force controller is dominant to the position controller. The way to provide this dominance is to use a PI force control loop working parallel to a PD position loop [11].

CHAPTER III

CONCEPTUAL DESIGN AND ANALYSIS OF THE MSS

The design of the MSS comprises the identification of the design specifications and the constraints on the defined specifications. The kinematical structure and the type of actuators are determined according to the comparative study of alternative actuation mechanisms for the optimum model support system for the AWT. Although a detailed design of the MSS in technical drawing level is out of scope of this thesis, the conceptual design is taken into consideration carefully trying to foresee the problems that can arise during the later phases of design. In addition, the kinematical analysis is performed and the inverse dynamic equations are constructed.

3.1 DESIGN SPECIFICATIONS

In this section, the design requirements will be clarified for the MSS that is designed in this thesis. The technical specifications for purchasing (TSP) [2] of an MSS prepared by TÜBİTAK-SAGE Aerodynamic Division is the main reference used for this purpose.

In order to simulate the relative motion between the aircraft and store model completely, the proposed MSS should be capable of performing motion in all axes which requires the use of a 6-DOF manipulator.

TSP defines a working volume given in Table.3.1. The corresponding model positions are specified to occur in all combinations and available in all model positions. Since the MSS will never position the model at maximum locations in all combinations, the described cubic volume is considered to be unreasonable. Therefore, the requirement defined about the working volume is not taken into account. However, it is aimed to have the largest possible working volume.

Table.3.1 The Working Volume Defined in TSP.

Required Movement	Properties
Pitch	-5° to +40°
Yaw	-40° to +40°
Roll	± 180°
Movement Range in Flow Direction	From 1.75 m to 3.5 m from the beginning of the test section
Movement Range in Lateral Direction	±1.4 m from the center line of the test section
Movement Range in Vertical Direction	From the floor of the test section to 2.2 m height

Another important requirement of the MSS is related with the aerodynamics of the test section. TSP does not allow the blockage ratio, which is defined as the ratio of cross sectional area of the MSS in the wind direction to the test section cross section, to exceed 10%.

The external loading that MSS should withstand is tabulated in TSP. These values are given in Table.3.2.

Table.3.2 External Loading Defined by the TSP

Load Types	Loading for the Aircraft Model	Loading for the Store Model
Weight of the Model	1471 N	245 N
Force in x direction	±375 N	±80 N
Force in y direction	±1000 N	±225 N
Force in z direction	±1000 N	±225 N
Rolling Moment	±150 N.m	±15 N.m
Pitching Moment	±150 N.m	±15 N.m
Yawing Moment	±100 N.m	±10 N.m

3.2 COORDINATE FRAMES

In order to develop the equations of motion, there should be a non-rotating and non-accelerating inertial frame for which the Newton's laws are valid. In this thesis, the inertial frame $Oxyz$ is taken as the earth-fixed reference frame $\mathfrak{F}^{(a)}$ attached to the test section floor seen in Figure.3.1. In Figure.3.1, the body-fixed frame $\mathfrak{F}^{(b)}$ is also shown as $O_b x_b y_b z_b$.

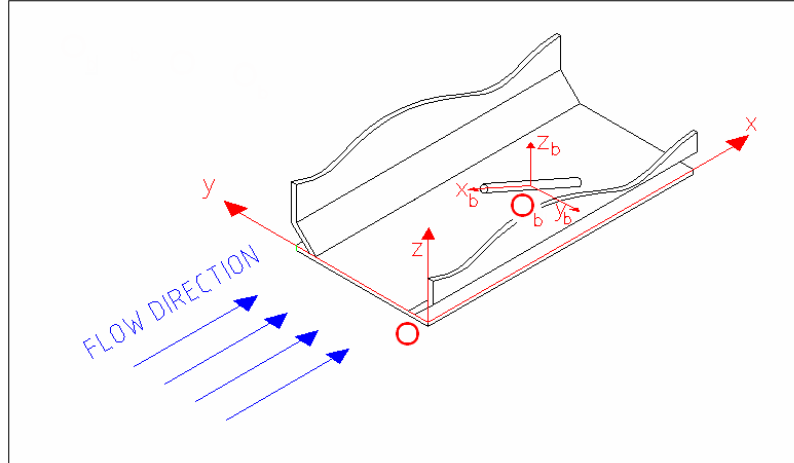


Figure.3.1 Earth-Fixed and Body-Fixed Coordinate Frames

An arbitrary physical vector can be expressed as different column vectors in different reference frames such as $\bar{r}^{(a)}$ in reference frame $\mathfrak{S}^{(a)}$ and $\bar{r}^{(b)}$ in reference frame $\mathfrak{S}^{(b)}$. The transformation between these two column vectors actually represented the same physical can be achieved by using an orthogonal 3x3 transformation matrix called as the direction cosine matrix $\hat{C}^{(a,b)}$ representing a transformation from the reference frame $\mathfrak{S}^{(b)}$ to reference frame $\mathfrak{S}^{(a)}$ and defined as

$$\hat{C}^{(a,b)} = \begin{bmatrix} c(\theta) \cdot c(\psi) & -c(\theta) \cdot c(\psi) & s(\theta) \\ c(\theta) \cdot s(\psi) + s(\phi) \cdot s(\theta) \cdot c(\psi) & c(\phi) \cdot c(\psi) - s(\phi) \cdot s(\theta) \cdot s(\psi) & -s(\phi) \cdot c(\theta) \\ s(\phi) \cdot s\psi - c(\phi) \cdot s(\theta) \cdot c(\psi) & s(\phi) \cdot c(\psi) + c(\phi) \cdot s(\theta) \cdot s(\psi) & c(\phi) \cdot c(\theta) \end{bmatrix} \quad (3.1)$$

where

- c : cosine trigonometric function
- s : sine trigonometric function
- Ψ : rotation angle about the z-axis in reference frame a

- Θ : rotation angle about the y-axis in reference frame a
- ϕ : rotation angle about the x-axis in reference frame a

Using this direction cosine matrix, the transformation can be achieved by

$$\begin{bmatrix} r_x^{(a)} \\ r_y^{(a)} \\ r_z^{(a)} \end{bmatrix} = \hat{C}^{(a,b)} \cdot \begin{bmatrix} r_x^{(b)} \\ r_y^{(b)} \\ r_z^{(b)} \end{bmatrix} \quad (3.2)$$

3.3 THE R-R-P-R-R-R CONFIGURATION

The three alternative configurations to position the model in x, y, and z axes are

- Three prismatic joints(P-P-P), seen in Figure.3.2 and Figure.3.3
- One revolute and two prismatic joints (R-P-P), seen in Figure.3.4
- Two revolute and a prismatic joints (R-R-P), seen in Figure.3.5

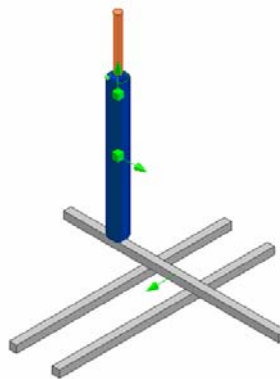


Figure.3.2 Three Prismatic Joint Configuration in x-y-z Kinematic Order

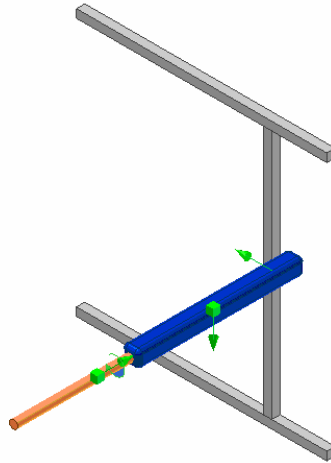


Figure.3.3 Three Prismatic Joint Configuration in y-z-x Kinematic Order

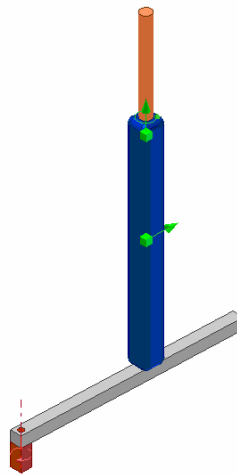


Figure.3.4 One Revolute and Two Prismatic Joint Configuration

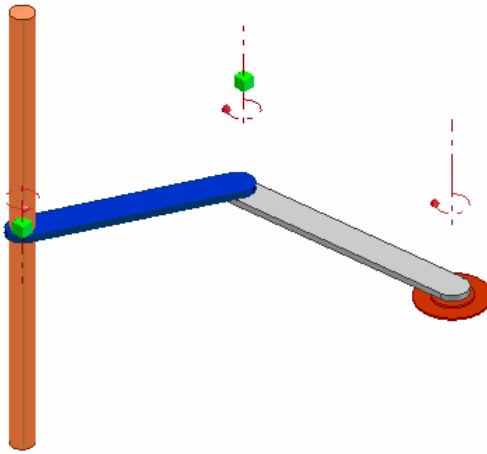


Figure.3.5 Two Revolute and One Prismatic Joint Configuration

At the evaluation stage of these alternative configurations, the most important design aspects are selected as the geometrical, kinematical, and aerodynamic applicability. The aspects like strength, weight, and cost are not easy to foresee at this stage of the design.

Among these alternatives two revolute and one prismatic joint (R-R-P) configuration is selected. The main advantage of this configuration is the opening left for the motion of the mechanism, can easily be closed by the mechanism itself with a mechanical design as seen in Figure.3.6.

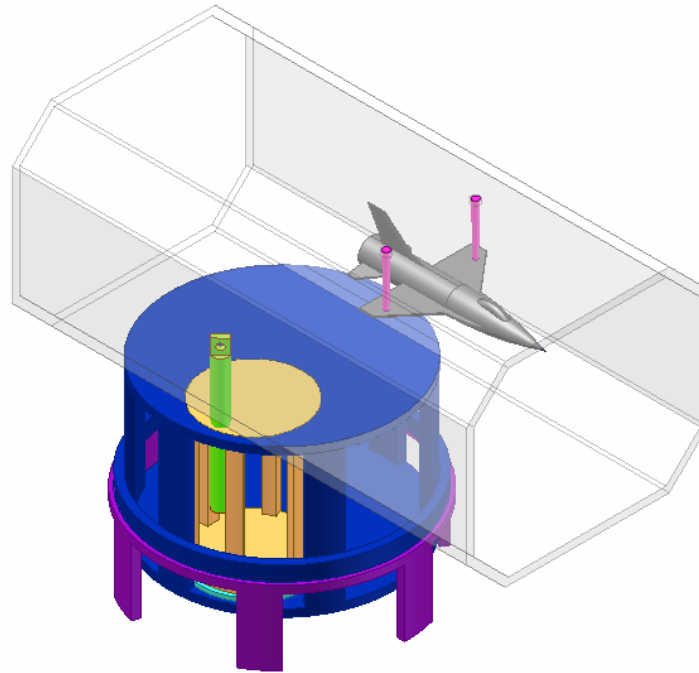


Figure.3.6 The Two Revolute One Prismatic Joint Configuration in the Tunnel

The actuators and the structure of the joints can be located outside of the test section resulting in a smaller blockage rate. Additionally, since the physical joints are located under the test section, it is also possible to increase the rigidity in those axes as much as needed. The two main disadvantages of this configuration are as follows: (i) The mechanism is heavier compared to other configurations and (ii) it should be constructed at the ground floor of the test section of the AWT.

After deciding on the translational positioning mechanism, the mechanisms related to the orientation of the model are determined. Due to the two revolute joints, the yaw angle is affected with the position of the model so it must be corrected. For this purpose, a revolute joint is placed after the prismatic joint.

The actuator of the joint is observed to be placed outside the test section so that it does not affect the flow.

The remaining degrees of freedom in pitch and roll motions are unavoidably actuated by the systems located in the test section. The kinematic sequence of these joints is decided by the locations of their actuators. The conceptual design of this compact pitch and roll motion system is held by considering the blockage rate and finally the pitch-roll sequence seen in Figure.3.7 is selected since the pitch actuator can be hidden at the back of the structure and the relatively small roll actuator can be located in the sting.

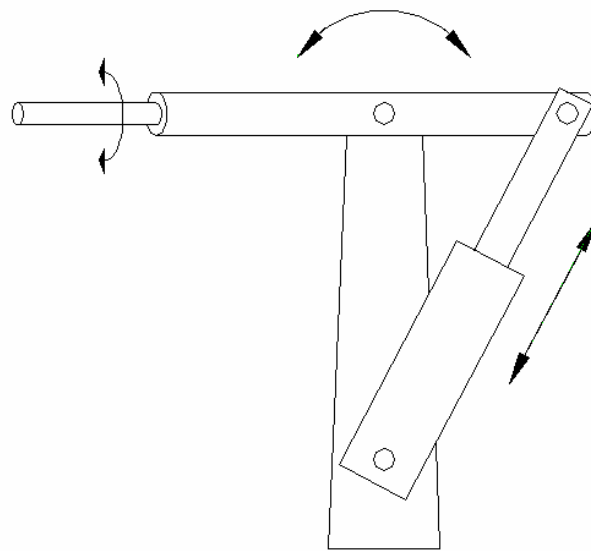


Figure.3.7 Actuating the Degrees of Freedom in the Test Section

So in the resulting configuration seen in Figure.3.8, the translational movement in x and y directions will be supplied by two consecutive revolute joints about

vertical axis. The third joint, which is the prismatic one, will allow motion in the z direction. The fourth revolute joint with a vertical axis is to control the yaw angle. The fifth revolute joint will allow the pitching motion and finally the last revolute joint will give the mechanism a degree of freedom in the roll.

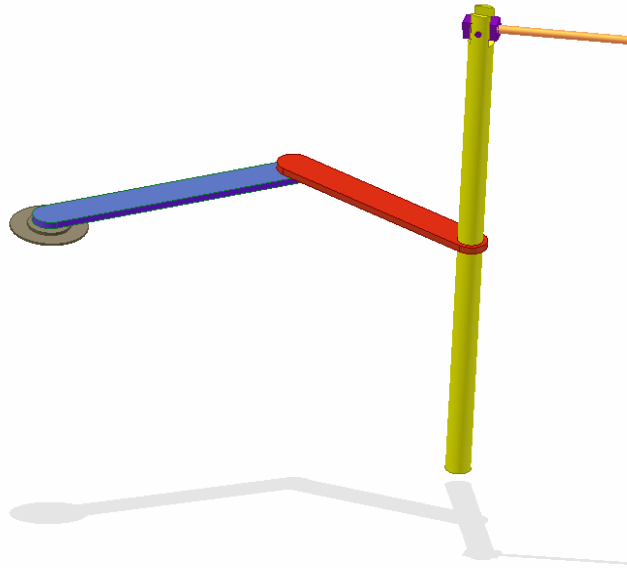


Figure.3.8 R-R-P-R-R-R Configuration

3.4 CONCEPTUAL DESIGN

Translation in x and y Axes

The first constraint while deciding the parameters of the first two links is that the mechanism should be capable of positioning the model in the workspace described. Also the workspace should not contain singular points of the mechanism where the manipulator's Jacobian matrix is not invertible. The singularity analysis for two consecutive revolute joints (R-R) can be seen in

Appendix.A. During the motion around a singular point or the kinematical boundary, actuator saturation is observed due to a tremendous increase in required torques, resulting in deviation from the desired trajectory. The origin of the mechanism, which is one of the many possible singular points, is placed outside of the workspace to avoid this problem, as seen in Figure.3.9. The intended workspace is placed off-centric covering the area enclosed between [1.0 m, 3.4 m] on x-axis and [1.0 m, 2.6 m] on y-axis.

So considering different possibilities on the geometry, the final mechanism is decided to have the origin at (2.2 m, 0, 0) in the earth fixed frame defined in Section.3.2. After locating the origin at the defined position and taking the link lengths as 1750 mm and 1500 mm, the obtained workspace is sufficient.

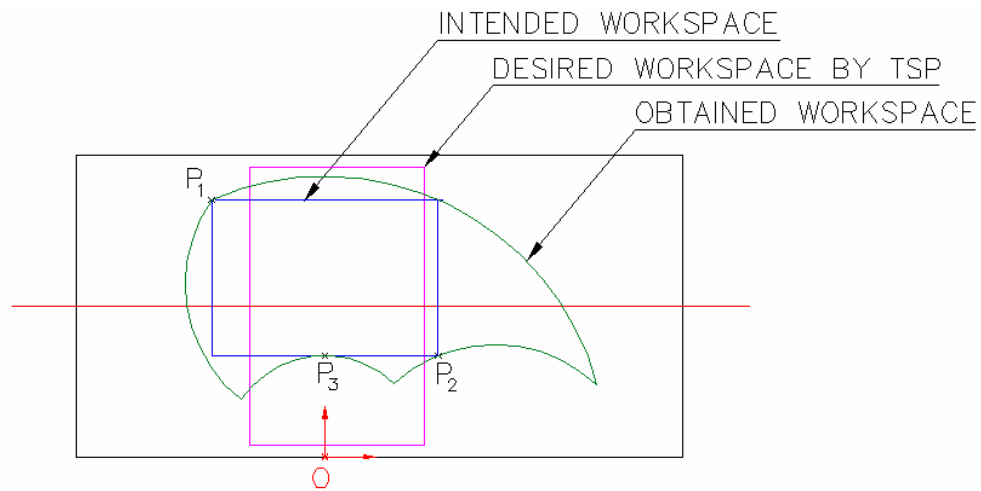


Figure.3.9 Workspace in x-y Plane

The points P_1 , P_2 and P_3 shown on Figure.3.9 are the corresponding maxima locations for the first two link angles. The information about these points are given in Table.3.3.

Table.3.3. Information about the Points Given in Figure.3.9

	$x_{(0)}$ (mm)	$y_{(0)}$ (mm)	θ_1 (deg)	θ_2 (deg)
P ₁	-1140	2596	86.8	58.7
P ₂	1140	1022	-12	124.4
P ₃	0	1022	31.3	144.3

So the intervals of θ_1 and θ_2 are obtained as

$$-12^\circ < \theta_1 < 87^\circ \quad (3.3)$$

$$58^\circ < \theta_2 < 145^\circ \quad (3.4)$$

Since these first two joints require relatively large torques, the joints are decided to be actuated by linear actuators. To avoid bending problems in the actuators, the maximum strokes of the linear actuators are limited to 500 mm. To minimize the required forces throughout the operating range of these revolute joints, the axes of the linear actuators are taken perpendicular to the moment arm when the link is in the middle of the operating range. With these constraints, the connection locations of the tip and the base points of two linear actuators on the links are obtained by simple geometric calculations. In Figure.3.10 the conceptual design of the first two links can be seen.

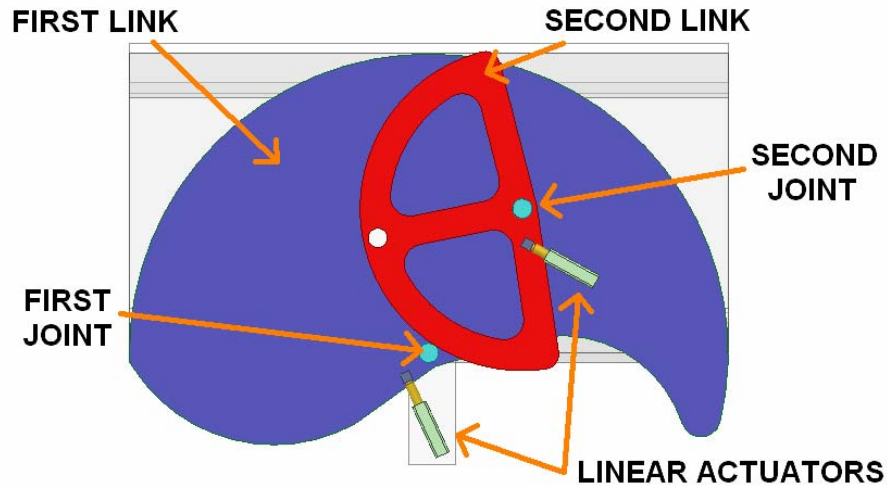


Figure.3.10. Bottom View of the Test Section with the First Two Links

In order to allow the motion and keep the test section closed, the interface of the mechanism with the test section is critical. For this purpose, the floor of the test section is opened out, determining the workspace. Since the geometry of the opening is taken directly from the arcs of the mechanism, the resulting geometry of the first link looks like snail shell at the conceptual design stage. Also to allow relative rotation between first link and the second, a circular slot is left blank on the first link and the second link is designed as a semi-circle to close the slot on the first link. Figure.3.11 shows the geometry of the opening on the test section floor and the geometry of the links.

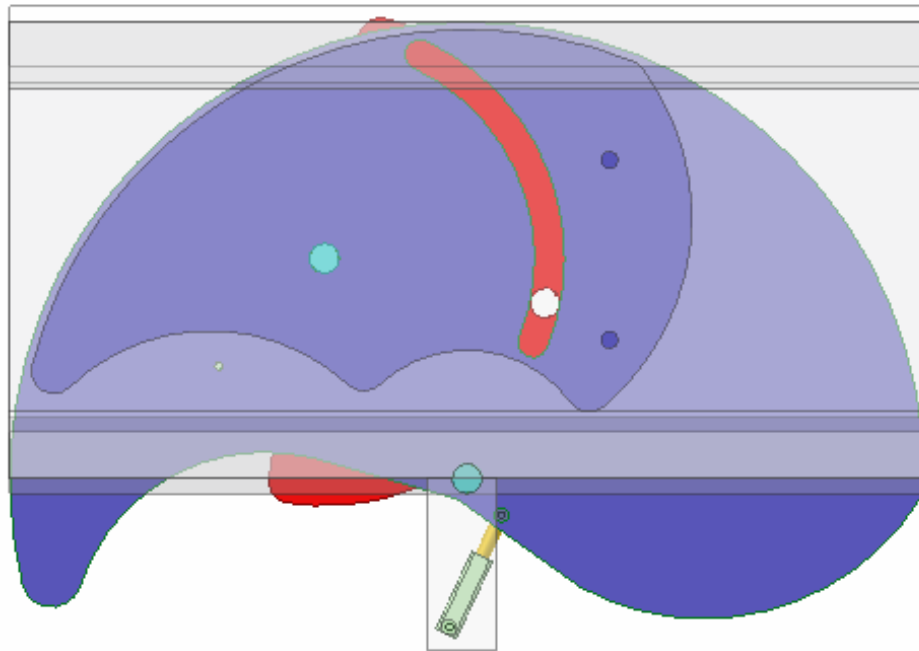


Figure.3.11. Top View of the Test Section with the First Two Links

Translation in z-Axis

In order to actuate and support the third link going into the test section, there is a structure going down at the bottom part of the second link as seen in Figure.3.12.

A prismatic joint is preferred to satisfy the z-axis positional requirements. A rotary actuator is selected since a linear actuator's dead length decreases the stroke of this joint. A ball screw is used to convert the rotary motion to linear and linear guides are assembled on the second link to support the z-axis movement.

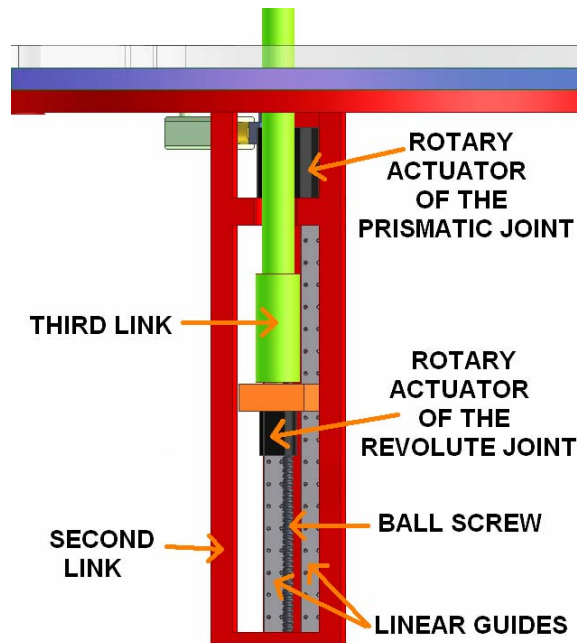


Figure.3.12 Side View of the Prismatic and Fourth Revolute Joint

The limits of z-axis motion are strongly dependent on physical constraints of the wind tunnel and the mechanical design of the MSS. At this conceptual design stage from the constructed solid model seen in Figure.3.13, the limits of this axis are observed to be as

$$0 < z < 1540 \text{ mm} \quad (3.5)$$

The third link is the first link that is located in the test section. For that reason its surface geometry is also important. In this thesis, it is assumed to have a circular cross section but a suitable NACA geometry can be covered around this link to increase its aerodynamic appropriateness.

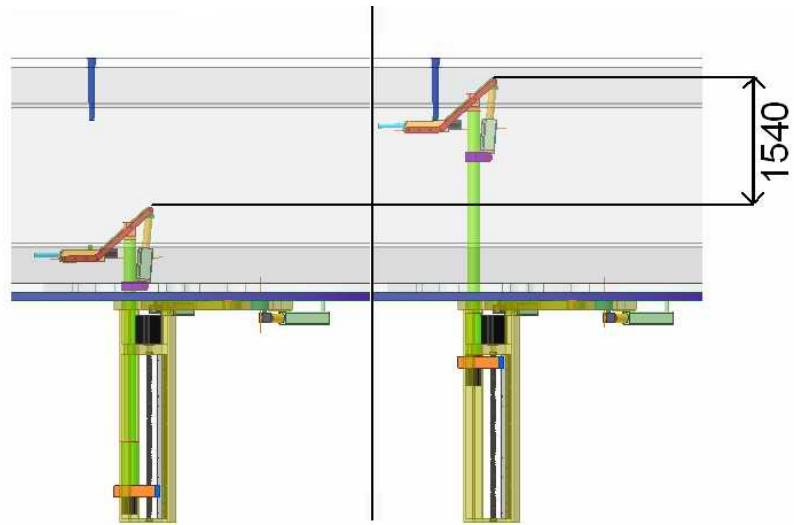


Figure.3.13 Limits of the Motion in z-axis

Rotation around z-Axis (Yaw)

As stated in Table.3.1 the required motion in yaw angle is $\pm 40^\circ$ in the flow direction. However, when the earth-fixed coordinate system is considered for the MSS, the yaw angle requirement is

$$140^\circ < \psi < 220^\circ \quad (3.6)$$

Since the fourth revolute joint, which is acting on the yaw angle, is also responsible to correct the orientation errors caused by the x-y motion on the yaw angle, the overall span of this joint should be greater. The θ_4 span is found by the formulation:

$$\psi = \theta_1 + \theta_2 + \theta_4 \quad (3.7)$$

$$\theta_{4,MAX} = \psi_{MAX} - \theta_{1,MIN} - \theta_{2,MIN} \quad (3.8)$$

$$\theta_{4,MIN} = \psi_{MIN} - \theta_{1,MAX} - \theta_{2,MAX} \quad (3.9)$$

By using equations (3.3), (3.4), (3.8), and (3.9), the span of the joint is determined as;

$$-92^\circ < \theta_4 < 174^\circ \quad (3.10)$$

A rotary actuator is used to drive this motion. After the torque requirements are determined, the output torque of the actuator will be increased with proper transmission elements.

Rotation around y-Axis (Pitch)

The actuator of this joint has to be located in the test section of the wind tunnel. For that reason while determining the actuation type, the aerodynamic aspects are considered. In case of a rotary actuator, unavoidably the actuator or the transmission system would create a disturbance on the flow. Because of that a linear actuator of stroke 200 mm, that is located behind the main structure of the MSS, is preferred to maintain the required pitch angle motion of

$$-5^\circ < \theta < 40^\circ$$

(3.11)

The effect of this actuator on the flow increases with the increasing yaw angles. However, at small yaw angles, its effect on the blockage rate is negligible. The assembly can be seen in Figure.3.14.

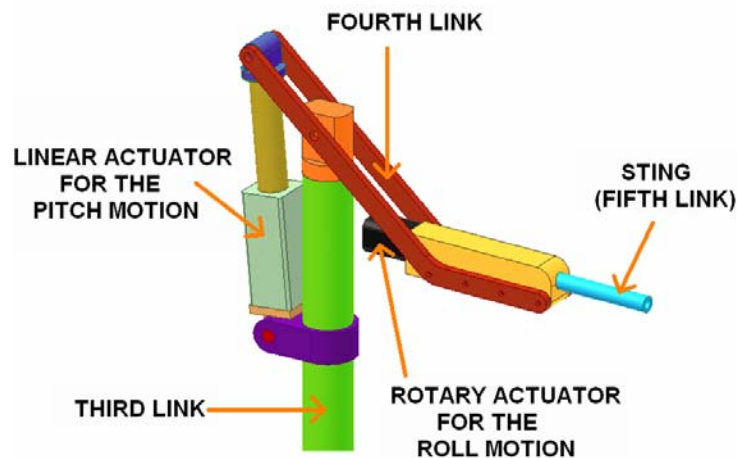


Figure.3.14. Last Two Links of the MSS

The main function of the fourth link is to keep the model away from the disturbed airflow due to MSS by making an offset distance between model and the MSS by two parallel arms. These two parallel arms providing increased rigidity in the test section is an advantage. Also the effect of this link on the flow will affect the tests much more than the others, for that reason exterior surface of the end part of this link, where the roll actuator is assembled, can be designed for better aerodynamic performance.

Rotation around x-Axis (Roll)

The sting, which is the final link of the manipulator, will carry the internal balance to collect the force data on the model and to form a mechanical interface with the model. The sting will be actuated directly to give the roll angle to the model as seen in Figure.3.14

3.5 FORWARD KINEMATICS OF THE MSS

The forward kinematics of a manipulator is the derivation of the general form of the transformation relating the frames attached to each link to the neighboring ones. Then these individual transformations are used to calculate the required variables of position, velocity, or acceleration which are needed in determining the dynamics of the manipulator.

The first step in forward kinematics study is to assign a coordinate frame to each link. The frames are assigned with the notation developed by Denavit and Hartenberg [13]. The frames attached to each link of MSS with the convention explained below can be seen in Figure.3.15.

According to definitions of Denavit and Hartenberg [14];

- $\bar{u}_3^{(k)}$: unit vector long the axis of joint (k+1)
- $\bar{u}_1^{(k)}$: unit vector along the common normal from $\bar{u}_3^{(k-1)}$ to $\bar{u}_3^{(k)}$
(If these vectors intersect, the direction is arbitrary)
- O_k : intersection point of $\bar{u}_3^{(k)}$ and $\bar{u}_1^{(k)}$
- A_k : intersection point of $\bar{u}_3^{(k-1)}$ and $\bar{u}_1^{(k)}$

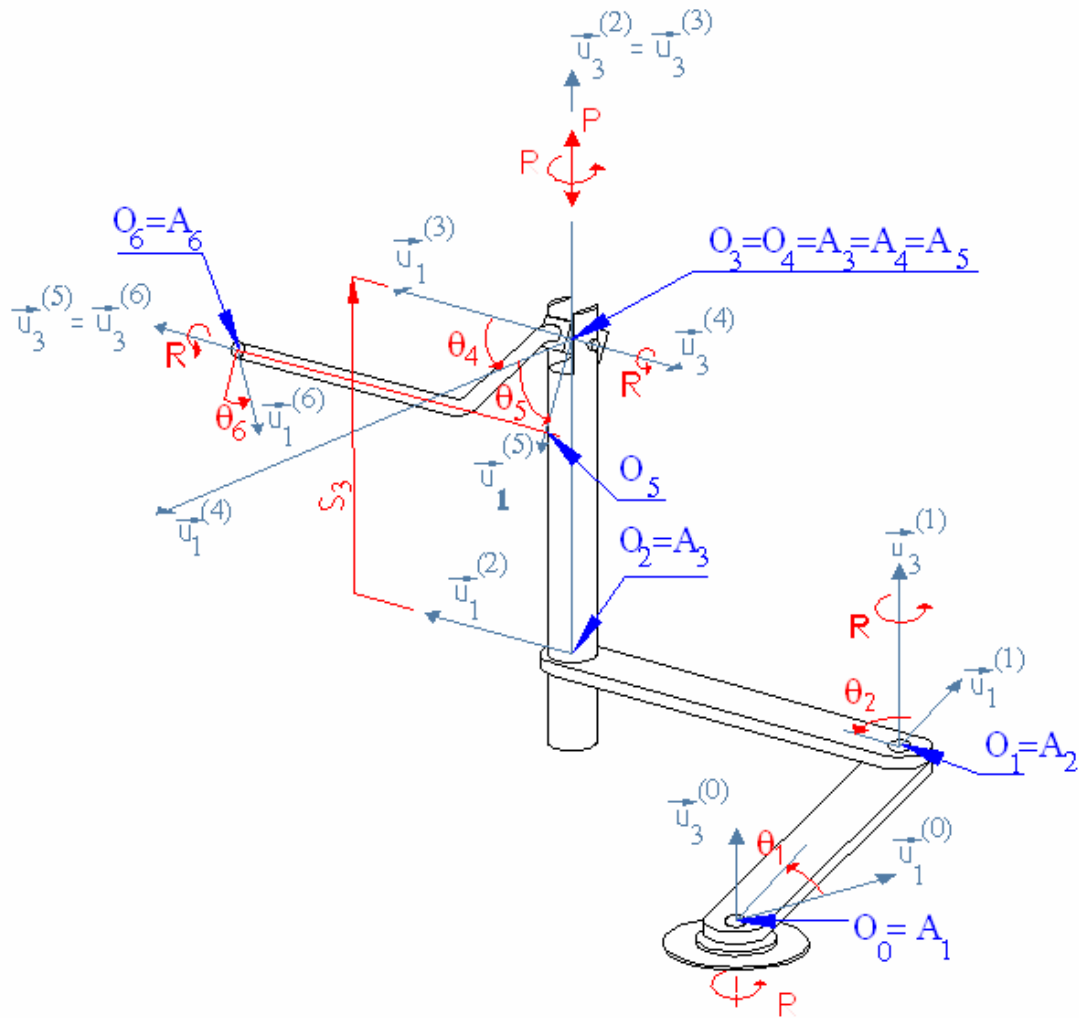


Figure.3.15 Coordinate Frames Attached to the MSS According to Denavit and Hartenberg Notation

Denavit and Hartenberg notation also describes four parameters in order to fully specify the configuration of frame k relative to frame $k-1$. The definitions of these parameters [14] are given below and the parameters of MSS are tabulated in Table.3.4.

- a_k : distance between $A_k O_k$ ($\bar{u}_3^{(k-1)}$ and $\bar{u}_3^{(k)}$ on $\bar{u}_1^{(k)}$)
 (Effective length of link k)
- α_k : angle from $\bar{u}_3^{(k-1)}$ to $\bar{u}_3^{(k)}$ about $\bar{u}_1^{(k)}$
 (Twist angle)
- s_k : distance between $\bar{u}_1^{(k-1)}$ and $\bar{u}_1^{(k)}$ on $\bar{u}_3^{(k-1)}$
- θ_k : angle from $\bar{u}_1^{(k-1)}$ to $\bar{u}_1^{(k)}$ about $\bar{u}_3^{(k-1)}$
 (Rotation angle)

Table.3.4 Denavit and Hartenberg Parameters

			Link 3			
	Link 1	Link 2	(Coincident Axes)		Link 4	Link 5
θ_k	Joint var.	Joint var.	0	Joint var.	Joint var.	Joint var.
a_k	1.75 m	1.5 m	0	0	0.8 m	0
α_k	0	0	-90	0	90°	0
d_k	0	0	Joint var.	0	0	0.3 m

After determining the parameters, the orientations of the links relative to the previous link are calculated according to [14] as

$$\hat{C}^{(k-1,k)} = e^{\bar{u}_3 \theta_k} \cdot e^{\bar{u}_1 \alpha_k} \quad (3.12)$$

where

- k : the number of the link whose orientation will be found
- \tilde{u}_n : the 3x3 cross product matrix generated from \bar{n} with the definition given by Equation (3.12)

$$\bar{n} \times \bar{p} = \tilde{n} \times \bar{p} \quad (3.13)$$

Resulting in

$$\begin{bmatrix} n_1 \\ n_2 \\ n_3 \end{bmatrix} \times \bar{p} = \begin{bmatrix} 0 & -n_3 & n_2 \\ n_3 & 0 & -n_1 \\ -n_2 & n_1 & 0 \end{bmatrix} \times \bar{p} \quad (3.14)$$

for any \bar{p} .

The orientation of a frame can be calculated in different link frames rather than the previous one using

$$\hat{C}^{(k-1,k+1)} = \hat{C}^{(k-1,k)} \cdot \hat{C}^{(k,k+1)} \quad (3.15)$$

For the tip point locations of the links relative to the previous link's tip point are calculated with the following formula [14]

$$\vec{r}_{(k-1)k}^{(0)} = \hat{C}^{(0,(k-1))} [a_k \cdot \cos(\theta_k) \cdot \bar{u}_1 + a_k \cdot \sin(\theta_k) \cdot \bar{u}_2 + s_k \cdot \bar{u}_3] \quad (3.16)$$

where $\vec{r}_{(k-1)k}^{(0)}$ is the vector from *the tip point of link k-1 to the tip point of link k* expressed in earth-fixed frame. The displacement vector can be summed up by using the Equation (3.17).

$$\vec{r}_{(k-1)(k+1)}^{(0)} = \vec{r}_{(k-1)k}^{(0)} + \vec{r}_{k(k+1)}^{(0)} \quad (3.17)$$

Applying these formulae to each joint for the parameters in Table.3.4 and using Equations (3.15) and (3.17), the tip point position and orientation can be calculated as

$$\hat{C}^{(0,6)} = e^{\bar{u}_3(\theta_1+\theta_2+\theta_4)} \cdot e^{\bar{u}_2(\theta_5)} \cdot e^{\bar{u}_3(\theta_6)} \quad (3.18)$$

$$\vec{r}_{06}^{(0)} = \begin{bmatrix} a_1 \cdot \cos(\theta_1) + a_2 \cdot \cos(\theta_{12}) + a_5 \cdot \cos(\theta_5) \cdot \cos(\theta_{124}) + d_6 \sin(\theta_5) \cdot \cos(\theta_{124}) \\ a_1 \cdot \sin(\theta_1) + a_2 \cdot \sin(\theta_{12}) + a_5 \cdot \cos(\theta_5) \cdot \sin(\theta_{124}) + d_6 \cdot \sin(\theta_5) \cdot \sin(\theta_{124}) \\ s_3 - a_5 \cdot \sin(\theta_5) + d_6 \cdot \cos(\theta_5) \end{bmatrix} \quad (3.19)$$

where;

$$\theta_{12} = \theta_1 + \theta_2$$

$$\theta_{124} = \theta_1 + \theta_2 + \theta_4$$

After finishing the positional analysis of the MSS, the calculations to determine the manipulator Jacobian, which is a time-varying linear transformation matrix, which maps the joint velocities to the Cartesian velocities of the tip of the arm, is held. In general it can be written that [12]:

$${}^0\mathbf{v} = {}^0\mathbf{J}(\Theta) \cdot \dot{\Theta} \quad (3.20)$$

where

Θ : vector of joint variables of the manipulator

${}^0\mathbf{v}$: a vector of Cartesian velocities in the earth-fixed frame (frame 0)

${}^0\mathbf{J}(\Theta)$: manipulator Jacobian for earth-fixed frame (frame 0)

The manipulator Jacobian can be defined as [14]

$$\hat{\mathbf{J}} = \begin{bmatrix} \bar{\mathbf{J}}_{r1} & \bar{\mathbf{J}}_{r2} & \bar{\mathbf{J}}_{r3} & \bar{\mathbf{J}}_{r4} & \bar{\mathbf{J}}_{r5} & \bar{\mathbf{J}}_{r6} \\ \bar{\mathbf{J}}_{a1} & \bar{\mathbf{J}}_{a2} & \bar{\mathbf{J}}_{a3} & \bar{\mathbf{J}}_{a4} & \bar{\mathbf{J}}_{a5} & \bar{\mathbf{J}}_{a6} \end{bmatrix} \quad (3.21)$$

where

$$\bar{\mathbf{J}}_{rk} = \frac{\partial \bar{\mathbf{r}}}{\partial \mathbf{q}_k} \quad (3.22)$$

$$\bar{J}_{ak} = \text{col} \left[\left(\frac{\partial \hat{C}}{\partial q_k} \right) \cdot \hat{C}^t \right] \quad (3.23)$$

It should be noted that “col” operation is the inverse operation of Equation (3.13). which forms a skew symmetric 3x3 matrix from a 3 element vector.

Taking the partial derivatives and making the necessary calculations, the elements of the Jacobian is obtained as:

$$\bar{J}_{r1} = \begin{bmatrix} -a_1 \cdot \sin(\theta_1) - a_2 \cdot \sin(\theta_{12}) - a_5 \cdot \cos(\theta_5) \cdot \sin(\theta_{124}) - d_6 \cdot \sin(\theta_5) \cdot \sin(\theta_{124}) \\ a_1 \cdot \cos(\theta_1) + a_2 \cdot \cos(\theta_{12}) + a_5 \cdot \cos(\theta_5) \cdot \cos(\theta_{124}) - d_6 \cdot \sin(\theta_5) \cdot \cos(\theta_{124}) \\ 0 \end{bmatrix} \quad (3.24)$$

$$\bar{J}_{r2} = \begin{bmatrix} -a_2 \cdot \sin(\theta_{12}) - a_5 \cdot \cos(\theta_5) \cdot \sin(\theta_{124}) - d_6 \cdot \sin(\theta_5) \cdot \sin(\theta_{124}) \\ a_2 \cdot \cos(\theta_{12}) + a_5 \cdot \cos(\theta_5) \cdot \cos(\theta_{124}) - d_6 \cdot \sin(\theta_5) \cdot \cos(\theta_{124}) \\ 0 \end{bmatrix} \quad (3.25)$$

$$\bar{J}_{r3} = \begin{bmatrix} 0 \\ 0 \\ 1 \end{bmatrix} \quad (3.26)$$

$$\bar{J}_{r4} = \begin{bmatrix} -a_5 \cdot \cos(\theta_5) \cdot \sin(\theta_{124}) - d_6 \cdot \sin(\theta_5) \cdot \sin(\theta_{124}) \\ a_5 \cdot \cos(\theta_5) \cdot \cos(\theta_{124}) - d_6 \cdot \sin(\theta_5) \cdot \cos(\theta_{124}) \\ 0 \end{bmatrix} \quad (3.27)$$

$$\bar{J}_{r5} = \begin{bmatrix} -a_5 \cdot \sin(\theta_5) \cdot \cos(\theta_{124}) + d_6 \cdot \cos(\theta_5) \cdot \cos(\theta_{124}) \\ -a_5 \cdot \sin(\theta_5) \cdot \sin(\theta_{124}) + d_6 \cdot \cos(\theta_5) \cdot \sin(\theta_{124}) \\ a_5 \cdot \cos(\theta_5) + d_6 \cdot \sin(\theta_5) \end{bmatrix} \quad (3.28)$$

$$\bar{J}_{r6} = \bar{0} \quad (3.29)$$

$$\bar{J}_{a1} = \bar{J}_{a2} = \bar{J}_{a4} = \begin{bmatrix} 0 \\ 0 \\ 1 \end{bmatrix} \quad (3.30)$$

$$\bar{J}_{a3} = \bar{0} \quad (3.31)$$

$$\bar{J}_{a5} = \begin{bmatrix} -\sin(\theta_{124}) \\ \cos(\theta_{124}) \\ 0 \end{bmatrix} \quad (3.32)$$

$$\bar{J}_{a6} = \begin{bmatrix} \cos(\theta_{124}) \cdot \sin(\theta_5) \\ \sin(\theta_{124}) \cdot \sin(\theta_5) \\ \cos(\theta_5) \end{bmatrix} \quad (3.33)$$

where;

$$\theta_{12} = \theta_1 + \theta_2$$

$$\theta_{124} = \theta_1 + \theta_2 + \theta_4$$

3.6 INVERSE DYNAMICS OF THE MSS

After focusing on the kinematic considerations, in this section the inverse dynamic analysis to calculate the actuator forces and torques for an instant, is formulated. The calculated actuator torques and forces are used as a feed forward compensation for the gravity, centrifugal and Coriolis forces at a specific instant of the MSS motion.

Knowing the position, velocity, and acceleration of the joints at a specific instant and the mass distribution of the robot, the Recursive Newton-Euler Formulation can be used [12]. The computation is composed of two parts. First, the forward recursion, propagating kinematic information from base to the end-effector, is held by applying Newton-Euler equations. Second, the backward recursion, propagating the forces and moments exerted on each link from the end-effector to the base to calculate the actuator forces and torques.

The Newton-Euler formulation for the Modified Denavit and Hartenberg summarized by Craig [12] is considered not to be suitable since his notation was not used in the kinematic formulation of the MSS. Instead, the Newton-Euler formulation summarized by Corke [15] is used and this formulation is given below.

Outward recursion:

First the outward recursion is held to calculate the accelerations of the mass centers and after that the inertial forces are calculated for each link.

If the axis $i+1$ is rotational

$${}^{i+1}\underline{\omega}_{i+1} = C^{(i+1,i)} ({}^i\underline{\omega}_i + \mathbf{c} \cdot \dot{\underline{q}}_{i+1}) \quad (3.34)$$

$${}^{i+1}\underline{\dot{\omega}}_{i+1} = C^{(i+1,i)} \{ {}^i\underline{\dot{\omega}}_i + \underline{z}_0 \cdot \ddot{\underline{q}}_{i+1} + {}^i\underline{\dot{\omega}}_i \times (\underline{z}_0 \cdot \ddot{\underline{q}}_{i+1}) \} \quad (3.35)$$

$${}^{i+1}\underline{\dot{v}}_{i+1} = {}^{i+1}\underline{\dot{\omega}}_{i+1} \times {}^{i+1}\underline{p}_{i+1} + {}^{i+1}\underline{\omega}_{i+1} \times \{ {}^{i+1}\underline{\omega}_{i+1} \times {}^{i+1}\underline{p}_{i+1} \} + C^{(i+1,i)} \cdot {}^i\underline{\dot{v}}_i \quad (3.36)$$

If the axis $i+1$ is translational

$${}^{i+1}\underline{\omega}_{i+1} = C^{(i+1,i)} \cdot {}^i\underline{\omega}_i \quad (3.37)$$

$${}^{i+1}\underline{\dot{\omega}}_{i+1} = C^{(i+1,i)} \cdot {}^i\underline{\dot{\omega}}_i \quad (3.38)$$

$$\begin{aligned} {}^{i+1}\underline{\dot{v}}_{i+1} &= C^{(i+1,i)} (\underline{z}_0 \cdot \ddot{\underline{q}}_{i+1} + {}^i\underline{\dot{v}}_i) + {}^{i+1}\underline{\dot{\omega}}_{i+1} \times {}^{i+1}\underline{p}_{i+1} + \dots \\ &\dots 2 \cdot {}^{i+1}\underline{\dot{\omega}}_{i+1} \times (C^{(i+1,i)} \cdot \underline{z}_0 \cdot \dot{\underline{q}}_{i+1}) + {}^{i+1}\underline{\omega}_{i+1} \times ({}^{i+1}\underline{\omega}_{i+1} \times {}^{i+1}\underline{p}_{i+1}) \end{aligned} \quad (3.39)$$

where

- i : link index
- ${}^{i+1}\underline{w}_i$: angular velocity of frame i in frame $i+1$
- ${}^{i+1}\underline{\dot{w}}_i$: angular acceleration of frame i in frame $i+1$

- ${}^{i+1}\underline{v}_i$: linear velocity of frame i in frame i+1
- ${}^{i+1}\dot{\underline{v}}_i$: linear acceleration of frame i in frame i+1
- \underline{z}_0 : unit vector in z direction
- \dot{q}_{i+1} : rate of change of joint variable

After calculating the motion variables of frames, the mass center accelerations are calculated by;

$${}^i\dot{\underline{v}}_i = {}^i\dot{\underline{w}}_i \times \underline{s}_i + {}^i\underline{w}_i \times ({}^i\underline{w}_i \times \underline{s}_i) + {}^i\dot{\underline{v}}_i \quad (3.40)$$

where

- ${}^i\dot{\underline{v}}_i$: linear acceleration of the center of mass of link i in frame i
- \underline{s}_i : position vector of the center of mass of link i with respect to frame i

The inertial forces and moments on links are calculated with the formulae:

$${}^i\underline{F}_i = m_i \cdot {}^i\dot{\underline{v}}_i \quad (3.41)$$

$${}^i\underline{N}_i = \underline{J}_i \cdot {}^i\dot{\underline{w}}_i + {}^i\underline{w}_i \times (\underline{J}_i \cdot {}^i\underline{w}_i) \quad (3.42)$$

where

- ${}^i\underline{F}_i$: inertial force on the center of mass of link i in frame i
- ${}^i\underline{N}_i$: inertial moment on center of mass of the link i in frame i
- m_i : mass of the link i
- J_i : moment of inertia of link i

Inward recursion

After calculating the required inertial forces, the actuator torques and forces for the required motion and required external forces are calculated by inward recursion with the formulae.

$${}^i\underline{f}_i = C^{(i,i+1)} \cdot {}^{i+1}\underline{f}_{i+1} + {}^i\underline{F}_i \quad (3.43)$$

$${}^i\underline{n}_i = C^{(i,i+1)} \left\{ {}^{i+1}\underline{n}_{i+1} + (C^{(i,i+1)} \cdot {}^i\underline{p}_j) \times {}^{i+1}\underline{f}_{i+1} \right\} + ({}^i\underline{p}_i + \underline{s}_i) \times {}^i\underline{F}_i + {}^i\underline{N}_i \quad (3.44)$$

where

- ${}^i\underline{f}_i$: force exerted on link i by link i-1
- ${}^i\underline{n}_i$: moment exerted on link i by link i-1

And finally the actuator forces and torques are calculated by the formula

$$\underline{Q}_i = \begin{cases} ({}^i \underline{n}_i)^T \cdot (\mathbf{C}^{(i,i+1)} \cdot \underline{z}_0) & \text{if the link } i+1 \text{ is rotational} \\ ({}^i \underline{f}_i)^T \cdot (\mathbf{C}^{(i,i+1)} \cdot \underline{z}_0) & \text{if the link } i+1 \text{ is translational} \end{cases} \quad (3.45)$$

where

\underline{Q}_i : force or torque exerted by the actuator at joint i

CHAPTER IV

CONTROLLER DESIGN

As stated in Chapter 2, there are two common types of store separation test methods using MSS. To accomplish the tests with the continuous and grid methods, MSS controller does not need to be more complex than a position controller since the time response of the system is not important for the validity of the tests. However, the side effect of this is that the internal balance data obtained during tests does not include the unsteady aerodynamics effects on the model.

In this chapter, the study on a controller, which minimizes the force error occurring on the internal balance and make a real-time store separation test possible, is proposed and verified. Finally, the designed controller is tuned for the mechanical model of the MSS.

4.1. CONTROLLER TOPOLOGY

During the wind tunnel tests, there should not be any external forcing on the model except the ones that will occur during flight, in order to simulate the motion of the object in the wind tunnel environment. In other words, the internal balance should read zero forcing during the tests for a perfect model by

similarity means. In order the model to behave during the tests as it will behave under the flying aircraft, the MSS should not exert any extra force on the model than the reference force values which are calculated in order to compensate for the differences in the inertial properties of the model and the real object. This ability of the MSS eliminates the model-matching problem defined in Chapter 1.

Physically, the force measurements of the internal balance are the forces, which the model support system has applied to the model, affect the trajectory of the model during the tests. Keeping in mind that the desired trajectory is not known, the parameters to investigate in order to decide upon the validity of the test are only the force measurements of the internal balance.

During a store separation test in the wind tunnel, whether the model hits the aircraft or not is observed. So a deviation from the trajectory that would occur aerodynamically should be avoided. The validity of a store separation test held with this approach can be decided upon examining the force measurements of the internal balance after the tests. The tests with internal balance force and moment measurements above a certain limit can be decided as invalid.

In this thesis, the designed controller for the MSS is going to minimize the force error between the desired forces and the internal balance measurements. At the beginning of the tests, an external force simulating the ejector forces will be applied to the model and then the model will move according to the aerodynamic forces under the control of the MSS controller until it reaches to the limits of the test section where the test ends.

In this type of a test, the effects of unsteady aerodynamics will be included in the test results since the system is expected to be capable of working real-time. To accomplish this task, the control block diagram seen in Figure.4.1 is developed.

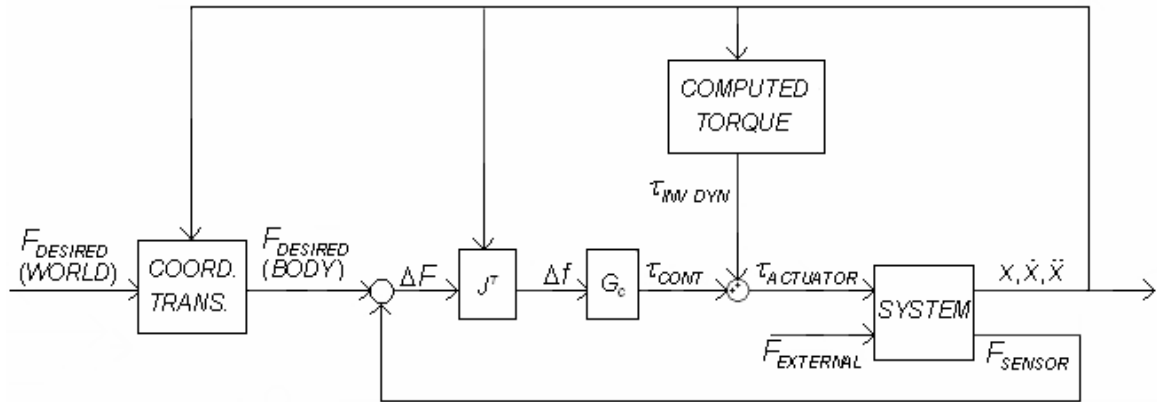


Figure.4.1 Force Controller Block Diagram

In the figure;

- $F_{DESIRED}$: force and torque vector of 6 components whose third component is the compensation for the weight of the model.
- ΔF : force error in Cartesian Space
- J : manipulator Jacobian
- Δf : force error in Joint Space
- G_c : controller gain
- τ_{CONT} : vector of torque input to the joints associated with the force controller
- $\tau_{INV DYN}$: vector of torque input to the joints associated with the inverse dynamics
- $\tau_{ACTUATOR}$: vector of total torque demand
- $F_{EXTERNAL}$: external force applied to object carried by the manipulator
- F_{SENSOR} : forcing on the end-effector by the object
- X, \dot{X}, \ddot{X} : vectors of joint variables and their derivatives

4.2. PRELIMINARY WORK

In order to validate this approach, a double pendulum problem case is used as a preliminary work to verify the approach. In this double pendulum problem, a double pendulum is modeled with an object attached to the tip point, which is instrumented with a force sensor to obtain the applied force data by the pendulum to the object as in the model support system case. (Figure.4.2 shows the modeled double pendulum.) The goal in this problem is to hold the object stationary for some time and then let the object free in order to observe zero forcing on the force sensor.

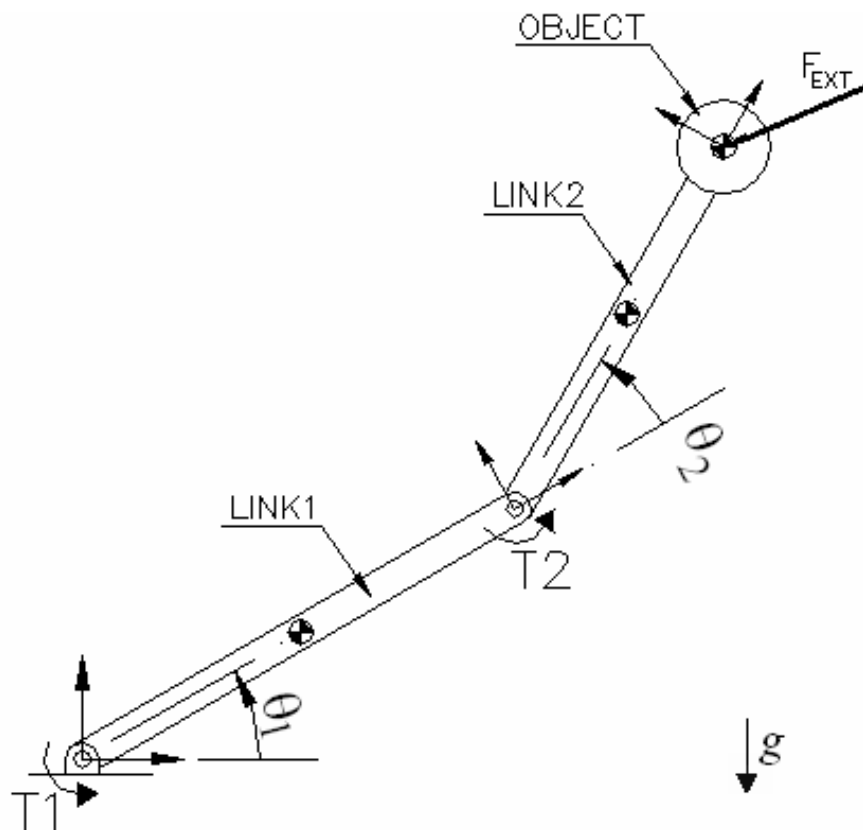


Figure.4.2 Modeled Double Pendulum

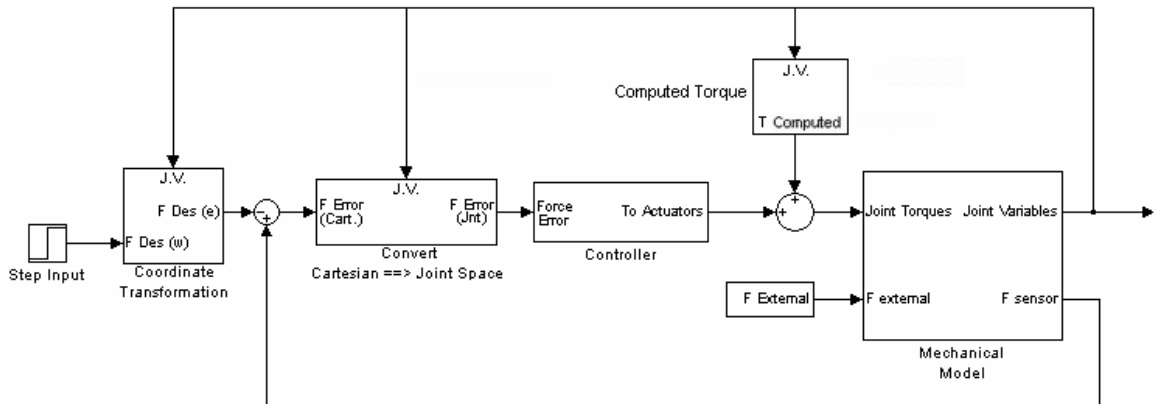


Figure.4.3 View of the MATLAB Simulink® Model for the Double Pendulum

In the MATLAB Simulink® model of a double pendulum seen in Figure 4.3, there are 5 important blocks. These are;

- Mechanical Model
- Coordinate Transformation
- Cartesian to Joint Space Converter
- Controller
- Computed Torque Block

By using MATLAB Simmechanics® tool, the double pendulum seen in Figure.4.2 is modeled mechanically as seen in Figure.4.4. The details of the revolute joint blocks seen in Figure.4.4 are shown in Figure.4.5.

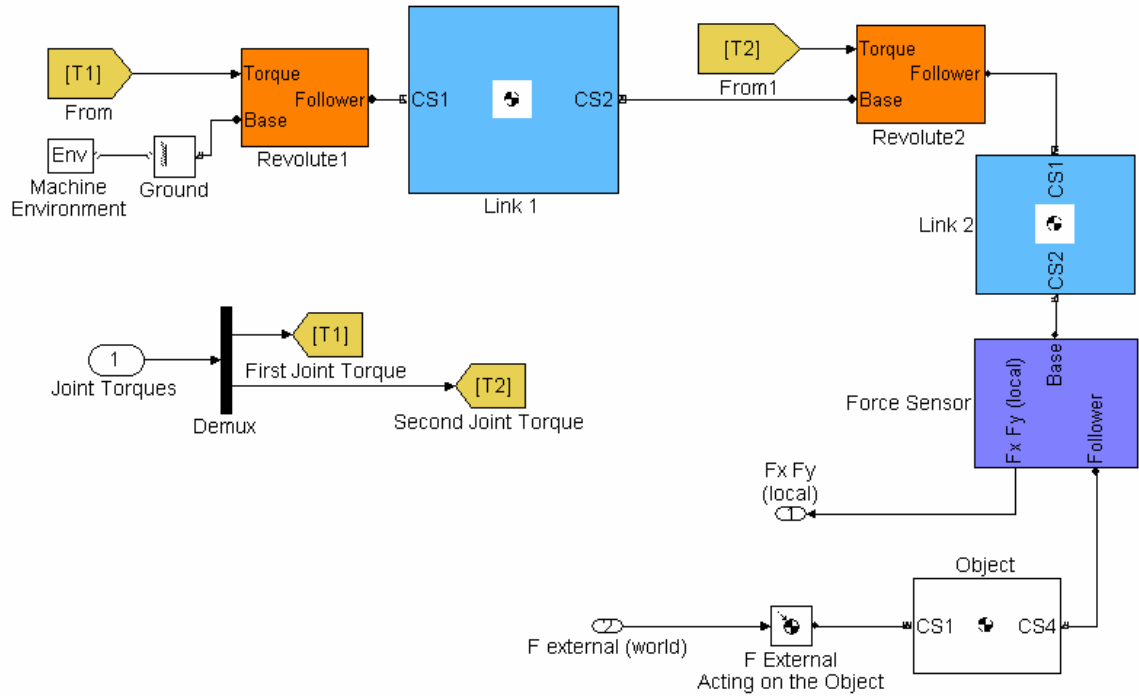


Figure.4.4 Simmechanics® Model of Double Pendulum

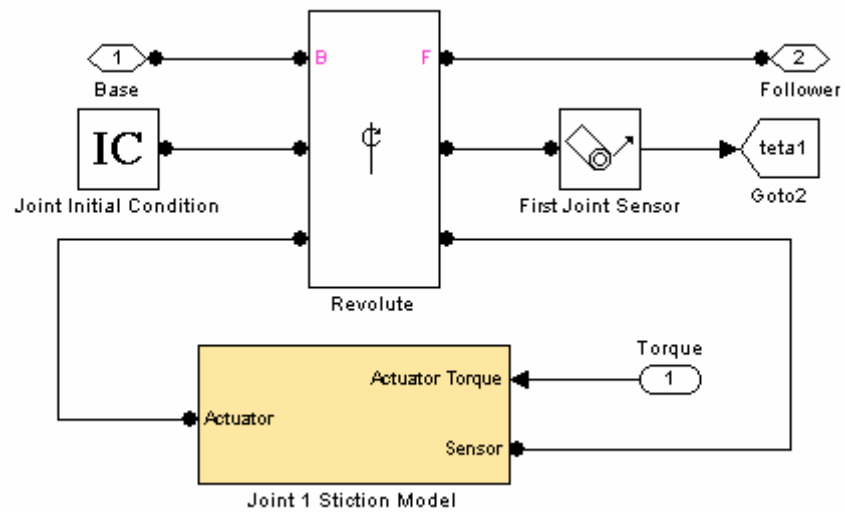


Figure.4.5 Details of the Revolute Joint Blocks

The joint torques are inputs to this Simmechanics[®] mechanical model, coming from the controller side calculations. The revolute joints are modeled with static and kinetic friction. The external force expressed in earth coordinates are manually adjusted as a constant by the user and by the help of this model, it is applied to the object. The links of the pendulum are taken as steel rods having circular cross section and the object's geometry is not taken into account. The parameters about the model pendulum are given in the Table.4.1. The force sensor data in end effector's coordinates are the outputs of this model which is feedback to the controller for proper operation.

Table.4.1 Parameters of the Double Pendulum Model

	Diameter (m)	Length (m)	Mass (kg)	I_{xx} (kg.m ²)	I_{yy} (kg.m ²)	I_{zz} (kg.m ²)
Link 1	0.09	2	100	0.10	33.38	33.38
Link 2	0.045	1	50	0.05	4.19	4.19
Object	----	----	3	1	1	1

Since the controller takes the error signal on joint axes, first it is needed to calculate the error in end effector's coordinates and then to convert the forcing in Cartesian space to joint space. Since the desired forces are in earth coordinates, a coordinate transformation block is embedded in the system. This block uses the θ_1 and θ_2 values in direction cosine matrices to transform the force values in earth coordinates to end effector's coordinates. After this transformation, the force sensor measurements are subtracted from the desired forces to calculate the force error in end effector's coordinates.

The force error is then converted to torque error in joint space by Equation (4.1) [12].

$$J^T = \begin{bmatrix} l_1 \cdot \sin(\theta_2) & l_2 + l_1 \cdot \cos(\theta_2) \\ 0 & l_2 \end{bmatrix} \quad (4.1)$$

where the matrix is the transpose of the manipulator Jacobian which relates the tip point position with respect to origin in end effector's coordinates.

The resulting torque error in joint space is then fed into the controller block. In this controller block, separate PID controllers for each joint are used. Since the successful controller with the simplest structure can be considered as the best controller, PID controllers are selected. PID controllers are widely used in similar industrial applications due to their simplicity. The PID controllers with the transfer function

$$G_c(s) = K_p + \frac{K_i}{s} + K_d s \quad (4.2)$$

are tuned afterwards using *Signal Constraint Block* of *MATLAB® (Rev.14) Simulink Response Optimization* directory. The resulting gains are tabulated in Table.4.2

Table.4.2 Resulting Optimal PID Parameters for Double Pendulum

Controller	Controller Parameters		
	Kp (N / N)	Ki (N.s / N)	Kd (N / N.s)
1	536	154	2153
2	618	13	1005

The controller output is added with a feed-forward signal which calculates the required torques to maintain the instantaneous motion of the double pendulum. The computed torque block is used as a feedforward compensation for the gravity, centrifugal and Coriolis forces. In other words the computed torque method is used as a disturbance estimator resulting in improvement in transient and steady state response of the applied system. As a natural result of this improvement the tracking performance of the system also increases. In a perfectly modeled system there is no need for a feedback controller after inserting a computed torque block. However, since the environmental conditions like friction, ambient temperature, wear, or aerodynamic forces in MSS case; can not be modeled perfectly, the PID controller is used as the feedback controller in order to compensate for the errors working parallel with the computed torque block. The effect of the computed torque method is discussed with forced motion simulation.

The double pendulum is tested; the results of a free fall without an external force and a forced motion are given below.

Free Fall

In the free fall demonstration, the pendulum is initially positioned with joint angles being equal to 60° and -40° for θ_1 and θ_2 respectively. Until $t = 0.1$ sec, the desired forces are given equal to the weight of the object to hold the model stationary and after $t=0.1$ sec, the desired forces are set to 0 (zero) in order the pendulum to let the object in a free fall under the effect of gravity in $-y$ direction. The simulation is terminated at $t=1$ sec before the mechanism reaches the workspace boundary. From Figure.4.6 to Figure.4.10 the obtained results can be examined for the free fall case.

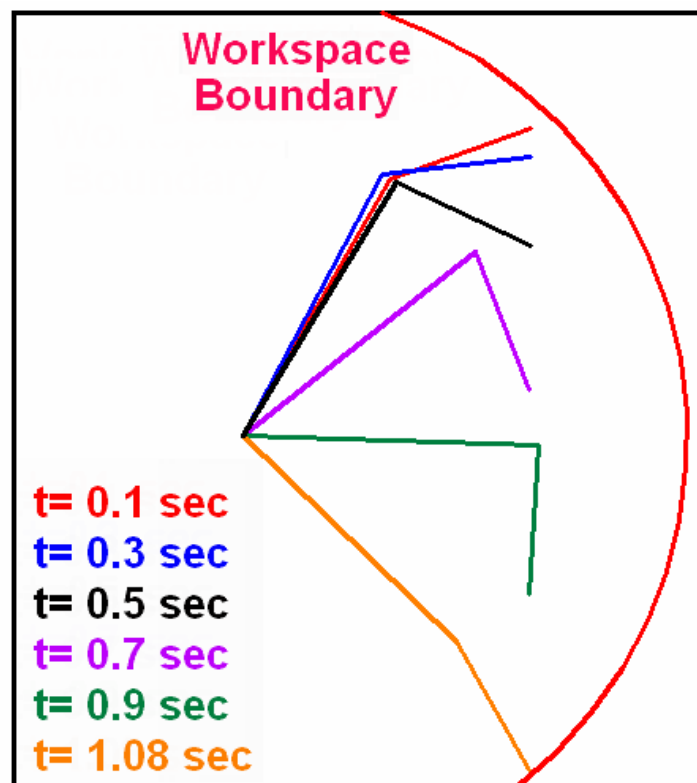


Figure.4.6 Free Fall Trajectory

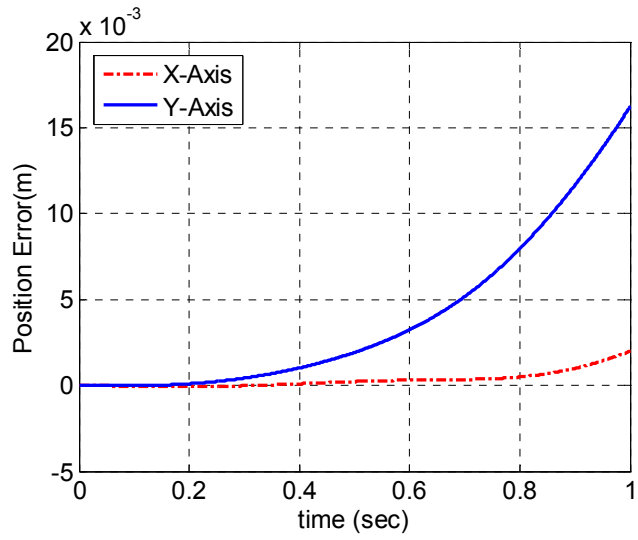


Figure.4.7 Position Error Occurred During Free Fall

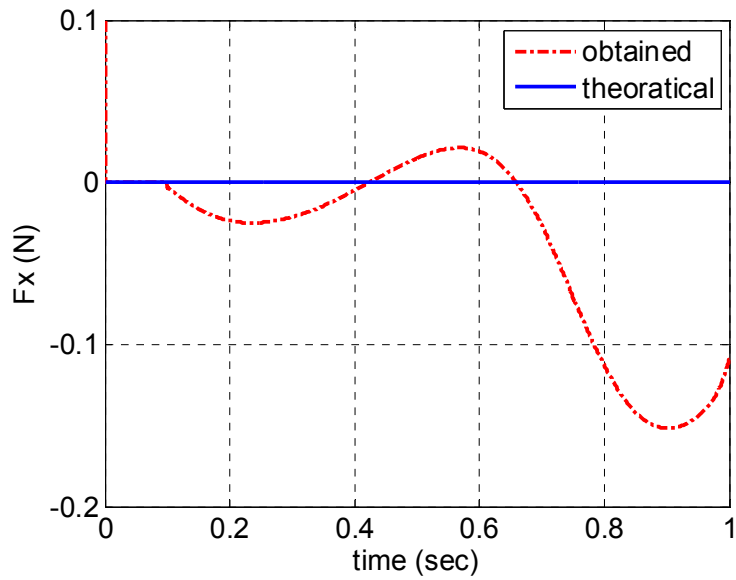


Figure.4.8 Force Sensor Measurement on x-Axis

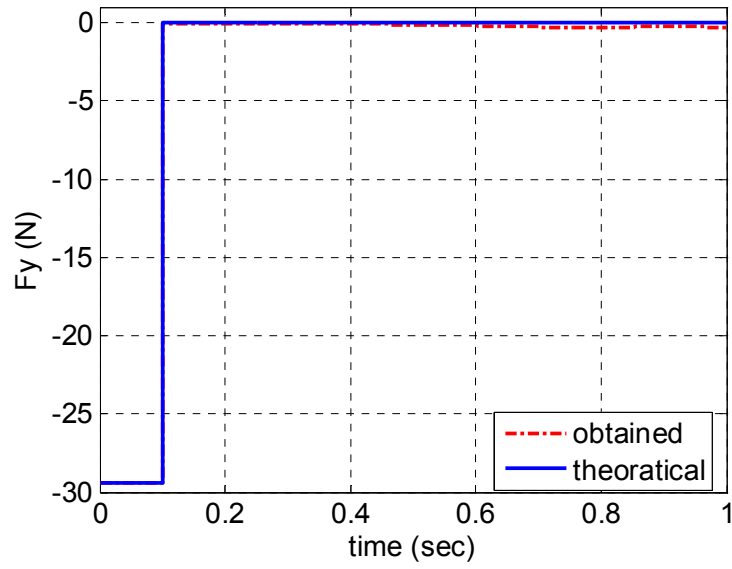


Figure.4.9 Force Sensor Measurement on y-Axis

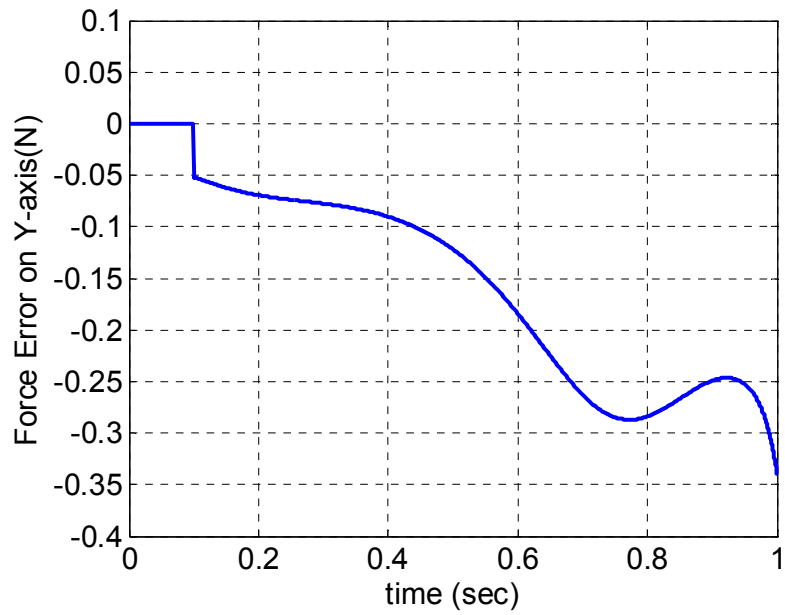


Figure.4.10 Force Error on y-Axis

Forced Motion

In the forced motion demonstration, the pendulum is initially positioned with joints angles being equal to 80° and 30° for θ_1 and θ_2 respectively. Until $t = 0.1$ sec, the desired forces are given equal to the weight and external forcing on the object to hold the model stationary and after $t=0.1$ sec the desired forces are set to zero in order the pendulum to let the object in motion under the effect of external force of -15N . The simulations are terminated at $t=1$ sec before the mechanism reaches the workspace boundary.

With this forced motion case two simulations are held: (i) without computed torque and (ii) with computed torque. Figure.4.11 shows the desired and obtained trajectory without the computed torque in order to give a brief idea about the path in the forced motion case. From Figure 4.12 to Figure.4.16 the results obtained without computed torque compensation can be examined.

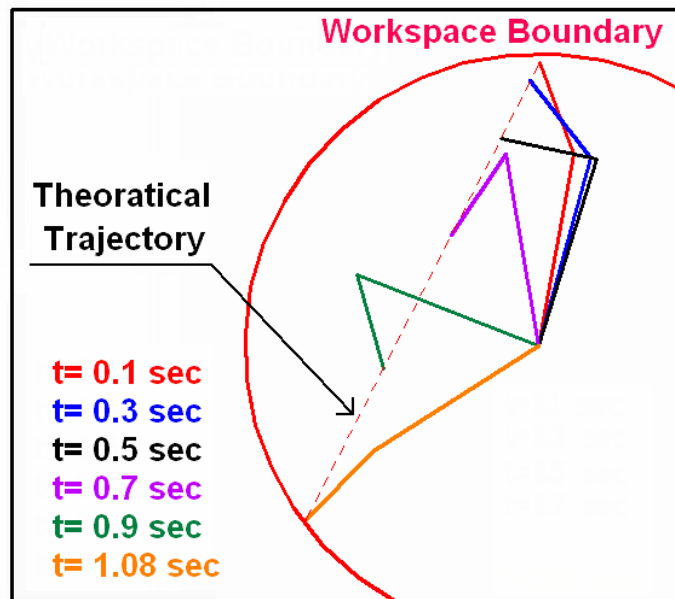


Figure.4.11 Forced Motion Trajectory

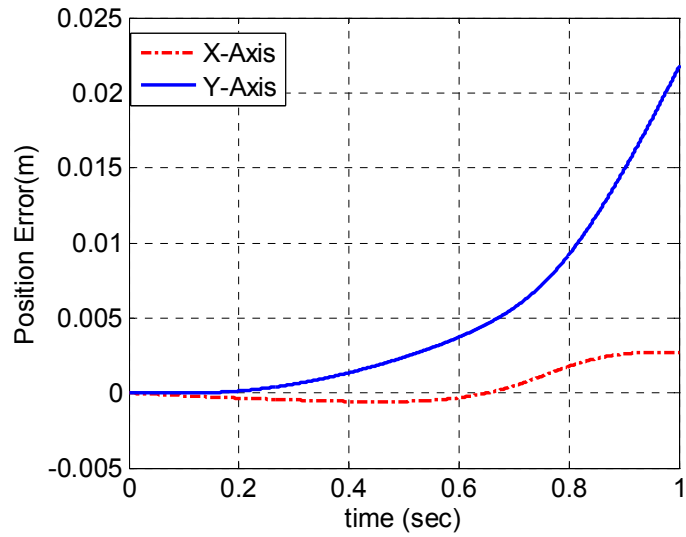


Figure.4.12 Position Error Occurred During Forced Motion without Computed Torque Compensation

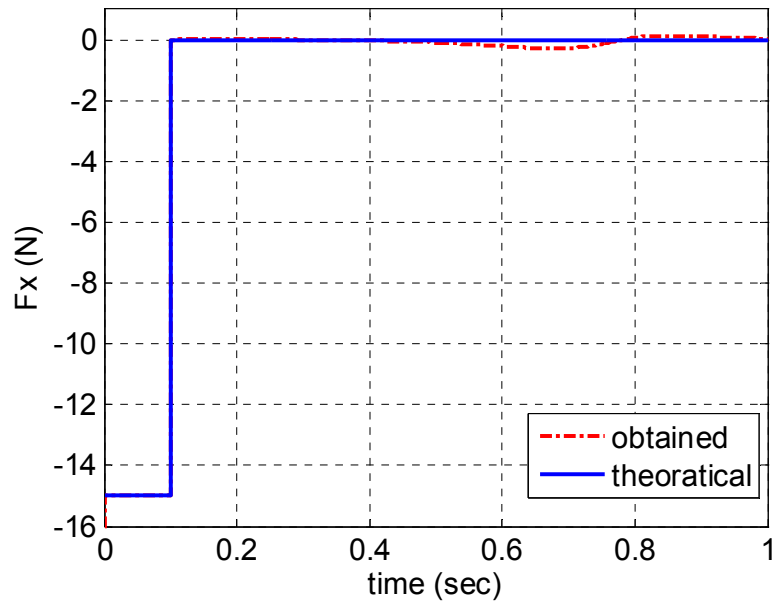


Figure.4.13 Force Sensor Measurement on x-Axis without Computed Torque Compensation

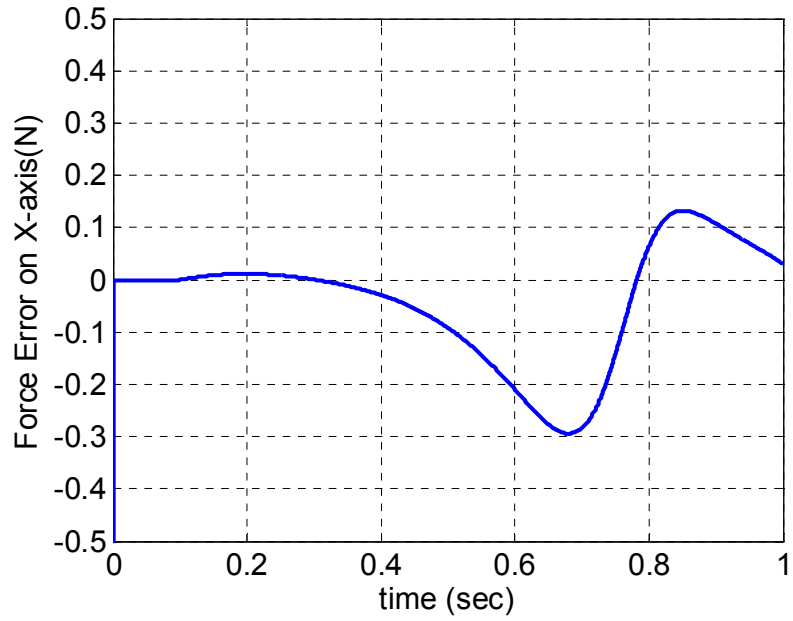


Figure.4.14 Force Error on x-Axis without Computed Torque Compensation

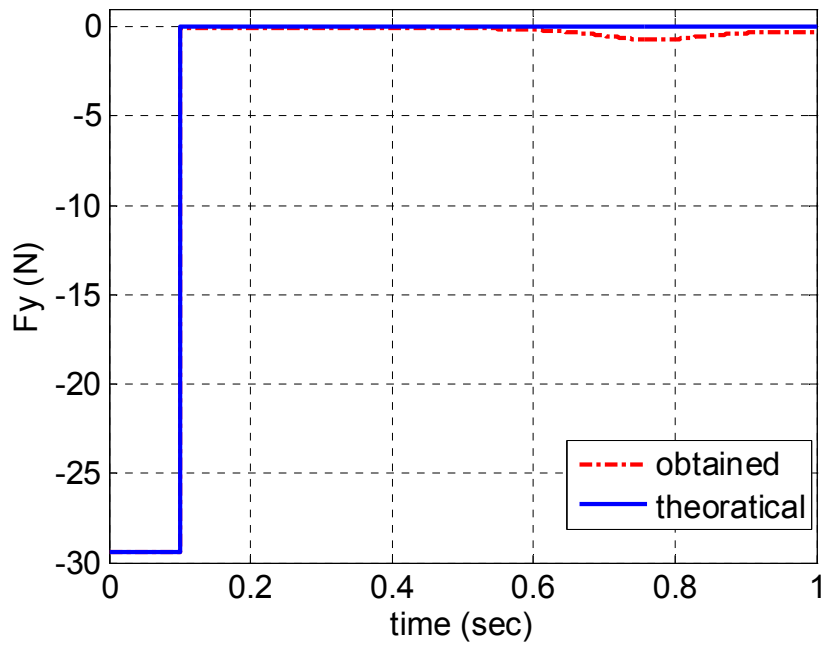


Figure.4.15 Force Sensor Measurement on y-Axis without Computed Torque Compensation

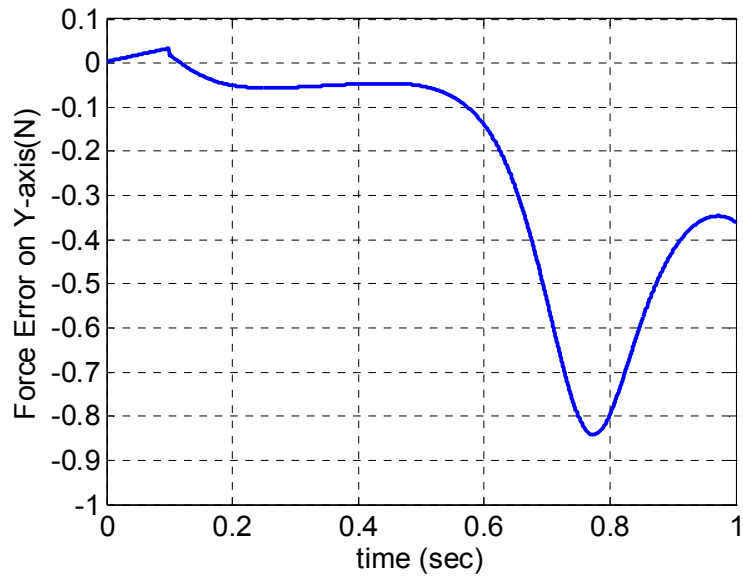


Figure.4.16 Force Error on y-Axis without Computed Torque Compensation

From Figure 4.17 to Figure.4.21, the results obtained with computed torque block can be examined.

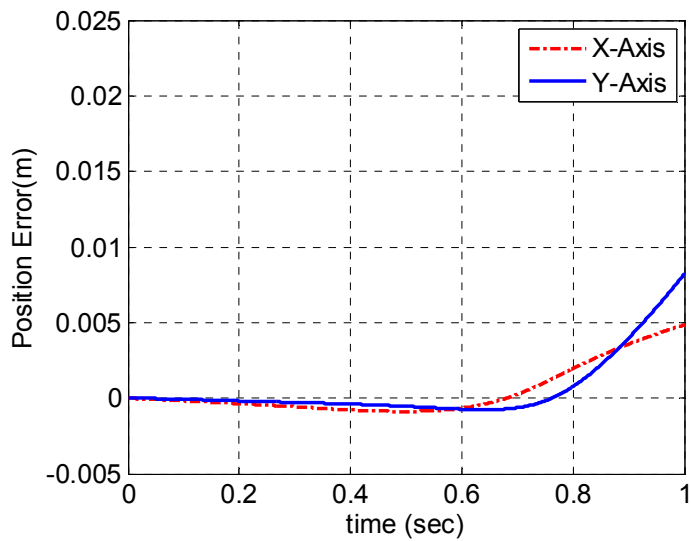


Figure.4.17 Position Error Occurred During Forced Motion with Computed Torque Compensation

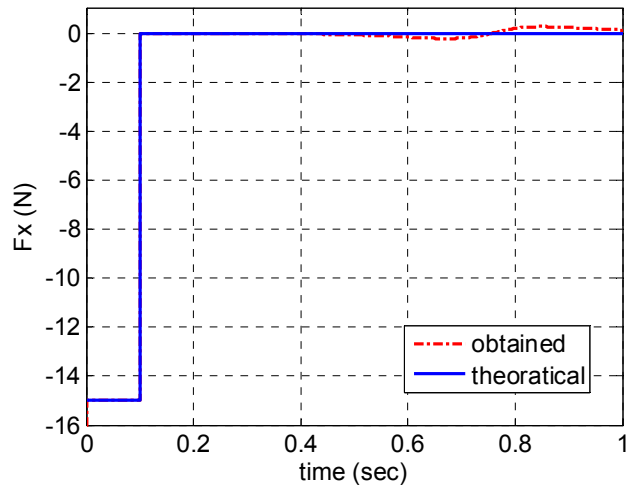


Figure.4.18 Force Sensor Measurement on x-Axis with Computed Torque Compensation

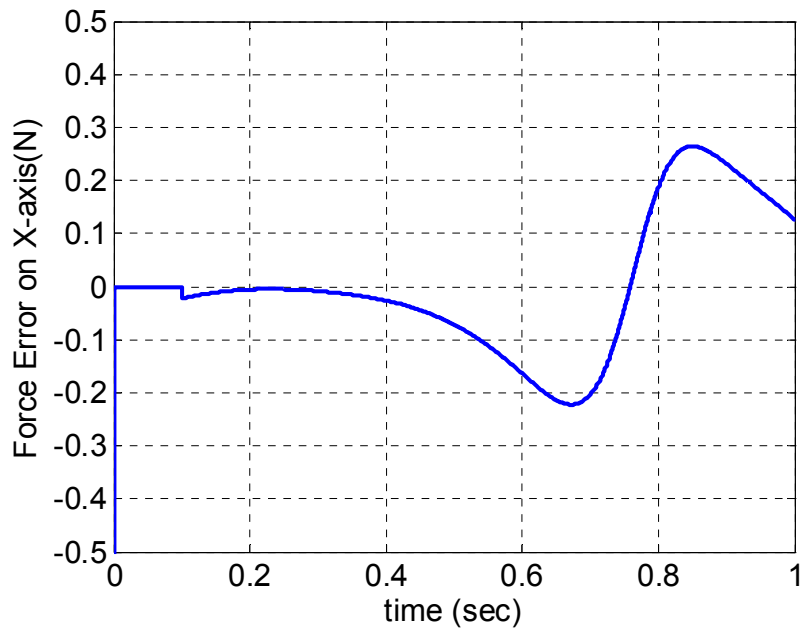


Figure.4.19 Force Error on x-Axis with Computed Torque Compensation

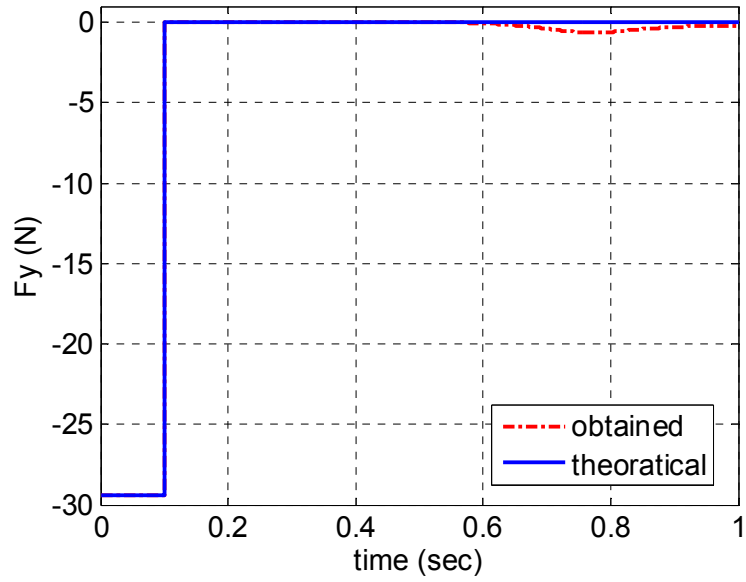


Figure.4.20 Force Sensor Measurement on y-Axis with Computed Torque Compensation

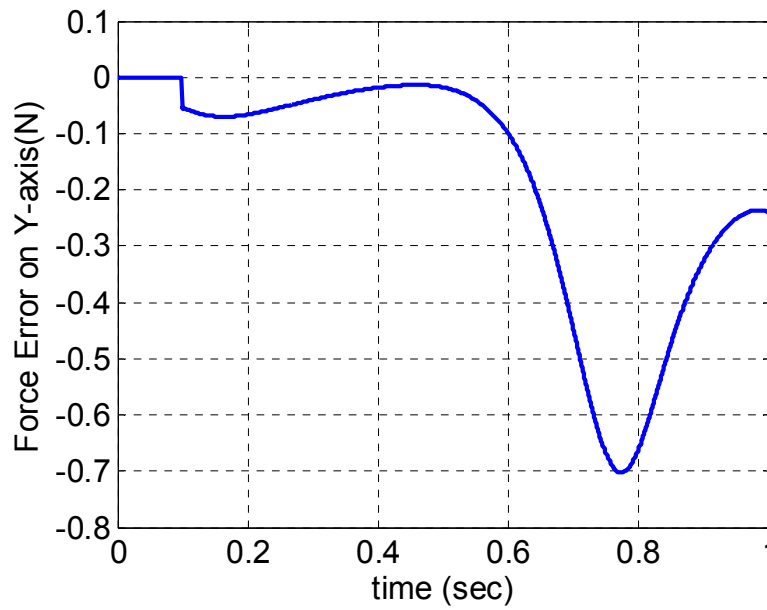


Figure.4.21 Force Error on Y-axis with Computed Torque Compensation

In these forced motion simulations, the computed torque compensation is observed to improve the results slightly. Since the constructed mechanical model is much more uniform than a real mechanism, the performance of the single feedback controller is also sufficient in the computer environment. However, in the case of a real system, the difference between the cases of with computed torque compensation and without computed torque compensation is expected to be greater. For this reason, it is decided to use the computed torque method in this work.

In addition to those, with this double pendulum preliminary work, it is seen that the used control approach satisfied the system requirements. However, there are some important points which should not be neglected behind these satisfactory results. First of all, the initial positions of the cases are carefully selected in order not to face a singular point during the simulations. Additionally, rather large controller gains are used resulting in high actuator torques in order to end up with an agile system that can regulate the force error in a small envelope.

As a conclusion of this double pendulum preliminary work, it is decided that the minimization on the force sensor measurement can be considered as an appropriate approach for the model support system controller with powerful actuators which results in an agile system. Although the conceptual mechanical design of the model support system is done aiming a singular-free workspace, it should be noted that the force control abilities of such a controller is position dependent.

4.3. CONTROL SYSTEM FOR THE MSS

After testing the performance of the approach in the previous section, the application of the verified approach to the MSS control problem is discussed in this section. For this purpose, some modifications to the preliminary blocks are introduced.

As in the double pendulum control problem, in the block diagram of MSS seen in Figure.4.22, there are 6 blocks. These are;

- Model Support System Module
- Computed Torque Controller
- Aerodynamic Module
- Cartesian to Joint Space Conversion
- Controller
- Coordinate Transformation

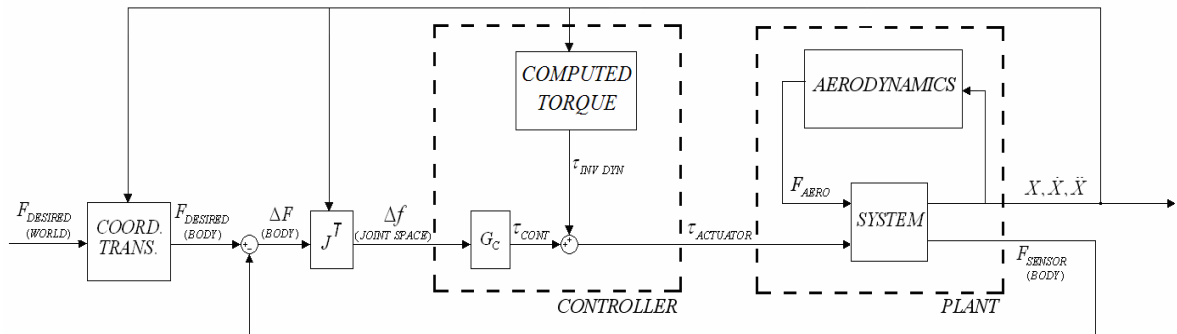


Figure.4.22 Block Diagram of the MATLAB Simulink® Model for the MSS

4.3.1 MODEL SUPPORT SYSTEM BLOCK

The interior of the mechanical model constructed using MATLAB[®] Simmechanics Tool is seen in Figure.4.23.

In this model, all joints on the kinematic chain of the MSS are modeled such that they include both static and kinetic friction. Also, it is assumed that all joints are instrumented with joint sensors in order to obtain the joint variables during the simulations. The mechanical properties of the bodies in this model are read from a MATLAB[®] m-file which is given in Appendix-A. This m-file is also used to calculate, the initial positions of the joints given the end-effector position and orientation. These initial conditions of the joints are fed to the mechanical model to position the model correctly at the beginning of the simulations.

In this model, there are two ground blocks where the first linear actuator and the first link are connected to the earth fixed reference frame. The first link is connected to the fixed frame by a revolute joint, which is actuated by a linear actuator whose details can be seen in Figure.4.24. The computed torque of the controller for the first revolute joint is fed into this block. By simple geometric calculations, this torque value is transformed into the force value, which can be considered as a transformation from joint space to actuator space. After this transformation, this force value is fed to the prismatic joint.

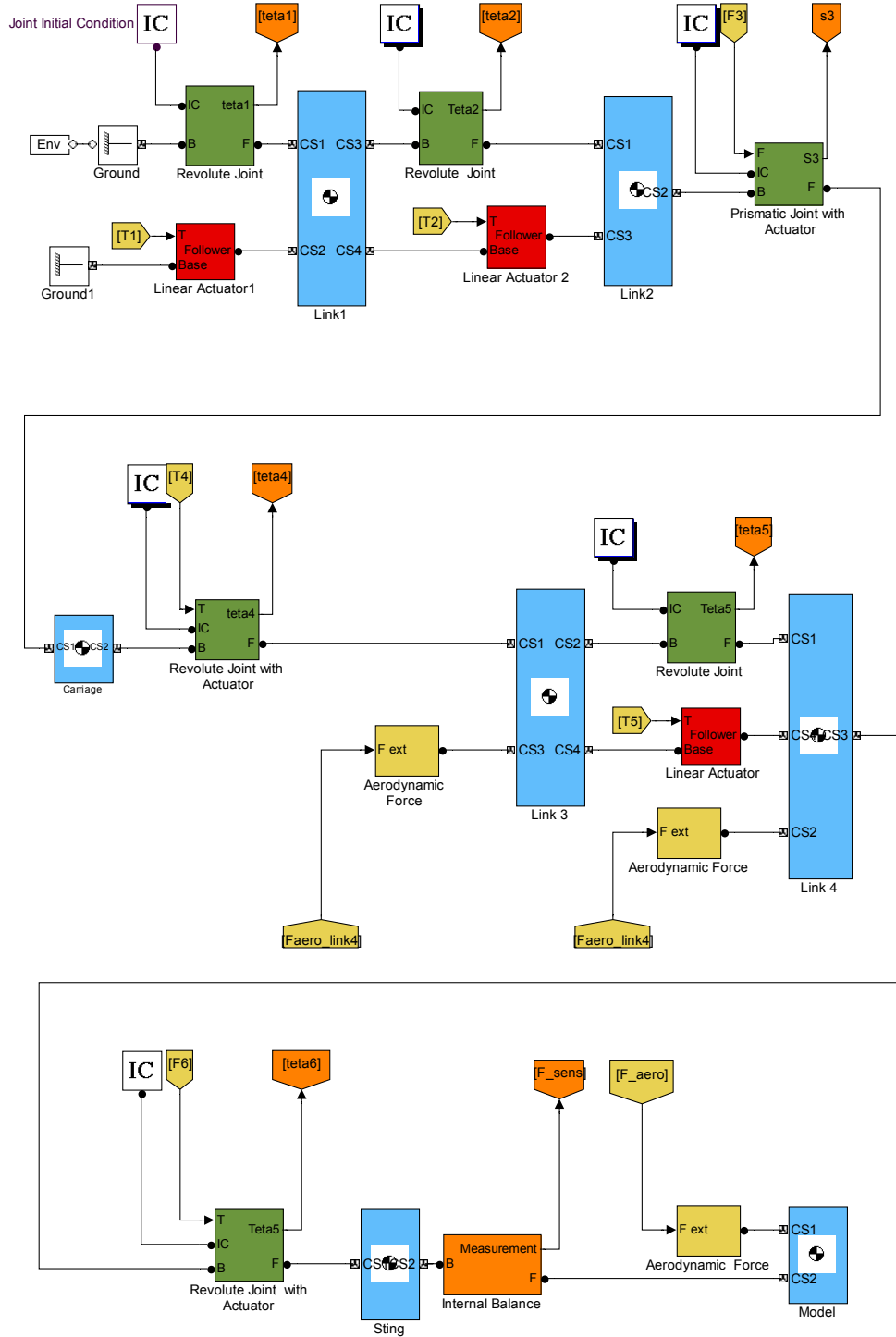


Figure.4.23 MATLAB[®] Simmechanics Model of the MSS

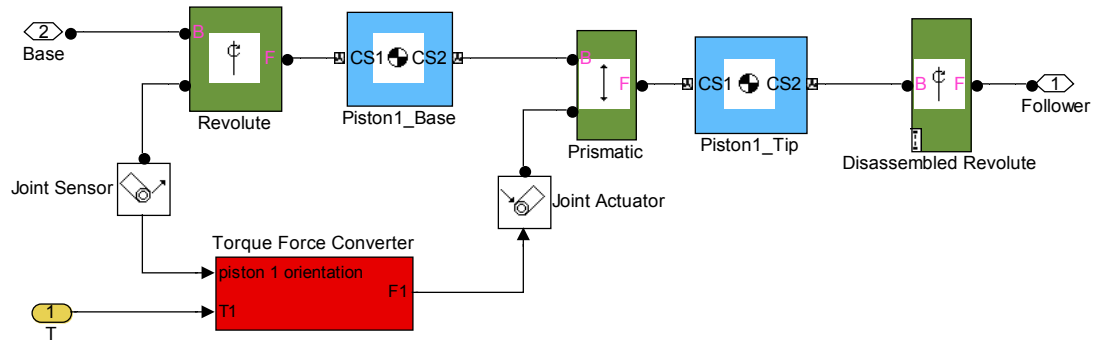


Figure.4.24 Linear Actuator Model

The structure of the second revolute joint is very similar to the first revolute joint. The second link is connected the first link by a revolute joint which is actuated by a linear actuator which is also connected to the first link.

The connection between the second link and the third link is maintained by consecutive prismatic and revolute joints with coincident axis. As in the conceptual design 3D model, a massless link is modeled in between them; in order to assume these consecutive joints as a cylindrical joint. However, the m-file in Appendix-B has the lines to modify these inertia values in future. The joints are actuated with the calculated force and torque values which are fed directly to the joint actuators.

The third and the fourth link are the links subject to air flow. The aerodynamic blocks connected to these links applies the calculated aerodynamic forces by the aerodynamic module as discussed in Section.4.3.3. These forces are applied on the geometric centers of the links in the test section.

Like the first two joints, the joint between the third and the fourth link is a revolute joint actuated by a linear actuator. Sting is connected to the fourth link by means of an actuated revolute joint.

The sting is the last link of the manipulator which is the component where the model is assembled to the MSS. In between the sting and the model, the internal balance is located. This connection is modeled as welded joint which is instrumented with a 6-axis force sensor.

The last component of the constructed model is the missile model. The force acting on this component is the aerodynamic force calculated by the aerodynamic module as discussed in Section.4.3.3.

4.3.2 COMPUTED TORQUE BLOCK

During the simulations, the joint variables are fed into the computed torque block and the change rates are calculated by differentiation. After this operation, the total 12 joint variables (position and velocity) are used into Corke's RNE block [15] which carries out the inverse dynamic calculations for MSS with the formulation summarized in Section.3.6. The output of this Computed Torque block is a vector of joint forces and torques which is used to compensate for the required forcing due to the instantaneous motion of the MSS, in order to increase the efficiency of the controller.

4.3.3 AERODYNAMIC MODULE BLOCK

The aerodynamic module block consists of two parts. One of them calculates the aerodynamic forcing on the store model in detail and the second part calculates the aerodynamic forcing acting on the links located in the test section.

Before going further with how the first part of the block works it is better to discuss the aerodynamics theory that this block depends on.

The aerodynamic coefficients depend on velocity, orientation, and the previous motion of the missile. However, the calculation of these coefficients as a function of all of these parameters is very difficult. In order to simplify these calculations, the effects of the roll angle, rate of change of pitch, yaw and roll angle on aerodynamic coefficients are neglected since they are relatively small in the basic finner geometry introduced in the next chapter.

After these assumptions, the aerodynamic module block is structured to calculate the coefficients as functions of Mach number, angle of attack and side-slip angle. The aerodynamic coefficients are required to be organized as 3D look-up tables in order to be interpolated during the calculation of aerodynamic forces and moments by the formulae taken from [16]. The results of the formulae given below are the forces and moments acting on the center of gravity of the basic finner in the body coordinate system which is given in Figure.4.25.

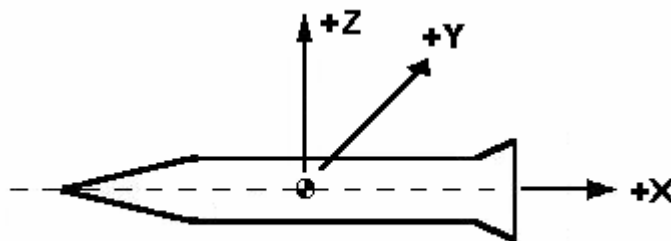


Figure.4.25 Coordinate System of Missile DATCOM

$$F_x = Q_d A C_A \quad (4.3)$$

$$F_y = Q_d A C_Y \quad (4.4)$$

$$F_z = Q_d A C_N \quad (4.5)$$

$$L = Q_d A d C_{LL} \quad (4.6)$$

$$M = Q_d A d C_M \quad (4.7)$$

$$N = Q_d A d C_{LN} \quad (4.8)$$

where

- Q_d : dynamic pressure
- A : cross sectional area of the object
- d : diameter of the object
- C_A : axial force coefficient
- C_Y : side force coefficient
- C_N : normal force coefficient
- C_{LL} : rolling moment coefficient
- C_M : pitching moment coefficient
- C_{LN} : yawing moment coefficient

- M : pitching moment
- N : yawing moment
- L : rolling moment

The block gets the instantaneous yaw and pitch angles during the simulations and interpolates the aerodynamic coefficients to be used in the formulae. After these calculations, the coordinate frame of the calculated force and torques are matched with the one used on the MSS seen in Figure.3.15.

The constants used in the equations from (4.3) to (4.8) are tabulated in Table.4.3

Table.4.3 Constants Used in Equations (4.3) to (4.8)

Constant	Value
Q_d	709.28 N/m ²
A	0.008 m ²
d	0.1 m

In the second part of the aerodynamic module, the aerodynamic forces acting on the third and the fourth link are calculated as functions of the test wind speed, yaw and pitch angles by simple fluid mechanics formula, Equation (4.9). The constants for these calculations are tabulated in Table.4.4

$$F = \frac{1}{2} \cdot C_D \cdot A \cdot \rho \cdot V^2 \tag{4.9}$$

where

C_D : drag coefficient

ρ : density

V : air velocity

Table.4.4 Constants Used to Calculate Aerodynamic Forcing on the Links

Constant	Value
$C_{D \text{ link3}}$	1.2
$C_{D \text{ link4}}$	1.2
d_{link3}	0.2 m
$A_{\text{link4, side}}$	0.12 m ²
$A_{\text{link4, top}}$	0.12 m ²
$A_{\text{link4, front}}$	0.08 m ²
ρ	1.2 kg/m ³

4.3.4 CARTESIAN TO JOINT SPACE CONVERTER BLOCK

As stated in Section 4.1, the force error on the Cartesian space can be converted to the joint space by multiplying with the transpose of the manipulator Jacobian. In this block, MSS Jacobian derived in Section.3.5 is embedded to perform this operation. The force error in Cartesian space at the input is transformed into the force error in the joint space and fed to the controller by this block.

4.3.5 CONTROLLER BLOCK

After achieving satisfactory results with two PID controllers in the double pendulum example, in the MSS problem PID controllers are used as well. For this purpose, 6 PID controllers each affecting a single joint actuator, are located in the block with the transfer function

$$G_c(s) = K_p + \frac{K_i}{s} + K_d s \quad (4.10)$$

The controller response requirements are determined as the force measurements on three axes are less than 0.8 N and the torque measurements on the three axes are 0.8 N.m for a 5 kg store model.

For these requirements using *Signal Constraint Block* of *MATLAB® (Rev 14) Simulink Response Optimization* directory, the PID controller parameters are tuned. The parameters of the test case used during the optimization process are tabulated in Table.4.5.

Table.4.5 Initial Conditions Used in Optimization

Parameter	Value
X	0 m
Y	1.5 m
Z	0.75 m
Yaw	-20°
Pitch	30°
Roll	0°
Wind Speed	0.1 Mach

The optimization process is started with the initial guesses for the PID parameters tabulated in Table.4.6.

Table.4.6. Initial Guesses of the PID Parameters

Controller	Controller Parameters		
	Kp [N/N]	Ki [N.s/N]	Kd [N/N.s]
1	500	50	50
2	500	50	50
3	120	50	50
4	60	50	50
5	30	50	50
6	10	50	50

After successive iterations the optimization process is ended up with the PID parameters tabulated in Table.4.7.

Table.4.7. Resulting Optimal PID Parameters

Controller	Controller Parameters		
	Kp (N / N)	Ki (Ns / N)	Kd (N / Ns)
1	4486	305	1534
2	6652	1750	88
3	1200	499	335
4	902	532	1799
5	511	90	45
6	25	9	12

CHAPTER V

SIMULATIONS OF THE MSS

5.1. THE MODEL MISSILE

During the simulations, the MSS will carry a model missile that is going to be moved under the effect of aerodynamic and gravitational forcing. For this purpose, a basic finner geometry seen in Figure.5.1 is chosen. The technical drawing of this geometry is given in Appendix. B Section.1.

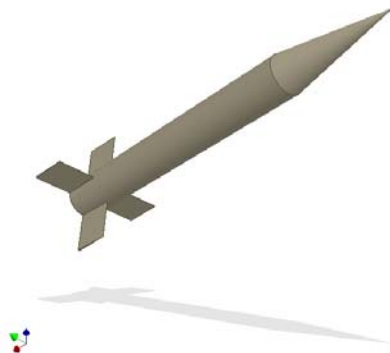


Figure.5.1. The Model Missile with Basic Finner Geometry

After selecting the geometry, the aerodynamic coefficients are found by using the software called “Missile DATCOM version 5/97” which is an aerodynamic design tool for preliminary design phase of missiles with its predictive accuracy

on the aerodynamic parameters. The reference coordinate system of the software is given in Figure.4.25 and the input file for the Missile DATCOM program is given in Appendix. B Section.2.

The range of motion for pitch angle and yaw angle are taken from Table.3.1. The aerodynamic coefficients found are given in Appendix. B. Section.3. These data are then organized as 3D look-up tables for MATLAB® in order to be interpolated by the aerodynamic module introduced in Section.4.3.4.

5.2. CASE STUDIES

In this section, the capabilities of the control system that is tuned in Section.4.3 will be demonstrated in three different cases. With the initial conditions tabulated in Table.5.1, these cases are:

- Case 1: A free fall when the tunnel is not blowing
- Case 2: At 0.1 M wind speed and -5° initial pitch angle
- Case 3: At 0.2 M wind speed and 30° initial pitch and -20° initial yaw angle

Table.5.1 The Initial Conditions of the Test Cases

	Case 1	Case 2	Case 3
X (m)	0	0	0
Y (m)	1.5	1.75	2
Z (m)	2.0	2.0	0.75
Yaw	0°	0°	-20°
Pitch	0°	-5°	30°
Roll	0°	0°	0°

Case 1

In Case 1; a free fall simulation of the basic finner geometry with a mass of 5 kg from 2 meters is performed. The simulation is terminated at 0.5 seconds before the model reaches the test section floor. The results obtained with this simulation are given in Figures 5.2 to 5.6

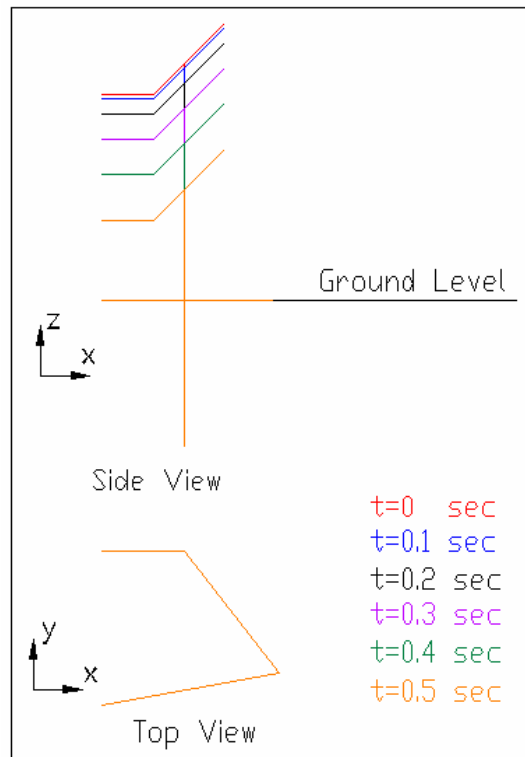


Figure.5.2 Wire Frame View of MSS at Specific Time Intervals of Case 1

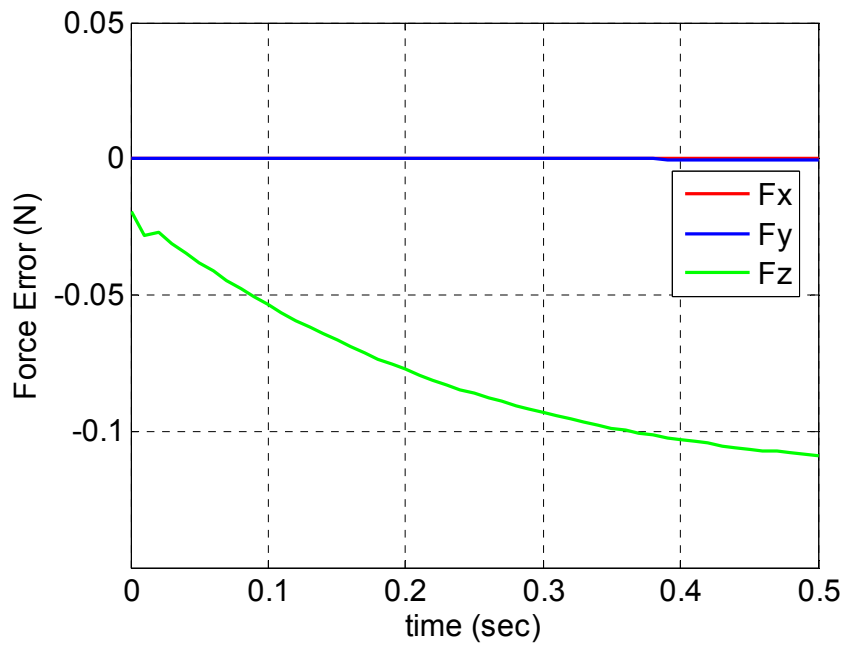


Figure.5.3 Force Error Occurred During Free Fall

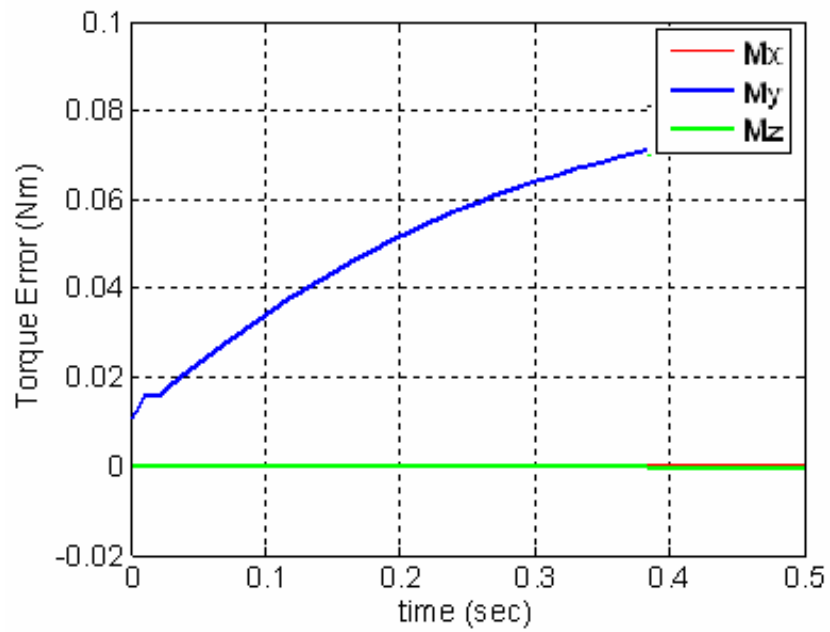


Figure.5.4 Torque Error Occurred During Free Fall

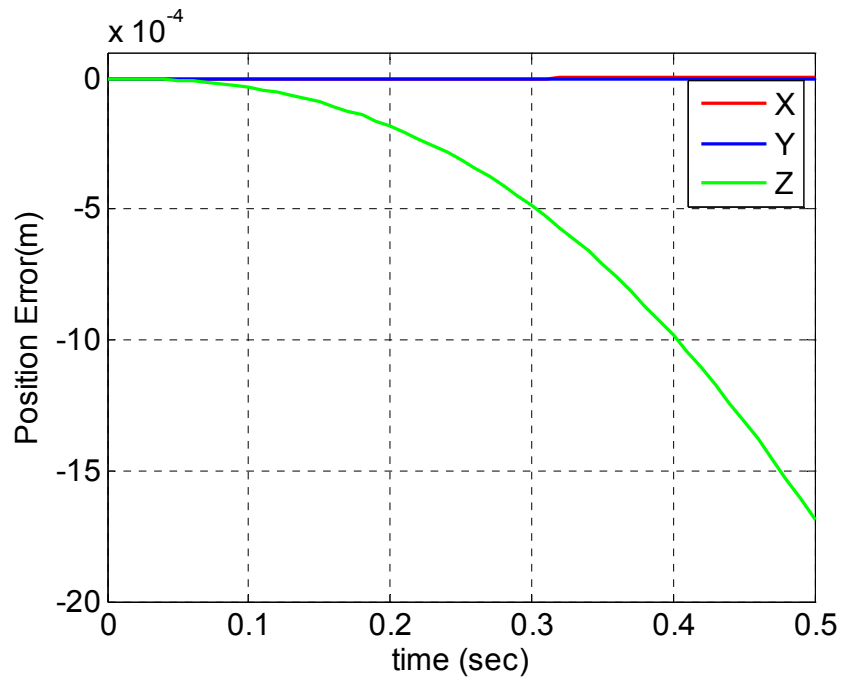


Figure.5.5 Position Error with Unconstrained Motion

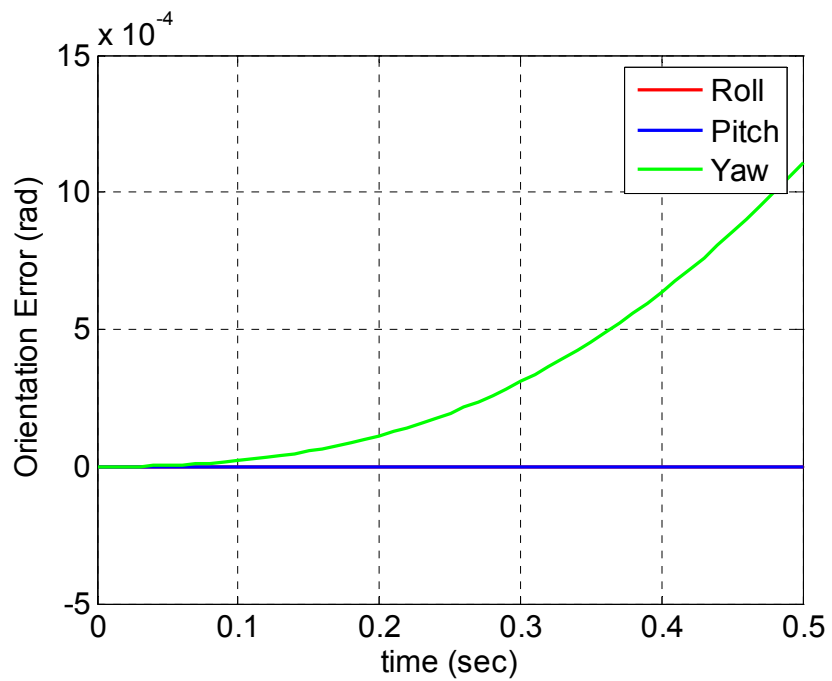


Figure.5.6 Orientation Error with Unconstrained Motion

Case 2

In Case 2; the basic finner geometry with a mass of 1 kg is left free in the flow of 0.1 Mach with -5° initial pitch angle. The simulation is terminated at 0.5 seconds before the model reaches the test section floor. The results obtained with this simulation are given in Figures 5.7 to 5.11

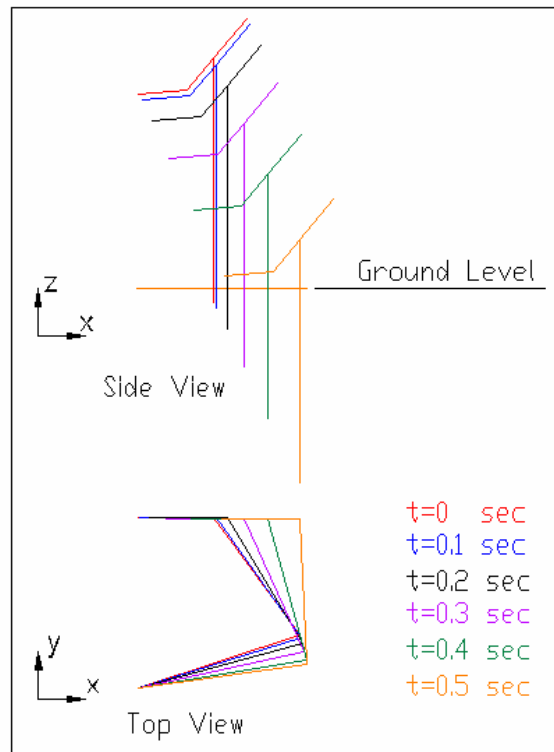


Figure.5.7 Wire Frame View of MSS at Specific Time Intervals of Case 2

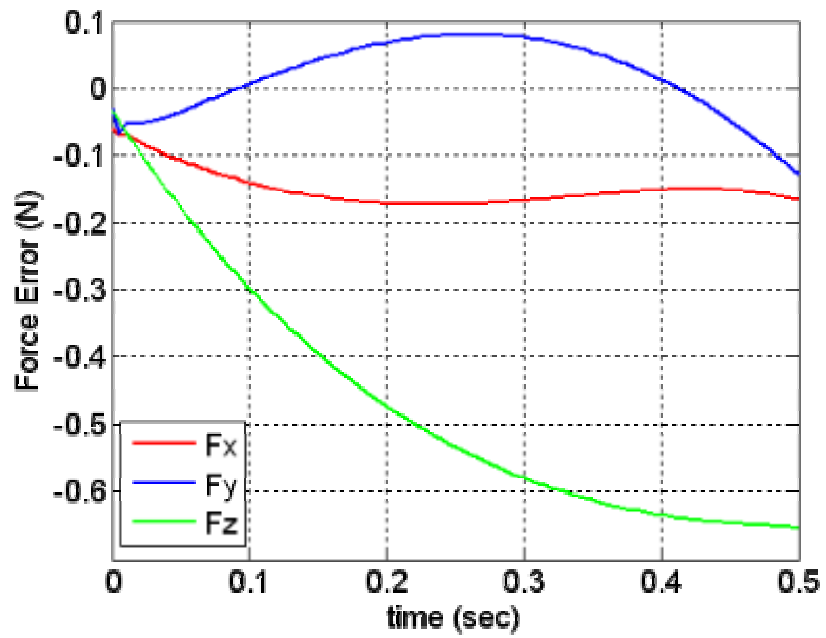


Figure.5.8 Force Error Occurred During Case 2

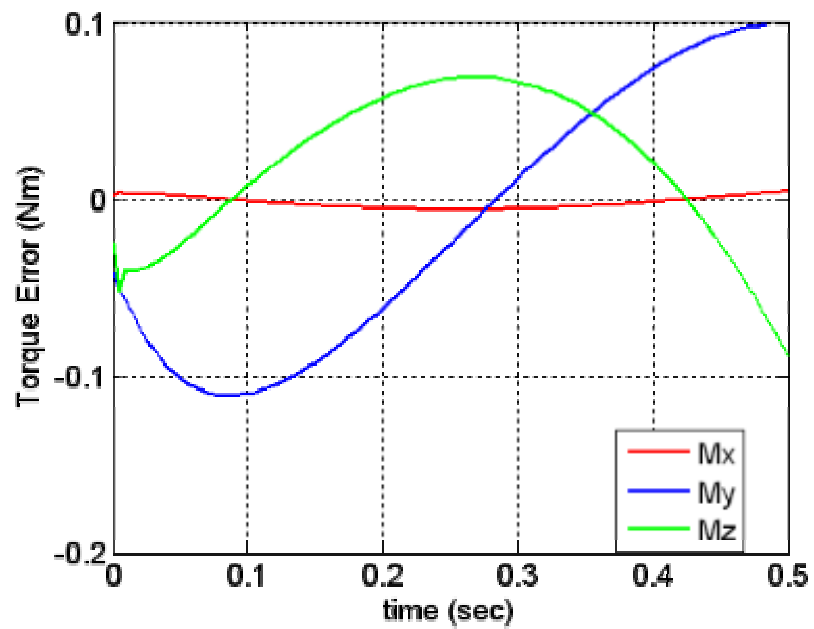


Figure.5.9 Torque Error Occurred During Case 2

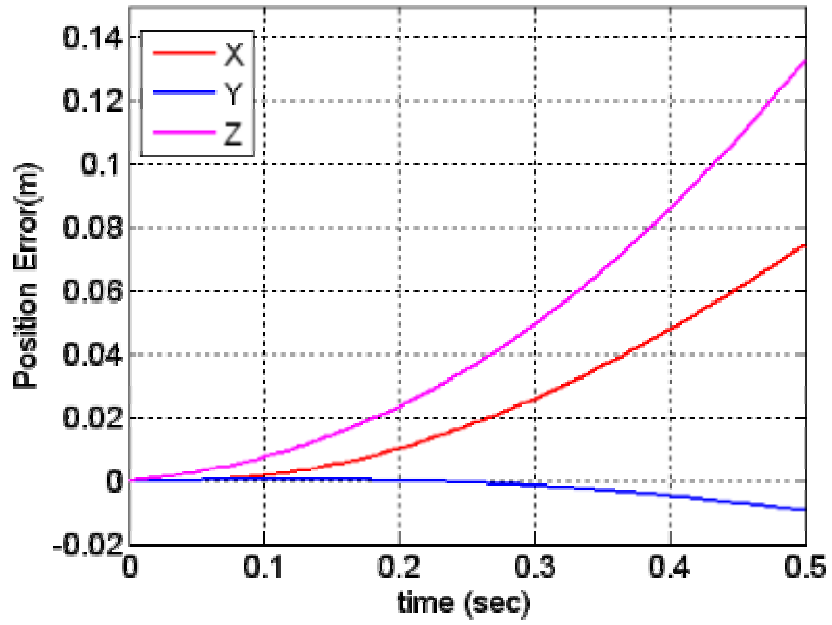


Figure.5.10 Position Error with Unconstrained Motion

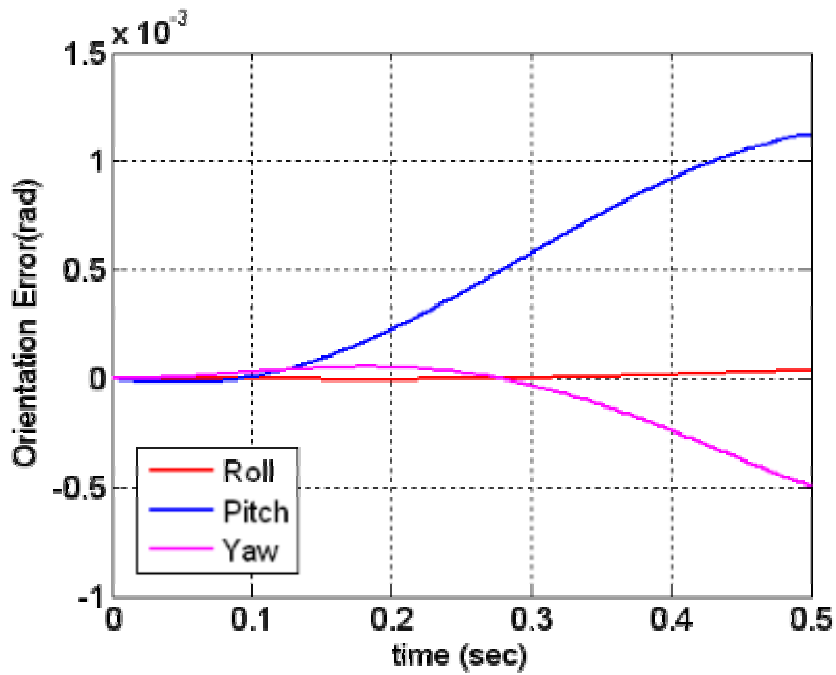


Figure.5.11 Orientation Error with Unconstrained Motion

Case 3

In Case 3; the basic finner geometry with a mass of 5 kg is left free in the flow of 0.2 Mach with 30° initial pitch angle and -20° initial side slip angle. The simulation is terminated at 0.5 seconds before the mechanism reaches the workspace boundary. The results obtained with this simulation are given in Figure 5.12 and 5.16

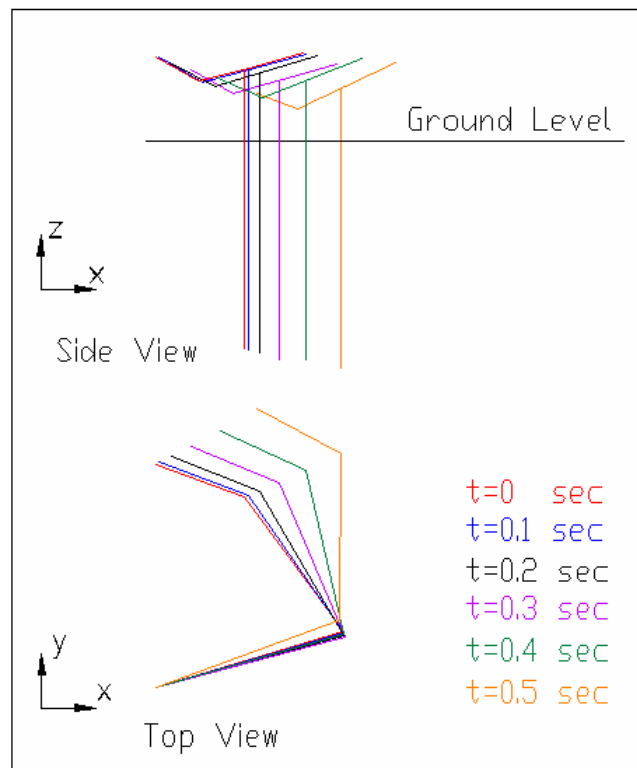


Figure.5.12 Wire Frame View of MSS at Specific Time Intervals of Case 3

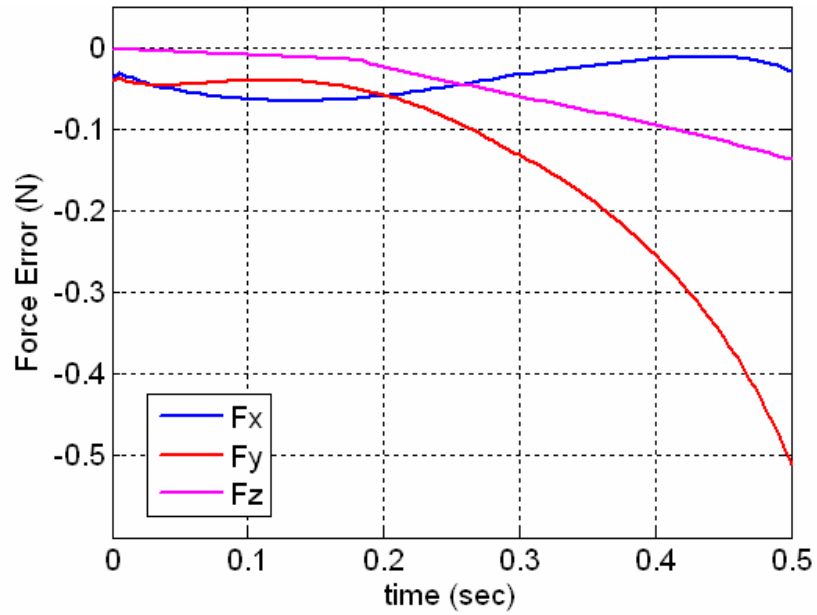


Figure.5.13 Force Error Occurred During Case 3

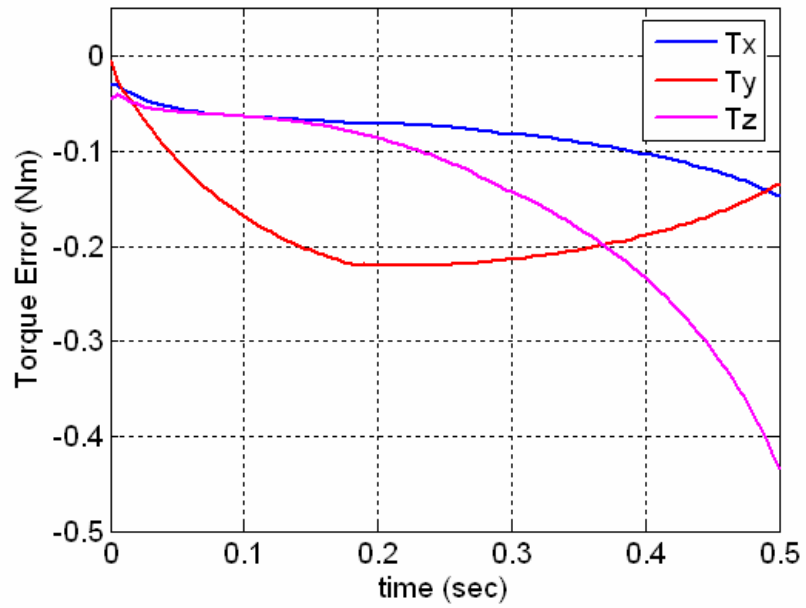


Figure.5.14 Torque Error Occurred During Case 3

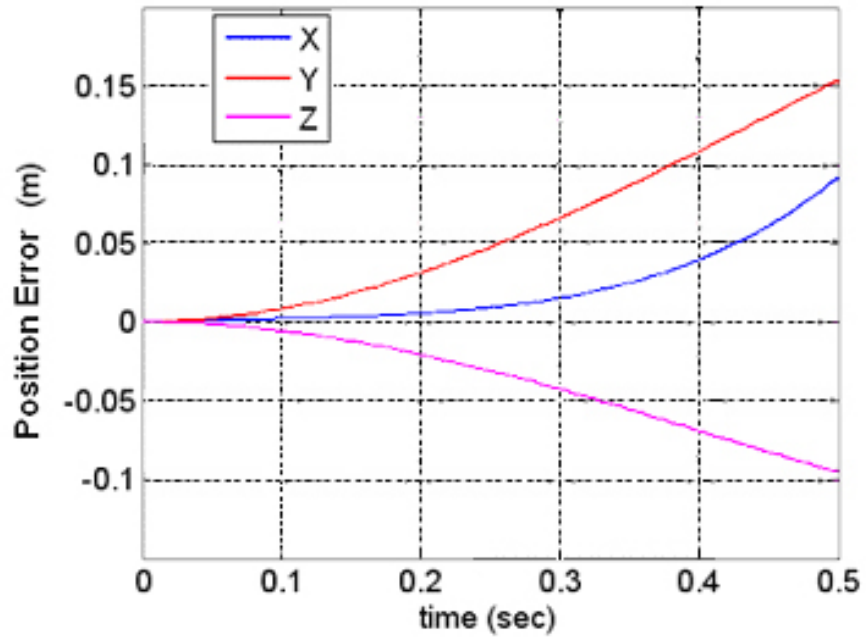


Figure.5.15 Position Error with Unconstrained Motion

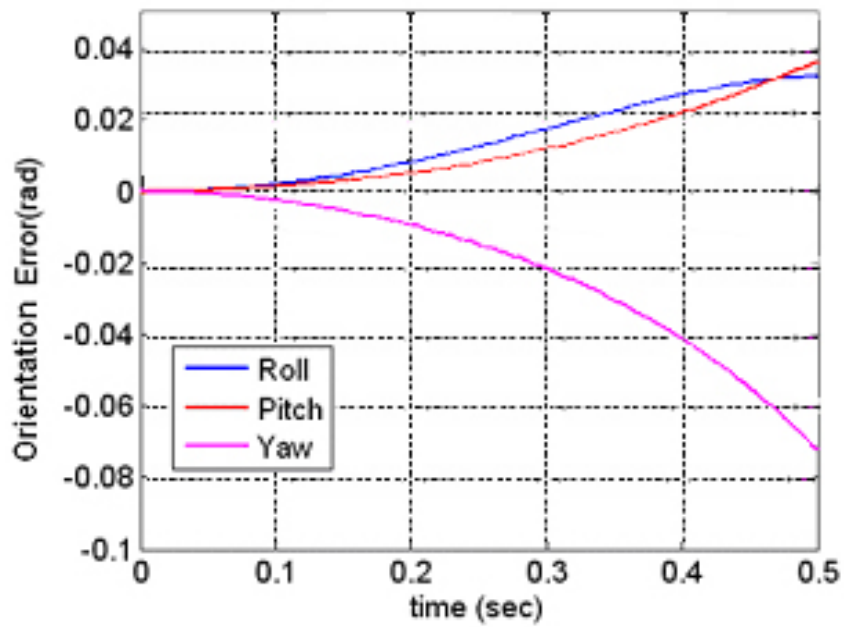


Figure.5.16 Orientation Error with Unconstrained Motion

5.3. DISCUSSION

In Case 1; the maximum error in z-axis is observed to be less than 2 mm in a travel of nearly 1.5 m. This position error is the result of the force measurement of about 0.1 N in z-axis. In Case 2; the maximum positioning error, which is the result of maximum 0.6 N interference of the MSS with a model of 1 kg mass, is computed as 14 cm. In Case 3, similar to Case 2; the 0.5 N maximum force error, results in a positioning error of 15 cm.

In these simulations, it is seen that the controller provides satisfactory results. However, during these simulations the actuators are not modeled with saturation since actuator selection is out of scope of this thesis. Therefore, in order to have a brief idea of actuator requirements, the actuators signals are examined for Case 3 and these actuator signals are tabulated in Table.5.2

Table.5.2 The Actuator Requirements for the Results Obtained

Actuator	Max. Forcing	Max. Power
1	4900 N	6000 W
2	1400 N	2000 W
3	650 N	200 W
4	300 N.m	600 W
5	450 N	200 W
6	8 N.m	5 W

These actuator inputs are reasonable. However, it should be kept in mind that these forces and torques are required to accelerate the MSS during the tests.

Due to the reason that the longer the acceleration phase lasts, the more reliable the tests become, during the acceleration phase the mechanism should travel most of its stroke and then in the remaining stroke the MSS should be decelerated safely. For this reason, the MSS should require much greater actuators to decelerate than to accelerate. As a conclusion; at the actuator selection phase of the design, the test durations and the available strokes on the joints should be carefully investigated.

CHAPTER VI

SUMMARY AND CONCLUSIONS

In this final chapter, a summary on the aims of this thesis, conceptual design of the proposed model support system, the technical background of the subject, the approach used, and some results obtained will be given. Major conclusions of the thesis work will be presented. In the last section, there will be some recommendations for the future work.

6.1. SUMMARY

In this study, two main aims are intended. One of them is to propose a conceptual mechanical design for a Model Support System with 6 degrees of freedom and the second one is to propose a control approach to this model support system concept which will allow the manipulator to be capable of performing store separation tests.

The main design criterion of a Model Support System is the blockage ratio which can be defined as the ratio of the manipulator's cross sectional area to the area of the test section. In order to keep this blockage ratio as low as possible, a design keeping four of the actuators outside the test section is selected. Since

the structural part of the system is located under the wind tunnel, the structural rigidity of the proposed system can be increased as much as needed to satisfy the design constraints. Although the system is rigid enough with a low blockage ratio, the mass properties of the links in the manipulator are rather high resulting in a bulky system.

The proposed control approach is based on the idea of minimizing the force measurements of the internal balance which is a force sensor assembled in between the model and the model support system. By minimizing the force measurements of the internal balance, the model will behave as if it is unconstrained. In other words, MSS will let the model move under the effect of aerodynamic forces and gravity only, resulting in a complete simulation of the separation problem in the wind tunnel environment.

To validate this approach a preliminary double pendulum case is studied and after obtaining satisfactory results, it is decided that this control approach can be applied to the MSS control problem.

To minimize the external effects of the MSS on the model motion, the internal balance values are compared with the desired forces that are aimed to be applied to the model. The manipulator Jacobian is used to distribute the six components of the force/torque error vector into the actuator space. Afterwards, these error signals transformed into joint space are used as the feedback information to the controller. Also to increase the efficiency of the controller, the inverse dynamics model of the proposed MSS is formed and used in order to compensate for the inertial force and torque requirements for the instantaneous motion of the manipulator. A MSS plant is modeled with MATLAB[®] Simmechanics Tool and embedded into the closed loop system model formed in MATLAB[®] Simulink environment.

For the controller tuning and the validation of the approach, an aerodynamic module is formed to calculate the aerodynamic forces on the model and the system as a function of Mach number, yaw angle, and pitch angle. Under the effect of these aerodynamic forces, the controller obtained satisfactory results upon minimization of the force error.

6.2. CONCLUSIONS

The proposed mechanical design of the six degree of freedom MSS is feasible with its low blockage ratio and high rigidity. At the mechanical design phase, the two revolute one prismatic joint configuration is selected in order the mechanism to close the gap that it requires. However later at the controller design phase, the mechanism is located off-centric in order to have a singular free workspace which is a cancellation of the described advantage. For this reason, another configuration with one revolute and two prismatic joints could also be selected with less computational problems with a similar mechanical design.

Although the control strategy developed appears to be satisfactory in accomplishing the desired task in the computer environment, some immediate problems are observed giving clues on the potential difficulties in the realization phase of this system,

First of all, the computational load of the controller with nonlinear manipulator dynamics is huge, indicating a potential difficulty in the real time application of feedforward computed torque strategy.

Secondly, the required actuator inputs to accomplish this task appear to be too large, indicating a need for using large actuators. Furthermore, two important

characteristics of real actuators; namely, the nonlinear actuator characteristics and long actuator response times for large actuators are expected to affect the performance of the system operation adversely.

The flexible nature of the links and the backlash problems in the actuators might create problems in the proper operation of the MSS. Although the static and kinetic friction is modeled in this thesis; in real life, friction will be a potential problem when the short test duration is considered. Also the blowing wind on the mechanism will behave as a disturbance on the mechanism. Although it can be modeled, it will always have an uncertainty.

6.3. RECOMMENDATIONS FOR FUTURE WORK

For the mechanical design of the MSS, first, the configuration for positioning the model on translational axis should be considered as stated in Section.6.2.

The kinematic variables are found by geometrical iterations in this study. An optimization on these variables can be held for better performance.

During the detailed mechanical design phase, the removal of the actuators of the last two joints (especially pitch actuator) located in the test section, could be considered. This could improve the blockage rate and related drawbacks might be overcome.

For the controller of the MSS, the system model can be improved with additional details like better friction models, actuator inertias, etc. This might allow to

design a more elaborate controller to deal with the coupling effects and the uncertainties in the system.

For the termination stage of the store separation test, an algorithm can be developed to compare the remaining span with the predefined maximum deceleration value. This algorithm can be used to decide the test termination point and start the system to decelerate in order the system to be stopped safely at the end of each test.

REFERENCES

- [1] Karail, K., “Image Based Flight Data Reconstruction Using Aeroballistic Range Yaw Cards”, METU Mechanical Engineering Department, M.Sc. Thesis, January 2005.
- [2] “Ankara Wind Tunnel Store Separation Test System Technical Specifications for Purchasing”, TÜBİTAK-SAGE, (Internal Document) April 2003.
- [3] Barlow, J.B., William, H.R.Jr., Pope. A. , “Low Speed Wind Tunnel Testing”, Wiley Interscience, 1999.
- [4] “Annual Report 2001”, DNW German-Dutch Wind Tunnels, URL: <http://www.dnw.aero/public/business.htm>, Last viewed: January 14, 2006.
- [5] “Report on Technical Trip to DNW&ARA”, TÜBİTAK-SAGE, (Internal Document), January 2003.

- [6] "Annual Report 2003", DNW German-Dutch Wind Tunnels, URL: <http://www.dnw.aero/public/business.htm>, Last viewed: January 14, 2006.
- [7] "Missile Model Support DNW-HST & DNW-SST", DNW German-Dutch Wind Tunnels, URL: <http://www.dnw.aero/public/business.htm>, Last viewed: January 14, 2006.
- [8] "Expo Review", Aerospace Testing International ISSN-1478-2774, p.40, June 2005.
- [9] Dede, M.İ.C., "Position / Force Control of Robot Manipulators", METU Mechanical Engineering Department, M.Sc. Thesis, April 2003.
- [10] Hogan, N., "Impedance Control: An Approach to Manipulation: Part.I: Theory", ASME Journal of Dynamic Systems, Measurements and Control, Vol. 107, pp.1-7, March 1985.
- [11] Chiaverini, S., Sciavicco L., "The Parallel Approach to Force / Position Control of Robotic Manipulators", IEEE Transactions on Robotics and Automation, Vol. 9, No. 4, pp.361-373, August 1993.
- [12] Craig, J.J., "Introduction to Robotics, Mechanics and Control", Addison-Wesley, 1989.

- [13] Denavit, J., Hartenberg, R.S., "A Kinematic Notation for Lower-Pair Mechanisms Based on Matrices", Journal of Applied Mechanics, pp.215-221, June 1955.
- [14] Özgören M.K., "A Kinematic Structure-based Classification and Compact Kinematic Equations for Six-dof Industrial Robotic Manipulators", Mechanism and Machine Theory, 36 (2001), 817-832.
- [15] Corke, P.I., " A Robotics Toolbox for MATLAB[®]", IEEE Robotics and Automation Magazine, Vol.3, No.1, pp.24-32, March 1996.
- [16] "Report on Flight Simulation Software", TÜBİTAK-SAGE, (Internal Document), January 2004.

APPENDIX A

SINGULARITY ANALYSIS FOR DOUBLE PENDULUM

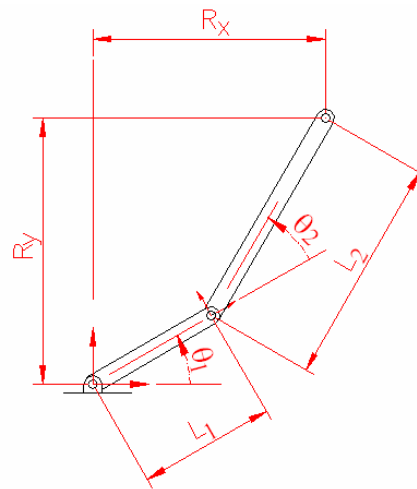


Figure.A.1 A simple R-R configuration

By using simple trigonometric relations

$$T_x = L_1 \cdot \cos(\theta_1) + L_2 \cdot \cos(\theta_1 + \theta_2) \quad (\text{A.1})$$

$$T_y = L_1 \cdot \sin(\theta_1) + L_2 \cdot \sin(\theta_1 + \theta_2) \quad (\text{A.2})$$

By squaring and adding these equations θ_2 can be found. Also since

$$\cos(\theta_1 + \theta_2) = \cos(\theta_1) \cdot \cos(\theta_2) - \sin(\theta_1) \cdot \sin(\theta_2) \quad (\text{A.3})$$

$$\sin(\theta_1 + \theta_2) = \sin(\theta_1) \cdot \cos(\theta_2) + \cos(\theta_1) \cdot \sin(\theta_2) \quad (\text{A.4})$$

The equations (A.1) and (A.2) can be rewritten in matrix form as

$$\begin{bmatrix} R_x \\ R_y \end{bmatrix} = \begin{bmatrix} L_1 + L_2 \cdot \cos(\theta_2) & -L_2 \cdot \sin(\theta_2) \\ L_2 \cdot \cos(\theta_2) & L_1 + L_2 \cdot \cos(\theta_2) \end{bmatrix} \cdot \begin{bmatrix} \cos(\theta_1) \\ \sin(\theta_1) \end{bmatrix} \quad (\text{A.5})$$

At conditions where $\Delta = 0$ a geometric singularity occurs

$$\Delta = (L_1 + L_2 \cdot \cos(\theta_2))^2 + (L_2 \cdot \sin(\theta_2))^2 \quad (\text{A.6})$$

Therefore, for a singularity to occur the required conditions are

$$L_1 = L_2 \quad (\text{A.7})$$

$$\theta_2 = \pi \quad (\text{A.8})$$

APPENDIX B

SUPPLEMENTARY MATLAB FILES

MATLAB[®] Simmechanics Model Initialization M-File

```
%%%%%%%%%%%%%%%%%%%%%%%%%%%%%%%%%%%%%%%%%%%%%%%%%%%%%%%%%%%%%%%%%%%%%%%%%%  
%% Initial Position Demands %%  
%%%%%%%%%%%%%%%%%%%%%%%%%%%%%%%%%%%%%%%%%%%%%%%%%%%%%%%%%%%%%%%%%%%%%%%%%%  
  
x=0.7708;  
y=1.5;  
yaw=-20*pi/180;  
  
%%%%%%%%%%%%%%%%%%%%%%%%%%%%%%%%%%%%%%%%%%%%%%%%%%%%%%%%%%%%%%%%%%%%%%%%%%  
%% Calculations to Reach %%  
%% Initial Position Demands %%  
%%%%%%%%%%%%%%%%%%%%%%%%%%%%%%%%%%%%%%%%%%%%%%%%%%%%%%%%%%%%%%%%%%%%%%%%%%  
  
t=(x^2+y^2-1.75^2-1.5^2)/(2*1.75*1.5);  
q(2)=acos(t);  
P=[x;y];  
J=[1.75+1.5*cos(q(2)) -1.5*sin(q(2));1.5*sin(q(2)) 1.75+1.5*cos(q(2))];  
Jt=inv(J);  
teta1=Jt*P;  
q(1)=atan2(teta1(2),teta1(1));  
q(3)=pi+yaw-q(2)-q(1);  
  
%%%%%%%%%%%%%%%%%%%%%%%%%%%%%%%%%%%%%%%%%%%%%%%%%%%%%%%%%%%%%%%%%%%%%%%%%%  
%% Joint Initial Conditions %%  
%%%%%%%%%%%%%%%%%%%%%%%%%%%%%%%%%%%%%%%%%%%%%%%%%%%%%%%%%%%%%%%%%%%%%%%%%%  
  
joint1_IC=q(1)*180/pi; %deg (calculated)  
joint2_IC=q(2)*180/pi; %deg (calculated)  
joint3_IC=0.0198; %deg  
joint4_IC=q(3)*180/pi; %deg (calculated)
```

```

joint5_IC=60;      %deg
joint6_IC=0;      %deg

%%%%%%%%%%

%%%%%%%%%%
%% Kinematic values of MSS %%
%%%%%%%%%%
a1=1.75;
a2=1.5;
a3=0;
a4=0;
a5=0.3;
a6=0;
d6=0.8;
c

%%%%%%%%%%
%% Mass Properties of Links %%
%%%%%%%%%%
m1=246; %kg
m2=103; %kg
m3=0; %kg
m4=44; %kg
m5=20; %kg
m6=5; %kg

% Ixx Iyx Izx Ixy Iyy Izy Ixz Iyz Izz
J1=[480 208.8 0 ; 208.8 387 0 ; 0 0 866 ];
J2=[113 0.14 18.13 ; 0.14 87 -0.07 ; 18.13 -0.07 87 ];
J3=[0 0 0 ; 0 0 0 ; 0 0 0 ];
J4=[31.1 0 0 ; 0 31.1 0 ; 0 0 0.15 ];
J5=[0.87 0 -0.24 ; 0 1 0 ; -0.24 0 0.22 ];
J6=[0.22 0 0 ; 0 0.22 0 ; 0 0 0.002];

%mass center locations of links in the corresponding link frames
c1=[-0.954;0.653;0]; %m
c2=[-0.647;0;0.494]; %m
c3=[0;0;0]; %m
c4=[0;0;-1.275]; %m
c5=[-0.029;0;0.02]; %m
c6=[0;0;-0.375]; %m

%%%%%%%%%%

%%%%%%%%%%
%% Geometric Locations of
%% Connection Points %%
%%%%%%%%%%
ground=[0;0;0];
%base of the mechanism

```

```

ground2=[ground(1)+0.12 ground(2)-0.991 0] ;
%the connection of piston1 base relative to the world
connectionpoint_link1_piston1=[-0.3288 0.05846 0];
% the connection point of the piston1 tip to link1
% (relative to the ground1 in link1 coordinates)
connectionpoint_link1_piston2=[-.222 -.9845 0];
% the connection point of piston2 base to link1
%(relative to the axis of the second revolute joint in link1 coordinates)
connectionpoint_link2_piston2=[0.0191 0.3645 0];
%the connection point of piston2 tip to link2
%(relative to the axis of the second revolute joint in link2 coordinates)

%%%%%%%%%%%%%%%%%%%%%%%%%%%%%%%%%%%%%%%%%%%%%%%%%%%%%%%%%%%%%%%%%%%%%%%%
%% Calculations for link Orientations %%
%% for linear Actuators %%
%% Due to Initial Conditions %%
%%%%%%%%%%%%%%%%%%%%%%%%%%%%%%%%%%%%%%%%%%%%%%%%%%%%%%%%%%%%%%%%%%%%%%%%

%calculation for piston1_IC
h01= sqrt(connectionpoint_link1_piston1(1)^2+connectionpoint_link1_piston1(2)^2);
h02= sqrt(ground2(1)^2+ground2(2)^2);
A04=atan2(0.05846,-0.3288)+joint1_IC*pi/180;
A02=atan2 (ground2(2) , ground2(1));
A05=2*pi()-A04+A02;
h04=sqrt(h01^2+h02^2-2*h01*h02*cos(A05));
A06=acos ( (h04^2+h02^2-h01^2) / (2*h04*h02) );
piston1_orient=pi()+A02+A06;
connection_l1_p1_IC=[(ground2(1)+h04*cos(piston1_orient)),(ground2(2)+h04*sin(piston1_orient)),0]

%calculation for piston2_IC
h11= sqrt(connectionpoint_link2_piston2(1)^2+connectionpoint_link2_piston2(2)^2);
h12= sqrt(connectionpoint_link1_piston2(1)^2+connectionpoint_link1_piston2(2)^2);
A14=atan2(0.3645,0.0191)+joint2_IC*pi()/180;
A12=atan2 (connectionpoint_link1_piston2(2) , connectionpoint_link1_piston2(1));
A15=2*pi()-A14+A12;
h14=sqrt(h11^2+h12^2-2*h11*h12*cos(A15));
A16=acos ( (h14^2+h12^2-h11^2) / (2*h14*h12) );
piston2_orient=pi()+A12+A16;
connection_l2_p2_IC=[(connectionpoint_link1_piston2(1)+h14*cos(piston2_orient)),(connectionpoint_l1_piston2(2)+h14*sin(piston2_orient)),0];

%calculation for piston3_IC
h21=0.300;
h22=0.590;
connectionpoint_link5_piston3=[-h21*cos(40/180*pi()) 0 -h21*sin(40/180*pi());
A22=(40+joint5_IC)*pi()/180;
h24=sqrt(h21^2+h22^2-2*h21*h22*cos(A22));
piston3_orient= atan2( h22+h21*cos(A22-pi/2), h21*sin(A22-pi/2));
connection_p3tip_ic=[-h21*sin(A22) -h21*cos(A22) 0];
p3_IC=sqrt(h21^2+h22^2-2*h21*h22*cos((joint3_IC+40)*pi/180));

```

```

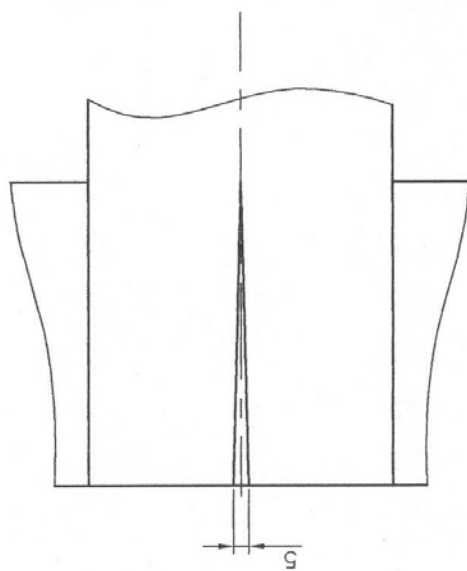
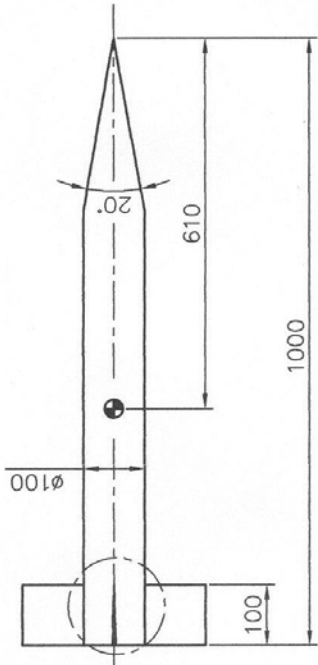
%robot object for robotic toolbox
%alpha A theta D sigma m rx ry rz Ixx Iyy Izz Ixy Iyz Ixz Jm G
L{1}=link([ 0 , 1.75 , 0 , 0 , 0 , 246 , -0.954 , 0.653 , 0 , 480 , 387 , 866 , 208.8 , 0 , 0
,0,0,0,0]);
L{2}=link([ 0 , 1.5 , 0 , 0 , 0 , 103 , -0.647 , 0 , -0.494 , 113 , 87 , 87 , 0.14 , -0.07 , 18.13
,0,0,0,0]);
L{3}=link([ 0 , 0 , 0 , 0 , 1 , 0 , 0 , 0 , 0 , 0 , 0 , 0 , 0 , 0 , 0 , 0,0,0,0,0]);
L{4}=link([ -pi()/2 , 0 , 0 , 0 , 0 , 44 , 0 , 0 , -1.275 , 31.1 , 31.1 , 0.15 , 0 , 0 , 0
,0,0,0,0]);
L{5}=link([ pi()/2 , 0.3 , 0 , 0 , 0 , 20 , -0.029 , 0 , .320 , 0.87 , 1 , 0.22 , 0 , 0 , -0.24
,0,0,0,0]);
L{6}=link([ 0 , 0 , 0 , 0.8 , 0 , 5 , 0 , 0 , -0.375 , 0.22 , 0.22 , 0.002 , 0 , 0 , 0
,0,0,0,0]);
mss=robot(L);
n=6;

```

APPENDIX C

INFORMATION RELATED TO THE SIMULATIONS

SECTION 1. Technical Drawing of Basic Finner Geometry



A (1:2)

TÜRKİYE BİLİMSEL VE TEKNİK ARAŞTIRMA KURUMU SAVUNMA SANAYİ ARAŞTIRMA VE GELİŞTİRME ENSTİTÜSÜ		TARİHİ		GİZLİLİK DEREJESİ	
TASARIMCI	ADI SOYADI	İMZA	TARİHİ	MALZEME	
ÇİZEN	MEHMET ULUSAL		30.08.2005		
KONT. EDEN					
KONT. EDEN					
KONT. EDEN					
ONAYLAYAN					
PROJE/KISIM	MODEL_SUPPORT_SYSTEM			BELGE NO	
ÜST BÜTÜN				SAYFA	

1. BU BELGE VE İÇERİĞİ TÜBİTAK-SAGE'YE AITIR.
2. ÇOCUKLARI VEYA KULLANILMASI TÜBİTAK-SAGE'NİN İZİNİNE BAĞLIDIR.
3. AKSİ BELİRTİLMEDİKÇE ÖLÇÜLER mm'DİR.
4. GENEL TOLERANSLAR ISO 2768-TS'NE GÖRE BELİRLENMİŞTİR.
5. BELİRTİLMİYEN YARIÇAP VE PAHLAR: --
6. TOPLAM KÜTLE: KÜTLE.GR



ÖLÇEK: 1/10

BASIC
FINNER_GEOMETRY

SECTION 2. Missile DATCOM Code to Obtain the Aerodynamic Coefficients

```
1 CASEID BASIC FINNER
2 DIM M
3 DERIV RAD
4 $REFQ
5 SREF= 0.007854,LREF= 0.1,LATREF= 0.100,
6 BLAYER=NATURAL,RHR=280.000000,XCG= 0.61,ZCG= 0.00000,
7 SCALE=1.0,
8 $END
9 $AXIBOD
10 TNOSE=CONICAL,
11 X0=0.0, LNOSE= 0.284,
12 DNOSE= 0.1 ,BNOSE= 0.0001,TRUNC=.FALSE.,
13 LCENTR= 0.716, DCENTR= 0.1, DEXIT= 0.000,
14 $END
15 $FINSET1
16 SECTYP=HEX,
17 NPANEL=4.,
18 PHIF=0.,90.,180.,270.,
19 XLE(1)=0.90,
20 XLE(2)=0.90,
21 STA=0.0,
22 SSPAN(1)=0.1,
23 SSPAN(2)=0.2,
24 CHORD(1)=0.1,
25 CHORD(2)=0.1,
26 ZUPPER=0.25,0.25,
27 LMAXU=0.9999,0.9999,
28 LFLATU=0.0001,0.0001,
29 $END
30 $FLTCON
31 NMACH= 3.0,NALPHA= 10.0,ALT= 0.00,
32 MACH(1)= 0.1, 0.2, 0.3,
33 ALPHA(1)= -5.000, 0.000, 5.000, 10.000, 15.000,
34 ALPHA(6)= 20.000, 25.000, 30.000, 35.000, 40.000,
35 $END
36 SPIN
37 DAMP
38 SAVE
39 NEXT CASE
40 $FLTCON
41 BETA=-40.00,
```

42 \$END
43 SPIN
44 DAMP
45 SAVE
46 NEXT CASE
47 \$FLTCON
48 BETA=-30.00,
49 \$END
50 SPIN
51 DAMP
52 SAVE
53 NEXT CASE
54 \$FLTCON
55 BETA=-20.00,
56 \$END
57 SPIN
58 DAMP
59 SAVE
60 NEXT CASE
61 \$FLTCON
62 BETA=-10.00,
63 \$END
64 SPIN
65 DAMP
66 SAVE
67 NEXT CASE
68 \$FLTCON
69 BETA=0.00,
70 \$END
71 SPIN
72 DAMP
73 SAVE
74 NEXT CASE
75 \$FLTCON
76 BETA=10.00,
77 \$END
78 SPIN
79 DAMP
80 SAVE
81 NEXT CASE
82 \$FLTCON
83 BETA=20.00,
84 \$END
85 SPIN
86 DAMP
87 SAVE

88 NEXT CASE
89 \$FLTCON
90 BETA=30.00,
91 \$END
92 SPIN
93 DAMP
94 SAVE
95 NEXT CASE
96 \$FLTCON
97 BETA=40.00,
98 \$END
99 SPIN
100 DAMP
101 SAVE

SECTION 3. Aerodynamic Coefficients of Basic Finner Geometry

CN Values

M=0.1

		Yaw Angle								
		-40	-30	-20	-10	0	10	20	30	40
Pitch Angle	-5	-0.82	-0.916	-1.085	-1.211	-1.234	-1.211	-1.085	-0.916	-0.82
	0	0	0	0	0	0	0	0	0	0
	5	0.824	0.916	1.085	1.211	1.234	1.211	1.085	0.916	0.824
	10	1.888	2.141	2.581	2.829	2.947	2.829	2.581	2.141	1.888
	15	3.181	3.736	4.348	4.711	4.683	4.711	4.348	3.736	3.181
	20	4.79	5.595	6.122	6.291	6.284	6.291	6.122	5.595	4.79
	25	6.449	7.215	7.428	7.402	7.37	7.402	7.428	7.215	6.449
	30	8.091	8.438	8.509	8.518	8.515	8.518	8.509	8.438	8.091
	35	9.3	9.59	9.733	9.785	9.797	9.785	9.733	9.59	9.3
	40	10.47	10.822	10.982	11.05	11.068	11.05	10.982	10.822	10.47

M=0.2

		Yaw Angle								
		-40	-30	-20	-10	0	10	20	30	40
Pitch Angle	-5	-0.70	-0.835	-1.036	-1.154	-1.174	-1.154	-1.036	-0.835	-0.70
	0	0	0	0	0	0	0	0	0	0
	5	0.701	0.835	1.036	1.154	1.174	1.154	1.036	0.835	0.701
	10	1.652	1.981	2.516	2.768	2.89	2.768	2.516	1.981	1.652
	15	2.822	3.495	4.264	4.689	4.664	4.689	4.264	3.495	2.822
	20	4.301	5.274	5.998	6.313	6.311	6.313	5.998	5.274	4.301
	25	5.834	6.806	7.219	7.352	7.382	7.352	7.219	6.806	5.834
	30	7.381	7.921	8.197	8.345	8.39	8.345	8.197	7.921	7.381
	35	8.452	8.919	9.215	9.372	9.42	9.372	9.215	8.919	8.452
	40	9.461	9.904	10.174	10.318	10.363	10.318	10.174	9.904	9.461

M=0.3

		Yaw Angle								
		-40	-30	-20	-10	0	10	20	30	40
Pitch Angle	-5	-0.56	-0.685	-0.866	-1.006	-1.021	-1.006	-0.866	-0.685	-0.56
	0	0	0	0	0	0	0	0	0	0
	5	0.565	0.685	0.866	1.006	1.021	1.006	0.866	0.685	0.565
	10	1.411	1.71	2.24	2.605	2.738	2.605	2.24	1.71	1.411
	15	2.476	3.142	3.968	4.556	4.601	4.556	3.968	3.142	2.476
	20	3.859	4.917	5.744	6.149	6.224	6.149	5.744	4.917	3.859
	25	5.314	6.507	7.013	7.243	7.311	7.243	7.013	6.507	5.314
	30	6.867	7.676	8.085	8.29	8.354	8.29	8.085	7.676	6.867
	35	7.868	8.67	9.072	9.275	9.332	9.275	9.072	8.67	7.868
	40	8.705	9.39	9.866	10.072	10.133	10.072	9.866	9.39	8.705

CM Values

M=0.1

		Yaw Angle								
		-40	-30	-20	-10	0	10	20	30	40
Pitch Angle	-5	0.437	0.671	1.332	2.013	2.339	2.013	1.332	0.671	0.437
	0	0	0	0	0	0	0	0	0	0
	5	-0.437	-0.671	-1.332	-2.013	-2.339	-2.013	-1.332	-0.671	-0.437
	10	-1.617	-2.279	3.868	-5.083	-5.747	-5.083	3.868	-2.279	-1.617
	15	-3.483	-4.988	-7.103	-8.677	-8.84	-8.677	-7.103	-4.988	-3.483
	20	-6.295	-8.438	-10.18	-11.03	-11.19	-11.03	-10.18	-8.438	-6.295
	25	-9.206	-11.04	-11.62	-11.68	-11.68	-11.68	-11.62	-11.04	-9.206
	30	-11.99	-12.30	-12.23	-12.23	-12.24	-12.23	-12.23	-12.30	-11.99
	35	-13.34	-13.26	-13.23	-13.21	-13.20	-13.21	-13.23	-13.26	-13.34
	40	-14.61	-14.46	-14.32	-14.22	-14.19	-14.22	-14.32	-14.46	-14.61

M=0.2

		Yaw Angle								
		-40	-30	-20	-10	0	10	20	30	40
Pitch Angle	-5	0.412	0.588	1.172	1.825	2.148	1.825	1.172	0.588	0.412
	0	0	0	0	0	0	0	0	0	0
	5	-0.412	-0.588	-1.172	-1.825	-2.148	-1.825	-1.172	-0.588	-0.412
	10	-1.615	-2.158	-3.656	-4.873	-5.555	-4.873	-3.656	-2.158	-1.615
	15	-3.515	-4.895	-6.97	-8.589	-8.759	-8.589	-6.97	-4.895	-3.515
	20	-6.4	-8.489	-10.23	-11.08	-11.25	-11.08	-10.23	-8.489	-6.4
	25	-9.47	-11.34	-11.91	-12.01	-12.03	-12.01	-11.91	-11.34	-9.474
	30	-12.62	-12.94	-12.93	-12.94	-12.95	-12.94	-12.93	-12.94	-12.62
	35	-14.32	-14.29	-14.23	-14.19	-14.17	-14.19	-14.23	-14.29	-14.32
	40	-15.9	-15.74	-15.57	-15.45	-15.41	-15.45	-15.57	-15.74	-15.9

M=0.3

		Yaw Angle								
		-40	-30	-20	-10	0	10	20	30	40
Pitch Angle	-5	0.275	0.353	0.784	1.356	1.664	1.356	0.784	0.353	0.275
	0	0	0	0	0	0	0	0	0	0
	5	-0.275	-0.353	-0.784	-1.356	-1.664	-1.356	-0.784	-0.353	-0.275
	10	-1.456	-1.793	-3.164	-4.358	-5.072	-4.358	-3.164	-1.793	-1.456
	15	-3.355	-4.547	-6.672	-8.406	-8.59	-8.406	-6.672	-4.547	-3.355
	20	-6.335	-8.436	-10.37	-11.36	-11.54	-11.36	-10.37	-8.436	-6.335
	25	-9.722	-11.81	-12.56	-12.84	-12.94	-12.84	-12.56	-11.81	-9.722
	30	-13.60	-14.06	-14.28	-14.38	-14.42	-14.38	-14.28	-14.06	-13.60
	35	-15.96	-16.02	-16.01	-15.99	-15.98	-15.99	-16.01	-16.02	-15.96
	40	-18.09	-17.9	-17.67	-17.54	-17.50	-17.54	-17.67	-17.9	-18.09

CA

M=0.1

		Yaw Angle								
		-40	-30	-20	-10	0	10	20	30	40
Pitch Angle	-5	1.08	1.11	1.10	1.15	1.15	1.15	1.10	1.11	1.08
	0	1.08	0.93	1.11	1.15	1.15	1.15	1.11	0.93	1.08
	5	1.08	1.11	1.10	1.15	1.15	1.15	1.10	1.11	1.08
	10	1.08	1.11	1.09	1.14	1.15	1.14	1.09	1.11	1.08
	15	1.08	1.11	1.05	1.12	1.14	1.12	1.05	1.11	1.08
	20	1.07	1.10	1.00	1.09	1.11	1.09	1.00	1.10	1.07
	25	1.07	1.09	1.11	1.01	1.04	1.01	1.11	1.09	1.07
	30	1.06	1.08	1.10	1.11	0.93	1.11	1.10	1.08	1.06
	35	1.06	1.07	1.09	1.10	1.10	1.10	1.09	1.07	1.06
	40	1.05	1.06	1.07	1.08	1.08	1.08	1.07	1.06	1.05

M=0.2

		Yaw Angle								
		-40	-30	-20	-10	0	10	20	30	40
Pitch Angle	-5	1.14	1.17	1.16	1.21	1.21	1.21	1.16	1.17	1.14
	0	1.14	1.01	1.17	1.21	1.21	1.21	1.17	1.01	1.14
	5	1.14	1.17	1.16	1.21	1.21	1.21	1.16	1.17	1.14
	10	1.14	1.17	1.14	1.20	1.21	1.20	1.14	1.17	1.14
	15	1.13	1.16	1.12	1.18	1.20	1.18	1.12	1.16	1.13
	20	1.13	1.16	1.07	1.14	1.17	1.14	1.07	1.16	1.13
	25	1.12	1.15	1.17	1.08	1.10	1.08	1.17	1.15	1.12
	30	1.12	1.14	1.16	1.17	1.01	1.17	1.16	1.14	1.12
	35	1.11	1.13	1.14	1.15	1.15	1.15	1.14	1.13	1.11
	40	1.10	1.12	1.13	1.14	1.14	1.14	1.13	1.12	1.10

M=0.3

		Yaw Angle								
		-40	-30	-20	-10	0	10	20	30	40
Pitch Angle	-5	1.28	1.32	1.31	1.36	1.36	1.36	1.31	1.32	1.28
	0	1.29	1.18	1.32	1.36	1.36	1.36	1.32	1.18	1.29
	5	1.28	1.32	1.31	1.36	1.36	1.36	1.31	1.32	1.28
	10	1.28	1.31	1.30	1.35	1.36	1.35	1.30	1.31	1.28
	15	1.28	1.31	1.27	1.33	1.35	1.33	1.27	1.31	1.28
	20	1.28	1.30	1.23	1.30	1.32	1.30	1.23	1.30	1.28
	25	1.27	1.30	1.32	1.24	1.27	1.24	1.32	1.30	1.27
	30	1.26	1.29	1.30	1.31	1.18	1.31	1.30	1.29	1.26
	35	1.26	1.28	1.29	1.30	1.30	1.30	1.29	1.28	1.26
	40	1.25	1.26	1.28	1.28	1.29	1.28	1.28	1.26	1.25

CY VALUES

M=0.1

		Yaw Angle								
		-40	-30	-20	-10	0	10	20	30	40
Pitch Angle	-5	11.06	8.52	6.29	2.92	0	-2.92	-6.29	-8.52	-11.06
	0	11.07	8.52	6.28	2.95	0	-2.95	-6.28	-8.52	-11.07
	5	11.06	8.52	6.29	2.92	0	-2.92	-6.29	-8.52	-11.06
	10	11.05	8.52	6.29	2.83	0	-2.83	-6.29	-8.52	-11.05
	15	11.02	8.52	6.26	2.83	0	-2.83	-6.26	-8.52	-11.02
	20	10.98	8.51	6.12	2.58	0	-2.58	-6.12	-8.51	-10.98
	25	10.92	8.49	5.88	2.37	0	-2.37	-5.88	-8.49	-10.92
	30	10.82	8.44	5.60	2.14	0	-2.14	-5.60	-8.44	-10.82
	35	10.69	8.33	5.23	2.01	0	-2.01	-5.23	-8.33	-10.69
	40	10.47	8.09	4.79	1.89	0	-1.89	-4.79	-8.09	-10.47

M=0.2

		Yaw Angle								
		-40	-30	-20	-10	0	10	20	30	40
Pitch Angle	-5	10.35	8.38	6.32	2.87	0	-2.87	-6.32	-8.38	-10.35
	0	10.36	8.39	6.31	2.89	0	-2.89	-6.31	-8.39	-10.36
	5	10.35	8.38	6.32	2.87	0	-2.87	-6.32	-8.38	-10.35
	10	10.32	8.35	6.31	2.77	0	-2.77	-6.31	-8.35	-10.32
	15	10.26	8.29	6.22	2.77	0	-2.77	-6.22	-8.29	-10.26
	20	10.17	8.20	6.00	2.52	0	-2.52	-6.00	-8.20	-10.17
	25	10.06	8.08	5.66	2.25	0	-2.25	-5.66	-8.08	-10.06
	30	9.90	7.92	5.27	1.98	0	-1.98	-5.27	-7.92	-9.90
	35	9.71	7.71	4.81	1.81	0	-1.81	-4.81	-7.71	-9.71
	40	9.46	7.38	4.30	1.65	0	-1.65	-4.30	-7.38	-9.46

M=0.3

		Yaw Angle								
		-40	-30	-20	-10	0	10	20	30	40
Pitch Angle	-5	10.12	8.34	6.21	2.71	0	-2.71	-6.21	-8.34	-10.12
	0	10.13	8.35	6.22	2.74	0	-2.74	-6.22	-8.35	-10.13
	5	10.12	8.34	6.21	2.71	0	-2.71	-6.21	-8.34	-10.12
	10	10.07	8.29	6.15	2.61	0	-2.61	-6.15	-8.29	-10.07
	15	10	8.21	6.02	2.56	0	-2.56	-6.02	-8.21	-10
	20	9.87	8.09	5.74	2.24	0	-2.24	-5.74	-8.09	-9.87
	25	9.65	7.92	5.35	1.97	0	-1.97	-5.35	-7.92	-9.65
	30	9.39	7.68	4.92	1.71	0	-1.71	-4.92	-7.68	-9.39
	35	9.07	7.37	4.42	1.56	0	-1.56	-4.42	-7.37	-9.07
	40	8.71	6.87	3.86	1.41	0	-1.41	-3.86	-6.87	-8.71

CLN VALUES

M=0.1

		Yaw Angle								
		-40	-30	-20	-10	0	10	20	30	40
Pitch Angle	-5	-14.20	-12.24	-11.16	-5.59	0	5.59	11.16	12.24	14.20
	0	-14.19	-12.24	-11.19	-5.75	0	5.75	11.19	12.24	14.19
	5	-14.20	-12.24	-11.16	-5.59	0	5.59	11.16	12.24	14.20
	10	-14.23	-12.23	-11.03	-5.08	0	5.08	11.03	12.23	14.23
	15	-14.27	-12.23	-10.75	-4.85	0	4.85	10.75	12.23	14.27
	20	-14.32	-12.23	-10.18	-3.87	0	3.87	10.18	12.23	14.32
	25	-14.39	-12.26	-9.33	-3.06	0	3.06	9.33	12.26	14.39
	30	-14.47	-12.30	-8.44	-2.28	0	2.28	8.44	12.30	14.47
	35	-14.54	-12.28	-7.41	-1.89	0	1.89	7.41	12.28	14.54
	40	-14.61	-11.99	-6.30	-1.62	0	1.62	6.30	11.99	14.61

M=0.2

		Yaw Angle								
		-40	-30	-20	-10	0	10	20	30	40
Pitch Angle	-5	-15.42	-12.95	-11.22	-5.39	0	5.39	11.22	12.95	15.42
	0	-15.41	-12.95	-11.26	-5.56	0	5.56	11.26	12.95	15.41
	5	-15.42	-12.95	-11.22	-5.39	0	5.39	11.22	12.95	15.42
	10	-15.45	-12.94	-11.09	-4.87	0	4.87	11.09	12.94	15.45
	15	-15.50	-12.94	-10.81	-4.64	0	4.64	10.81	12.94	15.50
	20	-15.57	-12.94	-10.23	-3.66	0	3.66	10.23	12.94	15.57
	25	-15.66	-12.94	-9.38	-2.88	0	2.88	9.38	12.94	15.66
	30	-15.74	-12.95	-8.49	-2.16	0	2.16	8.49	12.95	15.74
	35	-15.83	-12.91	-7.47	-1.83	0	1.83	7.47	12.91	15.83
	40	-15.90	-12.63	-6.40	-1.62	0	1.62	6.40	12.63	15.90

M=0.3

		Yaw Angle								
		-40	-30	-20	-10	0	10	20	30	40
Pitch Angle	-5	-17.52	-14.41	-11.50	-4.90	0	4.90	11.50	14.41	17.52
	0	-17.50	-14.42	-11.54	-5.07	0	5.07	11.54	14.42	17.50
	5	-17.52	-14.41	-11.50	-4.90	0	4.90	11.50	14.41	17.52
	10	-17.55	-14.39	-11.36	-4.36	0	4.36	11.36	14.39	17.55
	15	-17.60	-14.35	-11.04	-4.13	0	4.13	11.04	14.35	17.60
	20	-17.68	-14.28	-10.37	-3.16	0	3.16	10.37	14.28	17.68
	25	-17.78	-14.19	-9.41	-2.42	0	2.42	9.41	14.19	17.78
	30	-17.90	-14.07	-8.44	-1.79	0	1.79	8.44	14.07	17.90
	35	-18.01	-13.92	-7.38	-1.56	0	1.56	7.38	13.92	18.01
	40	-18.09	-13.60	-6.34	-1.46	0	1.46	6.34	13.60	18.09

CLL VALUES

M=0.1

		Yaw Angle								
		-40	-30	-20	-10	0	10	20	30	40
Pitch Angle	-5	-0.26	-0.22	-0.11	-0.01	0	0.01	0.11	0.22	0.26
	0	0	0	0	0	0	0	0	0	0
	5	0.26	0.22	0.11	0.01	0	-0.01	-0.11	-0.22	-0.26
	10	0.61	0.49	0.21	0	0	0	-0.21	-0.49	-0.61
	15	0.91	0.59	0.18	-0.04	0	0.04	-0.18	-0.59	-0.91
	20	0.94	0.46	0	-0.21	0	0.21	0	-0.46	-0.94
	25	0.56	0.13	-0.28	-0.36	0	0.36	0.28	-0.13	-0.56
	30	0.14	0	-0.46	-0.49	0	0.49	0.46	0	-0.14
	35	0.07	-0.03	-0.68	-0.56	0	0.56	0.68	0.03	-0.07
	40	0	-0.14	-0.94	-0.61	0	0.61	0.94	0.14	0

M=0.2

		Yaw Angle								
		-40	-30	-20	-10	0	10	20	30	40
Pitch Angle	-5	-0.24	-0.20	-0.10	-0.01	0	0.01	0.10	0.20	0.24
	0	0	0	0	0	0	0	0	0	0
	5	0.24	0.20	0.10	0.01	0	-0.01	-0.10	-0.20	-0.24
	10	0.59	0.48	0.21	0	0	0	-0.21	-0.48	-0.59
	15	0.90	0.60	0.18	-0.04	0	0.04	-0.18	-0.60	-0.90
	20	0.97	0.47	0	-0.21	0	0.21	0	-0.47	-0.97
	25	0.60	0.13	-0.28	-0.35	0	0.35	0.28	-0.13	-0.60
	30	0.18	0	-0.47	-0.48	0	0.48	0.47	0	-0.18
	35	0.09	-0.05	-0.70	-0.54	0	0.54	0.70	0.05	-0.09
	40	0	-0.18	-0.97	-0.59	0	0.59	0.97	0.18	0

M=0.3

		Yaw Angle								
		-40	-30	-20	-10	0	10	20	30	40
Pitch Angle	-5	-0.18	-0.15	-0.09	0	0	0	0.09	0.15	0.18
	0	0	0	0	0	0	0	0	0	0
	5	0.18	0.15	0.09	0	0	0	-0.09	-0.15	-0.18
	10	0.51	0.44	0.21	0	0	0	-0.21	-0.44	-0.51
	15	0.87	0.61	0.19	-0.04	0	0.04	-0.19	-0.61	-0.87
	20	1.04	0.52	0	-0.21	0	0.21	0	-0.52	-1.04
	25	0.70	0.15	-0.30	-0.33	0	0.33	0.30	-0.15	-0.70
	30	0.27	0	-0.52	-0.44	0	0.44	0.52	0	-0.27
	35	0.13	-0.11	-0.77	-0.48	0	0.48	0.77	0.11	-0.13
	40	0	-0.27	-1.04	-0.51	0	0.51	1.04	0.27	0